
Electronic Thesis and Dissertation Repository

7-3-2019 2:00 PM

Calcium Isotopes in the Saint Agatha Kettle Lake Deposits of Southern Ontario

Emma-Dawn Ferguson, *The University of Western Ontario*

Supervisor: Bouvier, Audrey, *The University of Western Ontario*

: Longstaffe, Fred J, *The University of Western Ontario*

A thesis submitted in partial fulfillment of the requirements for the Master of Science degree in Geology

© Emma-Dawn Ferguson 2019

Follow this and additional works at: <https://ir.lib.uwo.ca/etd>



Part of the [Geochemistry Commons](#), and the [Geology Commons](#)

Recommended Citation

Ferguson, Emma-Dawn, "Calcium Isotopes in the Saint Agatha Kettle Lake Deposits of Southern Ontario" (2019). *Electronic Thesis and Dissertation Repository*. 6293.

<https://ir.lib.uwo.ca/etd/6293>

This Dissertation/Thesis is brought to you for free and open access by Scholarship@Western. It has been accepted for inclusion in Electronic Thesis and Dissertation Repository by an authorized administrator of Scholarship@Western. For more information, please contact wlsadmin@uwo.ca.

Abstract

The St. Agatha kettle lake deposits, ON, Canada, contain a thick section of endogenic marl and coeval shelly fauna. Marl accumulation occurred from ~13,500 to ~8,200 cal yrs BP. This study examines controls on marl and shell $\delta^{44/42}\text{Ca}$, element ratios (Mg, Fe, and Ba), $\delta^{18}\text{O}$, $\delta^{13}\text{C}$, and $^{87}\text{Sr}/^{86}\text{Sr}$ ratios of marl calcite, shell aragonite, groundwater, and bedrock as proxies for paleolacustrine conditions. Results for *Interval A* (532.0 to 475.0cm) indicates a cooler, wetter climate, lower primary lake productivity and higher lake levels. *Interval B* (475.0 to 345.0cm) marks the onset of a closed lake system, warming climate, and perhaps Ca-limitation on marl calcite $\delta^{44/42}\text{Ca}$. Data for *Interval C* (345.0 to 192.0cm) suggest a reduction in lake depth, increased lakewater evaporation and greater lake productivity which continues into *Interval D* (192.0 to 128.0cm) before marl precipitation ceases. Marl calcite $\delta^{44/42}\text{Ca}$ is likely controlled by non-equilibrium processes in this freshwater system.

Keywords

Calcium isotopes, kettle lake, marl, paleolimnology, Saint Agatha, Ontario

Summary for Lay Audience

The St. Agatha kettle lake deposits, ON, Canada, contain a thick section of marl and mollusc shells. Marl is made up of calcite, while mollusc shells are mainly aragonite. Both occur in the sequentially deposited St. Agatha kettle lake deposits. Marl is a white to off-white calcium carbonate (CaCO_3)-rich sediment commonly found in shallow lakes that contain high concentrations of calcium (Ca) and bicarbonate (HCO_3^-). The marl at St. Agatha formed and accumulated as sequential laminae that have been dated from ~13,500 to ~8,200 years ago. This interval spans the change from the Pleistocene to Holocene Epochs, which was a period of great climate warming. The marl and shells should have recorded these changing conditions in their chemistry. We analyzed magnesium (Mg), iron (Fe), and barium (Ba) contents, and calcium (Ca)-, oxygen (O)-, carbon (C)-, and strontium (Sr)-isotope compositions of this marl and associated shells, using samples taken from cores throughout the lake sediments. A particular focus was placed on the Ca-isotope composition of the marl and shells. Very little is known about how Ca-isotope compositions change in marl lakes, and much could be learned by comparing its behaviour with the much better understood Sr-, O- and C-isotope tracers of water sources, climate and environment in such settings. Collectively, these data provide information about the environmental and climatic changes recorded in this kettle lake over this significant period of climate change. The changes deduced from the geochemical measurements can be subdivided into four *Intervals (A to D)*. From youngest to oldest, *Interval A* (located at 532.0 to 475.0cm depth) was a time of cooler, wetter conditions, higher lake levels, and lower primary lake organic productivity. *Interval B* (475.0 to 345.0cm) marked the beginning of a closed lake system (no outflow of water except through evaporation), warming climate, and a reduction in Ca-availability in lakewater. *Interval C* (345.0 to 192.0cm) was a time of progressively shallower lake level, increased evaporation and greater lake productivity which continued into *Interval D* (192.0 to 128.0cm) before marl formation ceased with the complete infilling and death of the lake.

Acknowledgements

I wish to thank a number of individuals whose guidance, patience, and encouragement over the last several years was paramount in the completion of this thesis. First and foremost I would like to extend a huge thank you to my supervisor Dr. A Bouvier for her never ending patience, guidance, and for being a fantastic resource throughout the duration of this project. Audrey, I am ever thankful for everything you have done for me, from your support, to teaching and training in the GEOMETRIC laboratory, the many research trips and research funding. The learning curve has been steep, the mistakes have been plenty, and the time spent was unforgettable; I would not have been as successful if it hadn't been for all you have done. You ignited a love for geochemistry, and for that I am ever grateful!

I would also like to express a sincerest thank you to my supervisor Dr. Fred J. Longstaffe, who has not only been an invaluable resource throughout this whole project, but has shown great patience and understanding along the way. Fred, I am honored to have been able to work with you and I thank you for extending me this opportunity. I will never forget all of your words of wisdom and many teachings. You and the amazing team of individuals you assembled have taught me more than I could have imagined throughout this project.

Without the dedication, hard work and patience of the research staff at Western University and Trent University, I would have been at a loss. To Dr. Blair Gibson, thank you for answering all of my questions, being a fantastic resource and always being available to run the ICPMS. To Dr. R Bastian Georg at Trent University, your expertise and wisdom knows no bounds, without which we would not have been able to conduct as many measurements as we did. Thank you for all of your help with the MC-ICPMS, for endless patience and always being a positive driving force behind all of our analytical sessions. For that I am forever thankful. I would also like to extend my appreciation to the staff at the Oil, Gas and Salt (OGS) Library, Liz Sutherland, Jordan Clark, Candace Freckelton, and Nikki Fortner for welcoming me so warmly to the OGS Library and aiding in core retrieval, identification, and sampling. To Tim Patterson of the Grand River Conservation Authority (GRCA), thank you for allowing me to accompany you in the collection of groundwater samples, and for being so patient and understanding. You were an invaluable resource and a great help during the whole process.

To my examination committee, Drs. Robert Linnen, Liz Webb, and Ron Martin, the time and effort you expended was much appreciated, as were your insights, questions and thoughtful revisions. I would also like to thank Dr. Roberta Flemming, who was Chair of my examination committee, for her time and efforts.

This project would not have been possible without the numerous funding agencies. Funding was provided by the Natural Sciences and Engineering Research Council of Canada Discovery Grant Program (AB, FJL), Canada Research Chairs Program (AB, FJL), Canada Foundation for Innovation (AB, FJL), Ontario Research Fund (AB, FJL), and the Faculty of Science, The University of Western Ontario (FJL).

I would also like to express my gratitude to the individuals I have shared research groups and laboratory space with. To the GEOMETRIC laboratory team: we worked in close quarters, shared resources and spent long hours in the lab together, but I couldn't have asked for a better group. You taught me how to be a better lab mate. To the Lake Pod, you were a kind and receptive audience, who welcomed an outsider into your midst with open arms. I have learned so much from each and every one of you, so I thank you for your input, your feedback and all of the amazing learning opportunities. I would also like to thank Jacob Walker for the provision of marl and shell samples, and access to unpublished oxygen and carbon isotope results for these samples. You were an invaluable resource!

Last but not least I would like to thank my parents Edward and Denise Ferguson, thank you for bringing me to Canada and giving me the opportunities to succeed, and for the crazy amount of love and support. To my siblings, Edward and Lorna Ferguson, while you drive me crazy and provide endless hours of torment, I would not be the person I am today without having had you by my side growing up, so a huge thank you to you both. To my better half Derek: thank you for the never ending love, for always making me feel like I could do whatever I set my mind to, and for always supporting me. You are my rock and were always there when I needed you most, thank you a thousand times over!

Table of Contents

Abstract.....	ii
Summary for Lay Audience.....	iii
Acknowledgements.....	iv
Table of Contents.....	vi
List of Tables.....	x
List of Figures.....	xii
List of Appendices.....	xvi
List of Abbreviations.....	xvii
Chapter 1.....	1
1 INTRODUCTION.....	1
1.1 Project Overview.....	1
1.2 Research Objectives.....	4
1.3 Stable Isotope Nomenclature.....	5
1.4 Project Background.....	5
1.5 Research Design.....	6
Chapter 2.....	9
2 BACKGROUND INFORMATION.....	9
2.1 Study Site.....	9
2.1.1 Saint Agatha Kettle Lake Deposits.....	9
2.1.2 Bedrock.....	11
2.1.3 Age of the Saint Agatha Marl Deposits.....	13
2.2 Calcium Isotopes.....	13
2.2.1 Calcium Isotope Standards.....	15
2.3 Measurement of Calcium Isotope Ratios.....	17

2.4 Calcium in Low Temperature Systems	21
2.4.1 Continental Calcium System	21
2.4.1a Mineral Crystallization	22
2.4.1b Shell Growth.....	23
2.4.1c Biologic Uptake	23
2.4.2 Calcium Carbonate Polymorphs.....	24
2.4.3 Ca-isotope Mineral-Water Geothermometers	25
2.4.4 Marl	26
Chapter 3.....	29
3 METHODOLOGY	29
3.1 Sample Collection	29
3.1.1 Marl Samples.....	29
3.1.2 Shell Samples	30
3.1.3 Groundwater samples.....	30
3.1.4 Bedrock Samples	32
3.2 Sample Preparation for Ca-isotope Analysis	33
3.2.1 Marl Sample Preparation.....	35
3.2.2 Shell Sample Preparation	36
3.2.3 Bedrock Sample Purification and Treatment	36
3.3 Column Chromatography.....	38
3.3.1 Calcium	38
3.3.2 Strontium.....	40
3.3.3 Calcium Column Blanks	41
3.4 Analytical Procedures	42
3.4.1 ICPMS	42

3.4.2	Ca-Isotope Measurements	43
3.4.3	Sr Isotope Measurements	45
Chapter 4	46
4	RESULTS	46
4.1	Elemental Concentrations	46
4.1.1	Marl	46
4.1.2	Aragonite Shells	49
4.1.3	Groundwater.....	53
4.1.4	Bedrock	54
4.2	Calcium-Isotope Ratios.....	56
4.2.1	SRM 915b	56
4.2.2	Marl	58
4.2.3	Aragonite Shells	61
4.2.4	Comparison of Marl Calcite and Aragonite Shells	63
4.2.5	Groundwater.....	64
4.2.6	Silicate Fraction from the Carbonate Bedrock Samples	65
4.3	Strontium Isotope Ratios.....	65
4.3.1	SRM 915b Sr-Isotope Ratios.....	65
4.3.2	Marl Sr-Isotope Ratios	66
4.3.3	Groundwater Sr-Isotope Ratios.....	68
4.3.4	Sr-Isotope Ratios of the Silicate Fraction from the Carbonate Bedrock Samples	68
Chapter 5	70
5	DISCUSSION	70
5.1	Lake Water Composition	70
5.1.1	Paleothermometers	70

5.2 Water History	74
5.2.1 Open or Closed Lake	78
5.3 Controls on the Isotopic Composition of St. Agatha Marl Calcite and Shell Aragonite ...	80
5.3.1 Oxygen Isotopes	83
5.3.1a Marl Calcite Oxygen.....	84
5.3.1b Shell Aragonite Oxygen	85
5.3.2 Carbon Isotopes	86
5.3.2a Marl Calcite Carbon	86
5.3.2b Shell Aragonite Carbon	88
5.3.3 Calcium Isotopes	88
5.4 Environmental History of St. Agatha Marl Calcite.....	91
5.4.1 Interval A (532.0 to 475.0cm)	94
5.4.2 Interval B (475.0 to 345.0cm)	95
5.4.3 Interval C (345.0 to 192.0cm)	97
5.4.4 Interval D (192.0 to 128.0cm)	99
5.4.5 Summary	100
Chapter 6.....	102
6 CONCLUSION.....	102
6.1 Future Work	105
References.....	107
Appendices.....	119
Curriculum Vitae	141

List of Tables

Table 2.1: The isotopes of calcium listed alongside their present abundances.	14
Table 3.1: Method for removal of OM and organic carbon from marl prior to column chromatography.	35
Table 3.2: Purification process applied to bedrock samples to isolate the carbonate, sulphate and silicate fractions in preparation for column chemistry.	37
Table 3.3: Protocol to separate the Ca fraction from matrix and interference elements using Eichrom DGA resin packed into a polypropylene Bio-Rad column, as adapted from Valdes et al. (2014).	39
Table 3.4: Protocol used to separate the Ca fraction from Sr using a Sr-specific resin after purification using Eichrom DGA resin, adapted from Valdes et al. (2014).	40
Table 3.5: Elemental standards for ICPMS analysis of carbonates.	43
Table 4.1: Elemental data for <i>G. parvus</i> , <i>V. tricarinata</i> and <i>Pisidium sp.</i> for two depths.	53
Table 4.2: Elemental concentrations of groundwater site W36 and W427.	54
Table 4.3: The abundance of various elements in the filtered (steps 3 to 7) and leachate (steps 8 to 10) fractions from the carbonate bedrock samples.	55
Table 4.4: The abundance of various elements in the carbonate bedrock arising from the silicate mineral content.	56
Table 4.5: Ca-isotope composition of each SRM 915b purified through the full column chromatography protocol.	57
Table 4.6: Ca-isotope value of unprocessed SRM 915b sample-standard bracketed against purified SRM 915b.	57
Table 4.7: Marl calcite $\delta^{44/42}\text{Ca}$ (‰) with 2SD and 2SE* relative to SRM 915b, all measured at ~4ppm.	60

Table 4.8: Shell aragonite $\delta^{44/42}\text{Ca}$ (‰) with 2SD and 2SE* relative to SRM 915b, all measured at ~4ppm.	62
Table 4.9: Ca-isotope results at two depths for coexisting <i>V. tricarinata</i> , <i>G. parvus</i> , and <i>Pisidium sp.</i> aragonite shells and coeval marl calcite.	63
Table 4.10: Ca-isotope values for groundwater.	64
Table 4.11: $\delta^{44/42}\text{Ca}$ (‰) of the silicate fraction from the carbonate bedrock samples.	65
Table 4.12: Sr-isotope compositions of marl calcite.	67
Table 4.13: $^{87}\text{Sr}/^{86}\text{Sr}$ ratios of water from overburden wells W36 and W427.	68
Table 4.14: $^{87}\text{Sr}/^{86}\text{Sr}$ ratios of bedrock samples.	69
Table 5.1: Marl calcite $\delta^{18}\text{O}$ (‰, VSMOW) and $\delta^{13}\text{C}$ (‰, VPDB) with depth (cm).	81
Table 5.2: <i>G. parvus</i> shell aragonite $\delta^{18}\text{O}$ (‰, VSMOW) and $\delta^{13}\text{C}$ (‰, VPDB) with depth (cm).	82

List of Figures

Figure 1.1: The location of the St. Agatha kettle lake deposits (Latitude: 43° 25' 49" N; Longitude: 80° 39' 55" W), indicated by the yellow marker, within southwestern Ontario. Major cities are indicated using red markers and large water bodies are labelled in blue text.	4
Figure 2.1: Cross section taken west-east across the Waterloo Moraine illustrating the boundaries of till sheets and underlying bedrock formations in relation to the St. Agatha kettle lake deposits (indicated with a red star). The dashed line dividing the Maryhill till sheet represents the Waterloo Sands (adapted from Kulak (2005))......	10
Figure 2.2: Location of the St. Agatha kettle lake deposits (indicated with a red star) and till sheet boundaries shown within the Kitchener-Waterloo area. Till sheets are labelled as follows: M - Mornington Till, T - Tavistock Till, Ma - Maryhill Till, P - Port Stanley Till, H - Unidentified till unit (adapted from Karrow (1974) using Karrow (1993), Kulak (2005), Stötler et al. (2010), Quaternary Geology and Paleozoic Geology, OGS Earth, and Carter and Fortner (2010))......	11
Figure 2.3: Map (adapted from OGSEarth, ©Queen's Printer for Ontario, 2018) detailing the bedrock formations in southwestern Ontario. The location of the St. Agatha kettle lake deposits are indicated with the yellow marker, and the formations of interest in this study are listed in the legend.....	12
Figure 2.4: A depiction of the global calcium cycle, focusing on the marine system, showing the major inputs and outputs of Ca to the ocean. The red arrows indicate outputs of Ca, while black arrows indicate inputs of Ca, with vegetation having minor direct inputs into the marine system.	21
Figure 2.5: A summation of the continental Ca-isotope cycle as it specifically relates to the St. Agatha lake deposits and associated carbonate-water Ca-isotope fractionation factors.....	28
Figure 3.1: Map showing the locations of the two wells sampled by the GRCA. W36 is located to the northeast and W427 to the southwest. The location of the town of Saint Agatha is indicated	

by the dark blue marker, while the St. Agatha kettle lake deposit is indicated by the green marker (adapted from Google Earth, 2018 and the PGMN from the Government of Ontario)..... 31

Figure 3.2: Cores 1119 (Latitude: 43° 58' 37.6" N, Longitude: 80° 53' 47.5" W) and 1120 (Latitude: 43° 58' 21.9" N, Longitude: 80° 56' 17.9" W) are the closest cored wells to the St. Agatha kettle lake deposits, indicated by the green marker, and which include most bedrock units of interest. They are located to the north near Minto, Ontario, indicated by the pink marker. (Image adapted from Google Earth, 2018, and the Oil, Gas and Salt Library, www.ogslibrary.com). 33

Figure 3.3: Bird's eye view of the Ca chromatographic column protocol, with each batch of samples accompanied by SRM 915b and a blank sample to ensure the consistency between sample batches. 41

Figure 4.1: Depth versus Ca-normalized concentrations (ppm) of St Agatha marl; with (a) Mg (dark blue), (b) Fe (green), (c) Mn (red) and Ba (light blue), and (d) Sr (purple)..... 47

Figure 4.2: Depth versus Ca-normalized concentrations of barium (Ba), magnesium (Mg) and iron (Fe) in marl calcite. Fe and Ba concentrations have been divided by a factor of 10. 48

Figure 4.3: Depth versus Mg/Ca, Fe/Ca and Ba/Ca ratios..... 49

Figure 4.4: Depth versus normalized minor and trace element concentrations (ppm) for *G. parvus*..... 50

Figure 4.5: (a) Depth versus normalized Mg concentration of marl calcite and shell aragonite *G. parvus*. The ~1m section of covariance is highlighted in the red box, (b) Normalized Mg concentration of marl calcite versus shell aragonite *G. parvus* for depths 191.5-299.5cm..... 51

Figure 4.6: Normalized Mg concentrations of shell aragonite (*G. parvus*) versus marl calcite for all depths. 52

Figure 4.7: Depth versus $\delta^{44/42}\text{Ca}$ (‰) obtained for marl calcite..... 59

Figure 4.8: Depth versus $\delta^{44/42}\text{Ca}$ (‰) of aragonite shell samples (*G. parvus*)..... 61

Figure 4.9: Depth versus $\delta^{44/42}\text{Ca}$ (‰) for marl calcite (black) and aragonite shells (<i>G. parvus</i>) (red).....	64
Figure 4.10: Depth versus marl calcite $^{87}\text{Sr}/^{86}\text{Sr}$	68
Figure 5.1: The calculated Ca-isotope composition of St. Agatha lake water, using Gussone et al. (2005) assuming a water temperature of 18°C and 27°C. The pink box outlines the range of $\delta^{44/42}\text{Ca}_{\text{water}}$ (‰) at 27°C and the green box outlines the range of $\delta^{44/42}\text{Ca}_{\text{water}}$ (‰) at 18°C. The purple box outlines the $\delta^{44/42}\text{Ca}_{\text{water}}$ (‰) of measured <i>G. parvus</i> using a temperature of 18°C with the average $\delta^{44/42}\text{Ca}_{\text{water}}$ of <i>G. parvus</i> indicated by the black arrow (+1.2‰). The blue dot indicates the average $\delta^{44/42}\text{Ca}$ (‰) of groundwater measured in this study, with the range in values shown by the blue arrows.	72
Figure 5.2: $^{87}\text{Sr}/^{86}\text{Sr}$ versus Sr concentration (ppm) of southwestern Ontario shallow and deep groundwater (diamonds) from Skuce (2014) and Skuce et al. (2015) compared with the results for St. Agatha marl calcite and two modern groundwater samples (squares).	76
Figure 5.3: $^{87}\text{Sr}/^{86}\text{Sr}$ ratios versus (a) Ca/Sr and (b) Mg/Ca for St. Agatha marl calcite.	78
Figure 5.4: $\delta^{18}\text{O}$ (‰) versus $\delta^{13}\text{C}$ (‰) of marl calcite illustrating the covariance between the two isotope systems.	80
Figure 5.5: Depth versus (a) $\delta^{18}\text{O}_{\text{marl}}$ (light blue) and $\delta^{18}\text{O}_{\text{shell}}$ (dark blue), and (b) $\delta^{13}\text{C}_{\text{marl}}$ (dark green) and $\delta^{13}\text{C}_{\text{shell}}$ (light green). Data courtesy J. Walker and F. Longstaffe (personal communication, 2017).	83
Figure 5.6: Dominant controls on the O-isotope composition of freshwater endogenic and biogenic carbonates (after Leng and Marshall, 2004).	84
Figure 5.7: Dominant controls on the C-isotope composition of freshwater endogenic (marl) calcite and biogenic (shells) aragonite.	87
Figure 5.8: Potential controls on the $\delta^{44/42}\text{Ca}$ of freshwater in the St. Agatha kettle lake system.	89

Figure 5.9: Depth versus $\delta^{44/42}\text{Ca}$ of marl calcite (red) and shell aragonite (black) of *G. parvus*.
See section figu for discussion of Intervals A-D. 91

Figure 5.10: Depth versus $\delta^{44/42}\text{Ca}$ (red), $\delta^{18}\text{O}$ (dark blue), $\delta^{13}\text{C}$ (green) and $^{87}\text{Sr}/^{86}\text{Sr}$ (light blue)
for marl calcite. Proposed Intervals A to D are outlined. 93

Figure 5.11: Controls on marl deposition in the St. Agatha kettle lake system. Depth (cm) versus
 $\delta^{44/42}\text{Ca}_{\text{marl}}$ (red) and $\delta^{18}\text{O}_{\text{marl}}$ (blue) (left), and $\delta^{13}\text{C}$ (green) and $\delta^{18}\text{O}$ (blue) (right). 101

Figure A1: $^{87}\text{Sr}/^{86}\text{Sr}$ ratios of brines from the Michigan and northern Appalachian Basins from
each of the formations identified (adapted from Burke et al. (1982) and Dollar et al. (1991)). 121

List of Appendices

Appendix A: Additional Methodology	119
Appendix B: Additional Data Tables and Figures	125

List of Abbreviations

Cal yrs BP – radiocarbon (^{14}C) dating of tree rings that corresponds to dates prior to 1950 and can be directly correlated with modern calendar years;

GRCA – Grand River Conservation Authority

IAPSO – International Association for the Physical Sciences of the Oceans

ICPMS – Inductively Coupled Plasma Mass Spectrometer

IRMS – Isotope Ratio Mass Spectrometry

LIS – Laurentide Ice Sheet

MC-ICPMS – Multi Collector Inductively Coupled Mass Spectrometer

NIST – National Institute of Standards and Technology

OM – organic matter, organic material

PGMN – Provincial Groundwater Monitoring Network; maintained by the GRCA

SRM – Standard Reference Material

TIMS – Thermal Ionization Mass Spectrometry

USGS – United States Geological Survey

VPDB – Vienna Pee Dee Belemnite; an isotope standard used in C-isotope studies

VSMOW – Vienna Standard Mean Ocean Water; an isotope standard used in O-isotope studies

Chapter 1

1 INTRODUCTION

1.1 Project Overview

The development of accurate and precise methodologies for measuring calcium (Ca) isotope ratios has allowed investigation of processes that cycle Ca in terrestrial and marine systems. The Ca-isotope systematics of continental freshwater systems, however, remains largely unexplored. In the present study we investigate the use of Ca-isotopes as a tracer of Pleistocene-Holocene climate and environmental variability as it is recorded in CaCO₃-rich marl and coeval mollusc shells deposited over several thousand years in a former kettle lake (St. Agatha) in southwestern Ontario. Samples from this deposit make possible (i) comparison of the Ca-isotope composition of coeval marl calcite and shell aragonite, (ii) evaluation of the dominant mechanisms and processes affecting the Ca-isotope compositions of neoformed marl calcite and biogenic aragonite, (iii) discrimination among possible water sources to the kettle lake using Sr-isotope ratios, (iv) development of a process-based understanding of how climatic and environmental conditions affecting this lake were reflected in isotopic variability over time, and by extension (v) how this model can be applied to other continental freshwater systems that have accumulated marl.

The St. Agatha deposit (an in-filled, former kettle lake) is located ~12km west of the city of Waterloo, Ontario, Canada within the township of Wilmont (Latitude: 43° 25' 49" N; Longitude: 80° 39' 55" W) (Figure 1) (Kulak, 2005). These kettle lake deposits offer a stratigraphic section that contains an interval of marl, a fine-grained soft sediment predominantly consisting of calcite (CaCO₃), deposited ~13,500 to ~8,200 cal years BP (Guillet, 1969; Thompson et al., 1997; Kulak, 2005; J. Walker and F. Longstaffe, personal communication 2017, 2019). Marl deposits commonly also incorporate biogenic and organic materials such as mollusc shells and plant matter, as well as clay, silt and fine sand (Guillet, 1969, Terlecky Jr., 1974). The white to off-white marl typically precipitates within topographic depressions, or kettle lakes, in regions with abundant carbonate bedrock. Kettle lakes in such terrains are typically fed by water that has come into contact with carbonate-rich units, and consequently have become enriched in calcium (Ca²⁺) and bicarbonate (HCO₃⁻) (Guillet, 1969; Terlecky Jr., 1974; Macdonald, 1982).

A kettle lake, such as the one once located near St. Agatha, is formed by the melting of a large block of ice that calved off during the retreat of a glacier (Warner et al., 1991). As the glacier retreats and temperatures rise, the ice block begins to melt leaving behind a large depression within the glacial material, typically tills; this depression then fills with water (Terlecky Jr., 1974; Kayler et al., 2018). The St. Agatha kettle lake formed during the retreat of the Laurentide Ice Sheet (LIS) approximately 14,000 years BP (Warner et al., 1991). The typically shallow kettle lakes are commonly spring-fed, closed systems that accumulate sediment (Terlecky Jr., 1974; Kayler et al., 2018), organic material and chemically precipitated marl calcite. These stratigraphic sequences can record conditions within the system from the time of lake formation until its demise once it becomes filled with sediment. The former St. Agatha kettle lake has now completely filled with material, including a thick interval (~400cm) of marl calcite. These sediments, and especially the marl calcite, can provide a record of the climatic and environmental conditions from the late Pleistocene- through to the Holocene era.

Southern Ontario is underlain by extensive carbonate bedrock formations that have contributed to the deposition of calcium-rich sediments, such as calcareous glacial tills and marl (Guillet, 1969; Turner et al., 1983). Glacial reworking of carbonate bedrock, such as Silurian dolomites, Ordovician limestones and Precambrian marble, within or near the St. Agatha area, contributed sediment to glacial tills formed during the advances and retreats of the LIS, and produced calcareous glacial drifts of varying thicknesses that blanket the topography of southwestern Ontario (Guillet, 1969; Carter and Fortner, 2010; Carter and Fortner, 2012). Surface water and groundwater percolating and flowing through carbonate bedrock formations and the glacial tills leaches Ca^{+2} and HCO_3^- (Guillet, 1969), which then enters kettle lakes such as the one that existed at St. Agatha. This provides the chemical components necessary for the precipitation of marl calcite.

In addition to the calcite comprising the marl at St. Agatha, calcium carbonate also occurs in aragonitic mollusc shells that are dispersed throughout the marl calcite (Kulak, 2005). The coeval precipitation of marl calcite and shell aragonite provides a unique opportunity to examine the Ca-isotope systematics of such low temperature systems. Whether the marl calcite or shell aragonite crystallizes in isotopic equilibrium with the lake waters or each other is not presently well understood. The nature of the signal that the Ca-isotope compositions might hold about the

changing environmental conditions during the time of marl calcite and shell aragonite precipitation is also unknown.

Marl crystallization is believed to be biologically aided by blue-green algae, otherwise known as cyanobacteria, in short periods of rapid accumulation referred to as “whiting” events (Grabau, 1920; Strong, 1978; Reynolds, 1984; Thompson et al., 1997). The extent to which this microbial mediation has affected the isotopic fractionation between dissolved Ca^{2+} and calcite precipitated from it is not fully understood. A comparison of isotopic results for marl calcite and coeval shell aragonite may reveal information about this and other aspects of Ca-isotope fractionation in freshwater systems. Experiments in controlled environments have demonstrated a systematic offset between the Ca-isotope compositions of calcite and aragonite precipitated from the same water column, which has been attributed to their differing bond strengths and crystal structures (Gussone et al., 2005; Colla et al., 2013; Gussone et al., 2015). It is presently unknown if the same offset occurs in natural systems, particularly those that are biologically mediated, and to what degree the composition of the source water will have on the resulting Ca-isotope compositions of both materials (Gussone et al., 2005).

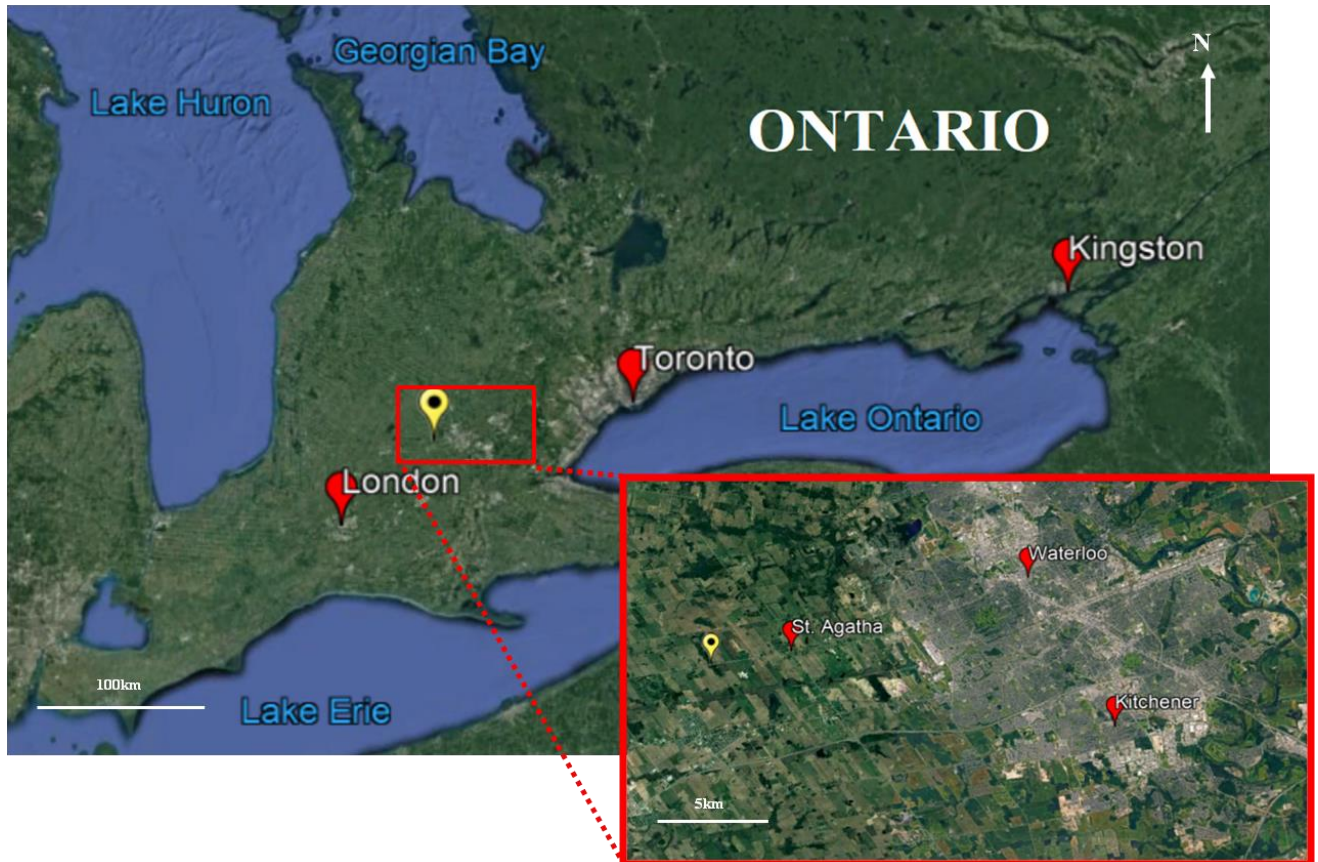


Figure 1.1: The location of the St. Agatha kettle lake deposits (Latitude: 43° 25' 49" N; Longitude: 80° 39' 55" W), indicated by the yellow marker, within southwestern Ontario. Major cities are indicated using red markers and large water bodies are labelled in blue text.

1.2 Research Objectives

A number of investigations have targeted the Ca-isotope systematics of marine environments through analysis of carbonate-rich sediments and foraminifera (Zhu and Macdougall, 1998; Kasemann et al., 2008). Freshwater Ca-isotope records, however, remain largely unexplored. Carbonates in freshwater systems are composed of calcite, aragonite or siderite (FeCO_3), with most current research exploring the variability in Ca-isotope fractionations between calcite and aragonite (Gussone et al., 2005). The variability in Ca-isotope compositions of calcite and aragonite, and the fractionation between them, offers insight into the mechanisms and processes controlling their formations and ultimately a greater understanding of Ca-isotopes in freshwater systems.

1.3 Stable Isotope Nomenclature

The nucleus of an atom contains an established number of protons and neutrons, with nuclei containing the same number of protons but differing number of neutrons being referred to as isotopes. Stable isotopes are those which do not radioactively decay, and many elements have more than one stable isotope (Coplen, 2011). It is therefore possible to measure the stable isotope ratio, or the ratio of the abundance of the heavy isotope to the light isotope of a given element (Sharp, 2007; Kayler et al., 2018). This stable isotope ratio is expressed as:

$$R = \frac{R_A}{R_B} \quad (1)$$

where R_A is the abundance of the heavy isotope and R_B is the abundance of the light isotope (Sharp, 2007).

The delta notation, or δ -value, is used to express the relative difference in abundance of two isotopes of the same element and is reported in parts per thousand (‰, per mille) relative to a given standard (Coplen, 2011). These isotope ratios are commonly measured using isotope ratio mass spectrometry (IRMS). Stable isotopes of an element will commonly fractionate during physical, chemical and biological processes, that is, the ratio of heavy to light isotopes of a given element will change from reactant to product, and/or as a product of isotopic re-equilibration between two phases containing the isotope of interest (Sharp, 2007; Coplen, 2011). In this study Ca-isotopes are reported in ‰ relative to National Institute of Standards and Technology (NIST) SRM 915b, which is a calcium carbonate standard (Heuser and Eisenhauer, 2008).

1.4 Project Background

In the present study, the Ca-isotopes of interest are ^{42}Ca and ^{44}Ca with the goal of obtaining $\delta^{44/42}\text{Ca}$ values for Ca carbonate-rich marl and shell species, groundwater, and bedrock from the St. Agatha kettle lake deposits. A significant portion of the previous work on Ca-isotopes has measured $\delta^{44/40}\text{Ca}$ (Tipper et al., 2006), given the much higher relative abundance of ^{44}Ca and the larger mass difference between ^{44}Ca and ^{40}Ca , relative to ^{44}Ca and ^{42}Ca (Skulan et al., 1997). Those analyses, however, were conducted using the double-spike method and Thermal Ionization Mass Spectrometry (TIMS) (Halicz et al., 1999; Tipper et al., 2006), unlike the present study in which Multi Collector Inductively Coupled Mass Spectrometry (MC-ICPMS) is

used to determine $\delta^{44/42}\text{Ca}$ values. Measuring ^{40}Ca is avoided due to the radiogenic β -decay of ^{40}K to ^{40}Ca (Schmitt et al., 2001; Tipper et al., 2006; Valdes et al., 2014; White, 2015), and interferences from the $^{40}\text{Ar}^+$ -plasma used in ICPMS and MC-ICPMS (Fietzke et al., 2004; Tipper et al., 2006; Rollion-Bard et al., 2007; Lehn et al., 2013). For these reasons, ^{42}Ca is measured in place of ^{40}Ca .

There currently exists no globally accepted standard for reporting Ca-isotope results, causing variability between laboratories. SRM 915a was a widely used standard until supplies were exhausted in 2006, which resulted in a switch to SRM 915b (Gills, 1995; Heuser and Eisenhauer, 2008). As a result, a conversion equation is required to compare δ -values obtained in this study to values obtained in earlier studies (see *2.1.1 Calcium Isotope Standards*). The International Association for the Physical Sciences of the Oceans (IAPSO) seawater standard (Wieser et al., 2004; Fietzke and Eisenhauer, 2006; Gothmann et al., 2016) is another commonly used material for Ca-isotope measurements for water in marine and riverine systems. The IAPSO standard, due to its differing matrix construction, is used primarily as a quality check on methodology.

1.5 Research Design

In the present study, Ca-isotopes were extracted and purified from Ca carbonate –rich materials (marl calcite), shell (aragonite), groundwater, and bedrock using column chromatography to eliminate matrix elements and any possible elemental interferences. Strontium (Sr) is a major elemental interference; it can have similar geochemical behaviour to Ca and easily replaces Ca in the crystal structure of carbonates, sulphates and phosphates (Matthews, 2014). In order to obtain high precision Ca-isotope ratios it is necessary to remove Sr from samples using column chromatography (Wieser et al., 2004). This process produced a suite of Sr-isotope samples for the marl calcite, groundwater and bedrock for which Ca-isotope compositions were also measured.

Prior to completing the column chromatographic protocols, a ThermoFisher iCap quadrupole ICPMS at Western University was used to determine the elemental compositions of samples as well as the ratios of key major and minor element pairs. The processing, extraction and purification protocols were carried out in the GEOMETRIC Laboratory at Western University, a clean laboratory designed to eliminate external and in-laboratory contamination (e.g. from dust,

equipment and materials) and to obtain pure Ca fractions (dissolved in nitric acid (HNO₃)) for high-precision isotopic compositions of the materials, and solutions prepared from them. Ca- and Sr- isotope measurements were conducted at the Trent University Water Quality Center, with the measurements of $\delta^{44/42}\text{Ca}$ performed using the Thermo Finnigan (Neptune) Multicollector ICPMS and the $^{87}\text{Sr}/^{86}\text{Sr}$ isotope ratios performed using the Nu Instrument Plasma II MC-ICPMS. The $\delta^{18}\text{O}$ (‰, VSMOW) and $\delta^{13}\text{C}$ (‰, VPDB) values were collected as part of another study in the Laboratory for Stable Isotope Science (LSIS) at Western University, but are used here in conjunction with the Ca-isotope and Sr-isotope measurements.

In addition to implementing the Ca-isotope method at Western, this research aims to measure and explain Ca-isotope fractionations within a continental freshwater system. The observed fractionations may be linked to the environmental conditions and history that have affected the freshwater system, such as temperature, pH, and extent of evaporation, or be connected to the water source (i.e. groundwater, surface water, precipitation). There may also be a link to the carbonate precipitation mechanism and its rate. For example, rapid marl deposition may be biologically mediated by blue-green algae rather than simply being a product of inorganic precipitation from the water column (Emrich et al., 1970; Terlecky Jr., 1974; Effler, 1984; Benson et al., 1991; Gussone et al., 2015). Accordingly, the following specific objectives are addressed in this study:

- i. To develop a method for accurate and precise Ca-isotope analysis of freshwater marl (calcite) and mollusc shells (aragonite), groundwater and carbonate bedrock,
- ii. To measure the Ca-isotope fractionations between coeval marl calcite and mollusc shell aragonite, groundwater and carbonate bedrock, and the Sr-isotope ratios of marl calcite, groundwater and carbonate bedrock,
- iii. To understand the sources and processes involved in determining the Ca-isotope composition of marl calcite and shell aragonite in the St. Agatha deposit, and
- iv. To test for patterns in Ca-isotope variation in marl and coexisting mollusc shell aragonite in the St. Agatha kettle lake system from the beginning to the end of marl precipitation,
- v. To relate the Ca-isotope variations to other chemical (elemental ratios) and isotopic parameters ($^{87}\text{Sr}/^{86}\text{Sr}$ isotope ratios, $\delta^{18}\text{O}$ and $\delta^{13}\text{C}$) that may carry information about environmental and climate change since deglaciation, and

vi. To extend these observations to freshwater marl systems in general.

Chapter 2

2 BACKGROUND INFORMATION

2.1 Study Site

The late-Wisconsin Glacial Episode shaped the landscape of Southern Ontario, resulting in an array of complex depositional features (Land and Water Policy Branch, Ministry of the Environment, 2009). These depositional features are a result of the advances and retreats of the Laurentide Ice Sheet (LIS), with this area of Ontario being one of the earliest to become deglaciated (Karrow, 1993; Stötler et al., 2010). The Ontario-Erie lobe from the east and the Huron-Georgian Bay lobe from the west contributed glacial deposits up to ~120m deep in areas, and formed many stratigraphic components intrinsic to this study (Karrow, 1993; Carter and Fortner, 2010). The Saint Agatha lake deposits reside within a depression in the Waterloo moraine (Kulak, 2005), which is composed primarily of fine sand and gravel, and is capped with glacial tills (Figure 2.1) (Karrow, 1993). Each till unit is geochemically unique as it is derived from a different source rock region and from a different glacial event (Stötler et al., 2010). These tills were a vital source of calcium to the St. Agatha deposits as were the calcareous bedrock formations found below.

2.1.1 Saint Agatha Kettle Lake Deposits

The St. Agatha kettle lake deposits are located in the Waterloo moraine within the Township of Wilmont, Ontario (Kulak, 2005). They are located approximately 12km west of the City of Kitchener-Waterloo (Kulak, 2005). The Waterloo Moraine incorporates many different stratigraphic components including sandy hills, ridges of sandy till, kames and kame moraines composed of outwash sands, all of which reflect the many glacial advances and retreats during the last glaciation (Stötler et al., 2010). These sands are capped with Maryhill Till (Figure 2.2). Within the Kitchener-Waterloo area, the glacial sediments are composed of many types of tills from the Ontario-Erie, Huron and Georgian Bay lobes, interspersed with glaciofluvial sediments (Karrow, 1993; Stötler et al., 2010). The glaciofluvial sediments consist primarily of outwash sand and gravel, and reworked material from older deposits (Karrow, 1993). As a result, the Saint Agatha kettle lake deposits are primarily underlain by Maryhill Till interspersed with

glaciofluvial outwash sediments, and sand and gravel (Karrow, 1974; Kulak, 2005; Stötler et al., 2010).

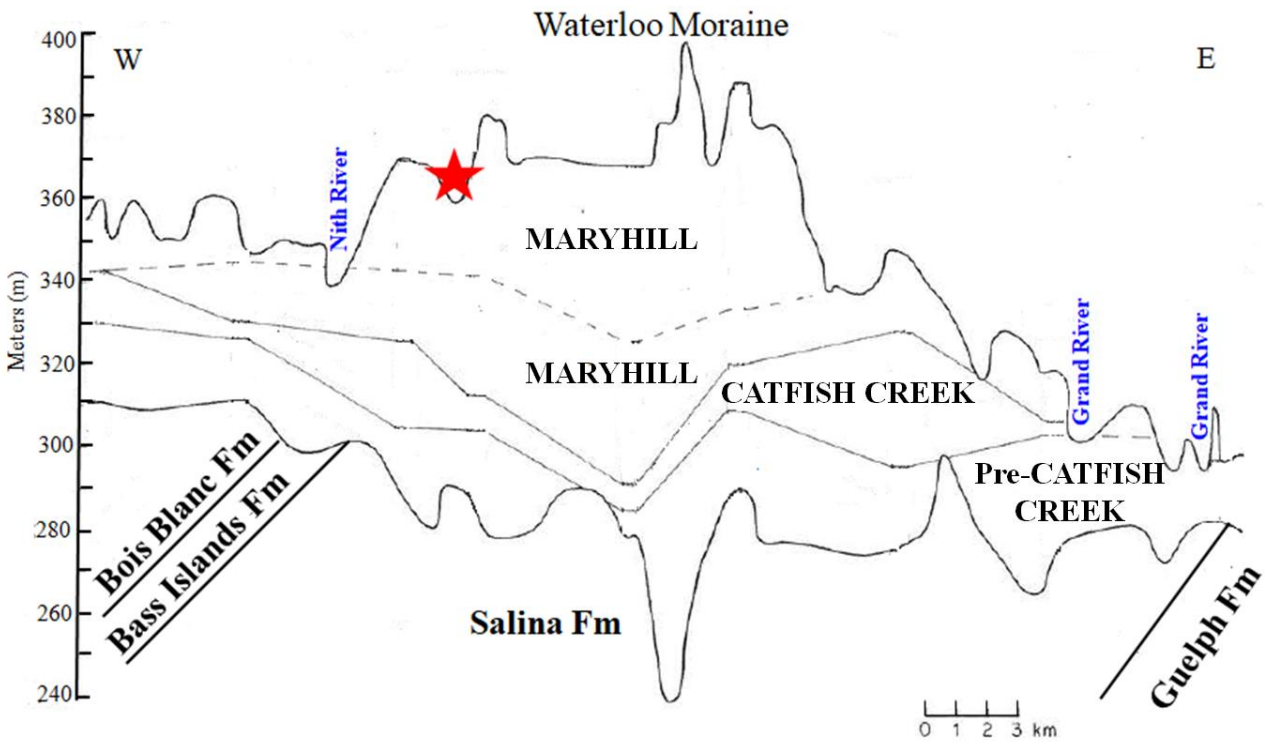


Figure 2.1: Cross section taken west-east across the Waterloo Moraine illustrating the boundaries of till sheets and underlying bedrock formations in relation to the St. Agatha kettle lake deposits (indicated with a red star). The dashed line dividing the Maryhill till sheet represents the Waterloo Sands (adapted from Kulak (2005)).

Kettle holes, or lakes, are typically associated with moraines, outwash tills and plains (Karrow, 1993), and are evidence of glacial activity. The kettle holes or lakes are formed from the melting of an ice-block that calved off from a larger, retreating ice sheet (Warner et al., 1991). The retreat of the last glacier covering Southern Ontario was estimated to have occurred at ~14,000 years BP leaving behind a glacial landscape.

A soil probe survey of the St. Agatha deposits identified an almost-flat sandy lake bottom overlain by marl and then covered by peat, soil and shallow water (Kulak, 2005). Complex layers of sandy to silty till underlie the St. Agatha deposits. These include the Catfish Creek Till, which is one of the earliest till units reported, and is widely distributed over Southern Ontario; it occurs between the Port Stanley Till and the Maryhill Till and sits atop part of the Waterloo moraine (Figure 2.2) (Karrow, 1974; Kulak, 2005; Land and Water Policy Branch, Ministry of the Environment, 2009; Stötler et al., 2010). Maryhill Till consists of clay till and extends north-

south along the edge of the Grand River. A comparison of the soil probe data and information published in the literature suggest that St. Agatha is immediately underlain predominantly by Maryhill Till, and is surrounded by glaciofluvial outwash deposits interspersed with minor deposits of Mornington Till. The Mornington Till which overlies the Tavistock Till, comprises primarily brown silty clay with a stony surface and extends easterly to the Conestogo River (Karrow, 1974). The Mornington Till was deposited by ice moving from the northwest (Lake Huron and Georgian Bay area) (Karrow, 1974). The boundaries of the Maryhill and Mornington tills are not sharply delineated and spatially there is interfingering of the two till units.

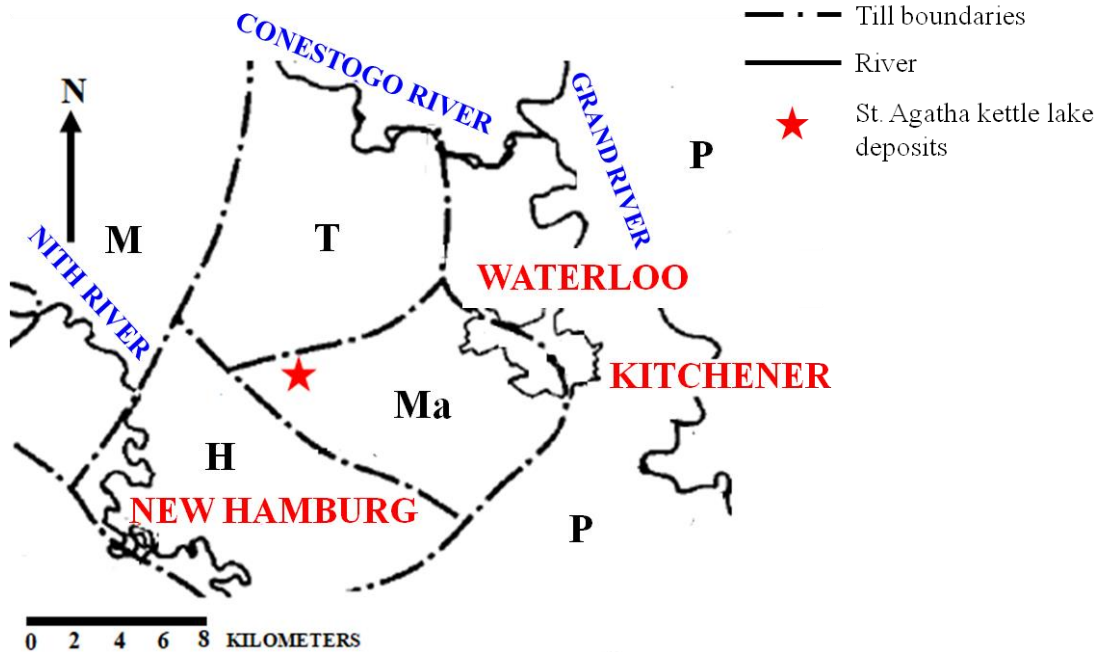


Figure 2.2: Location of the St. Agatha kettle lake deposits (indicated with a red star) and till sheet boundaries shown within the Kitchener-Waterloo area. Till sheets are labelled as follows: M - Mornington Till, T - Tavistock Till, Ma - Maryhill Till, P - Port Stanley Till, H - Unidentified till unit (adapted from Karrow (1974) using Karrow (1993), Kulak (2005), Stötler et al. (2010), Quaternary Geology and Paleozoic Geology, OGS Earth, and Carter and Fortner (2010)).

2.1.2 Bedrock

The St. Agatha kettle lake deposits reside atop glacial tills that are deposited overtop of the Upper Silurian bedrock, primarily of the Salina Formation (Figure 2.1, Figure 2.3). The Salina Formation variably consists of ~120 – 185m of interbedded shale, mudstone, dolostone, anhydrite, gypsum and halite, depending on location (Karrow, 1993). The maps of Armstrong and Dodge (2007), Carter and Armstrong (2010) and Stötler et al. (2010) suggest that Salina Formation units underlying the St. Agatha deposits consist of the Salina E member, with the

Salina C and Salina A members occurring to the northeast and the Salina F members to the southeast.

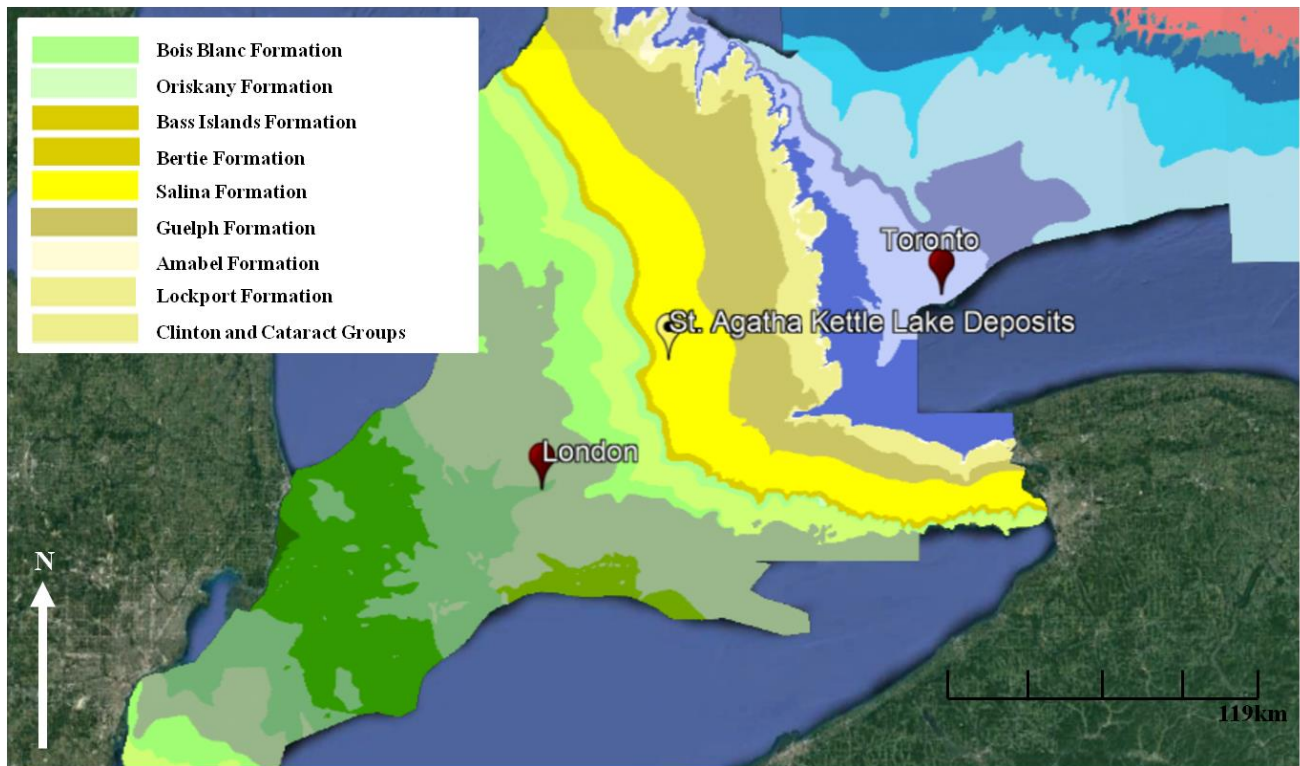


Figure 2.3: Map (adapted from OGSEarth, ©Queen’s Printer for Ontario, 2018) detailing the bedrock formations in southwestern Ontario. The location of the St. Agatha kettle lake deposits are indicated with the yellow marker, and the formations of interest in this study are listed in the legend.

Two cores (Well IDs: T011771 and T011773) from ~60km north of the St. Agatha deposit in this area provide some insight into the bedrock lithology underlying the region. The Salina F member is primarily a fine grained, compact grey dolomitic shale with porous dolomite-mudstone interbedded with layers of brown anhydrite. The Salina E member, which comprises the bedrock immediately underlying the St. Agatha kettle lake deposits, is composed of alternating layers of grey dolomitic shale, brown anhydrite, and grey to brown shaley dolostone. There are interbedded layers and veins of anhydrite throughout the grey dolomitic shale. The Salina C member consists of fine grained brown to grey dolomitic shale and shows little evidence of dissolution. The Salina A member varies depending on location, it can consist of A-1 carbonate, interbedded evaporite and anhydrite, and A-2 carbonate, salt, anhydrite, and shale. A-1 carbonate is light grey to brown, very fine grained with some anhydrite interbedding and fine shale laminae.

A-2 carbonate is very fine grained with veins and interbedded layers of anhydrite, and varies from light to dark grey. A-2 anhydrite is porous and contains shaley interlayers.

2.1.3 Age of the Saint Agatha Marl Deposits

There is currently no age-depth model for the St. Agatha marl stratigraphic section but some general observations are possible. Rising temperatures likely induced glacial melting and retreat of the last ice sheet from southern Ontario at ~15,000 years BP (Warner et al., 1991). Hence, onset of marl accumulation likely began sometime after deposition of Maryhill Till at ~15,000 – 14,000 years BP, as this is the till immediately underlying a portion of the St. Agatha kettle lake deposits (Kulak, 2005). As described by Kulak (2005), rapid colonization by plants, insects and molluscs was already occurring ~13,000 years BP. Hence, it can be inferred that marl began accumulating at St. Agatha between ~14,000 and 13,000 years BP (Terlecky Jr., 1974). Pollen analyses conducted by Kulak (2005) indicate that marl accumulation may have ceased at ~7000 years BP. A date of 5400 ± 55 ^{14}C cal BP has also been obtained for the peat-marl interface (J. Walker, personal communication, 2017). Using this date for the top of the marl succession, plus an assumed initial deposition age of ~13,500 years BP, the marl succession represents ~8,100 years of deposition. Assuming a constant rate of deposition, it can be inferred that each millimeter of marl calcite represents ~2 years of deposition primarily produced during rapid, summer whitening events.

2.2 Calcium Isotopes

Calcium is the 5th most abundant element in the silicate Earth and has 5 naturally occurring stable isotopes, ^{40}Ca , ^{42}Ca , ^{43}Ca , ^{44}Ca , ^{46}Ca (Table 2.1) (Zhu and Macdougall, 1998; Schmitt et al., 2001; Rollion-Bard et al., 2007; Valdes et al., 2014). A sixth isotope ^{48}Ca is radioactive, but considered to be stable due to its long half-life ($\sim 4.3 \times 10^9$ years) (Rollion-Bard et al., 2007; Valdes et al., 2014). Other radioactive isotopes include ^{41}Ca , ^{45}Ca and ^{47}Ca ; they are currently not considered in most Ca-isotope investigations (Gussone et al., 2016). The Ca-isotope system is considered a non-traditional, stable isotopic system because of the higher masses involved, relative to the traditional “light” isotopic systems such as hydrogen, oxygen, nitrogen and carbon.

The radiogenic β -decay of ^{40}K to ^{40}Ca is an additional complication. This process hinders measurement of non-radiogenic ^{40}Ca and determination of $^{44}/^{40}\text{Ca}$ ratios arising simply from fractionation in natural samples (Nelson and McCulloch, 1989; Halicz et al., 1999; Tipper et al., 2006; Rollion-Bard et. al., 2007). The ^{40}K isotope undergoes branched decay to $^{40}\text{Ar}^+$ and ^{40}Ca , by electron capture (ϵ) and β -decay, respectively (Isotope Geochemistry, 2003; Banner, 2003). It is not possible to predict how a ^{40}K atom will decay, but the probability of decay to each radiogenic daughter, or the decay constant (λ), is published in the literature. The $\lambda_{\epsilon} = 0.581 \times 10^{-10}$ and $\lambda_{\beta} = 4.962 \times 10^{-10}$, with a total $\lambda = 5.543 \times 10^{-10}/\text{year}$, and with associated half-lives of 11.93 Ga and 1.397 Ga (Isotope Geochemistry, 2003; Banner, 2003). Ca is a more abundant element than K, with ^{40}K being the least abundant of the K isotopes (0.012%) and ^{40}Ca being the most abundant of the Ca isotopes (96.94%) (Isotope Geochemistry, 2003; Tipper et al., 2006). This results in small $^{40}\text{K}/^{40}\text{Ca}$ ratios, and small variations in $^{40}\text{Ca}/^{42}\text{Ca}$ ratios due to radiogenic decay (Marshall and DePaolo, 1989; Nelson and McCulloch, 1989; Isotope Geochemistry, 2003). Marshall and DePaolo (1989) and Nelson and McCulloch (1989) exploited any possible radiogenic enrichment in rocks and minerals (such as arc island basalts, kimberlites, carbonatites and sediments from ancient terrains) by analyzing those with very high K/Ca ratios and concluded that enrichments in ^{40}Ca are measurable, particularly in the investigation of intra-crustal weathering processes (Nelson and McCulloch, 1989).

Table 2.1: The isotopes of calcium listed alongside their present abundances.

Isotope	Abundance (%)
^{40}Ca	96.94
^{42}Ca	0.647
^{43}Ca	0.135
^{44}Ca	2.086
^{46}Ca	0.004
^{48}Ca	0.187

(Zhu and Macdougall, 1998; Rollion-Bard et al., 2007; Fantle and Tipper, 2014; Valdes et al., 2014)

The isotopes of most interest in Ca-isotope studies are ^{44}Ca , ^{42}Ca and ^{40}Ca . The $^{44}\text{Ca}/^{40}\text{Ca}$ ratio has been favoured because of the large relative abundance of ^{40}Ca and the large mass difference between ^{40}Ca and ^{44}Ca which enhances isotopic fractionation in most processes (Baskaran, 2011;

Hoefs, 2015). The use of Thermal Ionization Mass Spectrometry (TIMS) has facilitated the precise and accurate determination of isotopic ratios involving ^{40}Ca as there are no analytical interferences during TIMS that affect this measurement. In the present study, however, the ratio of ^{44}Ca to ^{42}Ca ($\delta^{44/42}\text{Ca}$) is measured because of technical limitations of the MC-ICPMS method that was used (see 2.3 *Measurement of Calcium Isotope Ratios*).

2.2.1 Calcium Isotope Standards

One of the greatest challenges faced in early Ca-isotope investigations was the lack of a globally accepted standard of known purity (Gills, 1995). Standards offer a ubiquitous zero point against which isotope ratios are measured, allowing for easy comparison between laboratories, as well as seamless reporting in published literature. The variation in standards used in the past has made it difficult to compare published results (Hippler et al., 2003; Gussone et al., 2016). Holmden (2005) pointed out that absolute Ca-isotope ratios vary greatly between laboratories depending on the standard used, and the conversion equations required to compare inter-laboratory data resulted in errors and discrepancies in the literature. Hence, the universal use of an established reference standard is needed for accurate calibration and standardization of Ca-isotope data (Gills, 1995; Holmden, 2005).

Seawater was proposed as a widely available and accessible reference material by Zhu and Macdougall (1998) because of its measured homogeneity and high calcium concentration (~400mg/L) (Valdes et al., 2014). The Ca-isotope homogeneity of seawater is a direct result of the long residence time and the consistent mixing of oceans (Schmitt et al., 2001). It is widely believed that the Ca-isotope composition of seawater varied up to ~0.5‰ over geologic time due to the consistency in reporting of marine carbonates (Tipper et al., 2006). The National Institute of Standards and Technology (NIST), however, implemented the use of Standard Reference Material (SRM) 915a for the analysis of Ca-isotopes in 1995 (Gills, 1995). This general reference material was used until 2006 when its stock was exhausted, necessitating a switch to SRM 915b or SRM 1486 (Heuser and Eisenhauer, 2008; Valdes et al., 2014). SRM 915b is a calcium carbonate standard, while SRM 1486 is a bone meal standard used primarily in biological studies of biomineralization (Heuser and Eisenhauer, 2008). SRM 915b is reported to have a $\delta^{44/42}\text{Ca} = +0.35 \pm 0.01\text{‰}$ relative to SRM 915a (Valdes et al., 2014; Harouaka et al., 2016), or $\delta^{44/40}\text{Ca} = +0.72 \pm 0.02\text{‰}$ (converted using $\delta^{44/42}\text{Ca} \approx \delta^{44/40}\text{Ca} \times 0.488$, determined by

Holmden (2009)) (Valdes et al., 2014; White, 2015). Seawater has reported values of $\delta^{44/42}\text{Ca} = +0.92\text{‰}$, or $\delta^{44/40}\text{Ca} = +1.88\text{‰}$ relative to SRM 915a, or $\delta^{44/42}\text{Ca} = 0.57\text{‰}$ relative to SRM 915b.

There are many known published methods to convert between $\delta^{44/42}\text{Ca}$ and $\delta^{44/40}\text{Ca}$:

$$\delta^{44/42}\text{Ca} \approx \delta^{44/40}\text{Ca} \times 0.501 \quad (2)$$

(Martin et al., 2015)

$$\delta^{44/42}\text{Ca} \approx \delta^{44/40}\text{Ca} \times 0.476 \quad (3)$$

(White, 2015; Sime et al., 2005)

$$\delta^{44/42}\text{Ca} \approx \delta^{44/40}\text{Ca} \times 0.488 \quad (4)$$

(Holmden, 2009)

$$\delta^{44/42}\text{Ca} \approx \delta^{44/40}\text{Ca} \times 0.500 \quad (5)$$

(Hippler et al., 2003; Harouaka et al., 2016)

To determine equation 2, Martin et al. (2015) used the power fractionation law in order to convert between published $\delta^{44/40}\text{Ca}$ values and $\delta^{44/42}\text{Ca}$ values. The data was collected using a Thermo Neptune Plus MC-ICPMS with an Aridus desolvating nebulizer system for sample introduction without the use of a double spike. This approach is similar to that used in the present study, and may be an applicable conversion factor when comparing data sets. Equation 3, suggested by Sime et al. (2005) and White (2015) assumes equilibrium fractionation between marine biogenic carbonates and seawater. The use of biogenic marine carbonates formed in oceanic settings to determine this equation, as well as the assumption the system forms carbonates under equilibrium fractionation negates the use of the equation. It is currently unknown if equilibrium fractionation occurs in the crystallization of the Saint Agatha lake deposits. Holmden (2009) presents the use of Equation 4 for determining $\delta^{44/42}\text{Ca}$ from $\delta^{44/40}\text{Ca}$, as it is believed that a large portion of the variability in Ca-isotopes is a result of kinetic fractionation during crystallization of carbonate minerals. Kinetic fractionation during the crystallization of carbonate minerals is likely the case for Ca-isotope system that operated within the kettle lake (the lighter isotope, ^{42}Ca , has a strong preference for the solid phase over the liquid phase, and will therefore move more readily during marl calcite crystallization). The use of a double spike and MC-ICPMS was used to determine Equation 5, which was an approximation calculated from: $\delta^{44/42}\text{Ca} = (\delta^{44/40}\text{Ca}/43.956-39.963) \times (43.956 - 41.959)$, under

the working assumption that the samples were not artificially influenced by radiogenic ^{40}Ca (Hippler et al., 2003; Harouaka et al., 2016). While all equations offer the ability to convert $\delta^{44/40}\text{Ca}$ to $\delta^{44/42}\text{Ca}$, it is important to note the method by which each equation was obtained and to select the one most applicable to the study at hand. Equation 4 is used to convert between the Ca-isotope delta notations, since Holmden (2009) considered the possibility of kinetic fractionation in the determination of this equation.

Within the literature there are also conversion equations that allow for the direct comparison of a sample relative to the most widely used isotope standards (for $\delta^{44/40}\text{Ca}$).

SRM 915a-SRM 915b:

$$\delta^{44/40}\text{Ca}_{\text{sample/SRM 915a}} \approx \delta^{44/40}\text{Ca}_{\text{sample/SRM 915b}} + 0.72\text{‰} \quad (6)$$

(Gussone et al., 2005; Jacobson et al., 2008)

SRM 915b-Seawater:

$$\delta^{44/40}\text{Ca}_{\text{sample/SRM 915b}} \approx \delta^{44/40}\text{Ca}_{\text{sample/seawater}} + 1.88\text{‰} \quad (7)$$

(Gussone et al., 2005; Gussone et al., 2015)

For the most part, the most widely accepted conversion requires the addition of 0.35‰ to $\delta^{44/42}\text{Ca}$ analyzed against SRM 915b to obtain $\delta^{44/40}\text{Ca}$ relative to SRM 915a (Fantle and Tipper, 2014; Valdes et al., 2014; Owen et al., 2016). While available stocks remain exhausted, SRM 915a is still the most widely reported Ca-isotope standard. The data in this study are reported relative to a fresh aliquot of SRM 915b, which has a reported $\delta^{44/42}\text{Ca}$ of 0‰. Atlantic seawater was also processed alongside samples as a further check on the analytical protocol used; its expected $\delta^{44/42}\text{Ca}$ is +0.57‰ (White, 2015; Fantle and Tipper, 2014; C. Holdmen and A. Bouvier, personal communication, 2017).

2.3 Measurement of Calcium Isotope Ratios

Early investigations into Ca-isotope fractionations suggested that any natural variations should be observable between the smallest mass isotope ^{40}Ca and the largest mass isotope ^{48}Ca due to their large relative mass differences (Heumann and Luecke, 1973; Skulan et al., 1997) and the low abundances of Ca-isotopes beyond that of ^{40}Ca (Russell et al., 1978).

The investigations of Stahl (1968), Stahl and Wendt (1968), Heumann and Luecke (1973) and Russell et al. (1978) concluded that high analytical precision and accuracy were necessary to resolve the natural variations in Ca-isotopes. Work prior to 1973 was inconclusive in ascertaining the extent of fractionation effects between ^{48}Ca and ^{40}Ca in natural samples because of analytical limitations (Heumann and Luecke, 1973). Subsequent development of high precision techniques for measuring Ca-isotope ratios, however, has led to the ability of resolving even small mass dependent fractionations that were not attainable in the past (Hippler et al., 2003).

The precision of isotope analysis methods long remained a major limitation of Ca-isotope research, with the use of Thermal Ionization Mass Spectrometry (TIMS) being the preferred approach to these measurements (Baskaran, 2011). Measurement of Ca-isotopes by TIMS remained challenging because of low reproducibility arising from large and variable fractionation effects during analysis, as well as limited data output and often difficult sample preparations (Andr n et al., 2004). Subsequent development of (i) chemical separation (column chromatography) methods that improve the purification and preparation of the calcium fraction from samples, and (ii) high-precision Multi-Collector Inductively Coupled Plasma Mass Spectrometer (MC-ICPMS) techniques now allow larger numbers of samples to be analyzed, together with numerous standards under the same or similar analytical conditions (Gussone et al., 2016). The MC-ICPMS has revolutionized isotope geochemistry since the late 1990's as this instrument facilitates isotopic analysis of almost all elements, as well as different elements together if needed to correct for internal mass bias fractionation effects.

The precision and external reproducibility of Ca measurements has been largely resolved for TIMS using double-spiking. Double spiking requires the sample be mixed with two artificially enriched isotopes of known composition and concentration prior to purification using column chromatography (Lehn et al., 2013; Holmden, 2005; Morgan et al., 2011). This method is used to correct instrumental mass fractionation of elements with four or more stable isotopes as it ensures any fractionation occurring during column chromatography is corrected for at the same time as any mass discrimination occurring during the analysis at the mass spectrometer (Holmden, 2009; Baskaran, 2011). Once the isotope ratio is obtained from the TIMS, the predetermined composition of the double spike may be subtracted correcting instrument drift

after the fact (Holmden, 2005; Holmden, 2009; Morgan et al., 2011; Lehn et al., 2013).

Measurements using TIMS allows for the quantification of ^{40}Ca , but the double spiking method experiences instrument drift and a lower reproducibility than measurements using MC-ICPMS (Holmden, 2009; Lehn et al., 2013).

Ca-isotope measurements using high precision MC-ICPMS has several associated challenges; most notably (i) the inability to measure ^{40}Ca , (ii) the need to fully eliminate matrix elements, and (iii) interferences induced by the sample introduction system employed. The inability to measure ^{40}Ca results from of intense interferences with argon (Ar)-plasma, the gas used in MC-ICPMS measurements, and subsequently the $^{40}\text{Ar}^+$ ion beam, both of which are an essential part of the technique (Hippler et al., 2003; Baskaran, 2011). On one hand, ^{40}Ca is the most abundant of the six naturally occurring stable Ca-isotopes (Table 2.1), and the abundance of other Ca-isotopes is much smaller. On the other hand, ^{40}Ca contents are affected by additions from radiogenic decay of ^{40}K (Heuser and Eisenhauer, 2008), for which corrections must be made. The low relative abundances of the remaining Ca-isotopes, however, can be ameliorated by using high precision MC-ICPMS (Lehn et al., 2013), and chemical separation using column chromatography can help avoid elemental interferences from the sample matrix (Wieser et al., 2004; Sime et al., 2005).

Column chromatography separates the matrix elements from the sample to obtain the purest Ca-isotope fraction possible (Fantle and Tipper, 2014). The presence of matrix elements in a sample during analyses can inhibit the collection of precise and accurate Ca-isotope data (Fantle and Tipper, 2014). Elemental interferences can include $^{48}\text{Ti}^+$, $^{26}\text{Mg}^{16}\text{O}^+$ or $^{88}\text{Sr}^{+2}$ (because the mass spectrometer measures mass/charge [m/z]) (Wieser et al., 2004). Any Sr present will have a large influence on Ca-isotope measurements as its mass is double that of the Ca isotopes of interest, particularly as it commonly follows Ca in sample matrices (Halicz et al., 1999; Sime et al., 2005). This can form double-charged ions, such as $^{88}\text{Sr}^{2+}$, $^{86}\text{Sr}^{2+}$ and $^{84}\text{Sr}^{2+}$, in the plasma which exhibit strong spectral interferences on $^{44}\text{Ca}^+$, $^{43}\text{Ca}^+$ and $^{42}\text{Ca}^+$ (Sime et al., 2005). Strontium removal is possible through the addition of a second chromatographic protocol calibrated to fully eliminate this matrix element. Corrections for Sr^{+2} ion interference can be resolved by measuring $^{87}\text{Sr}^{+2}$ on calcium mass 43.5 during analyses (Tipper et al., 2006; Owen et al., 2016).

While column chromatography eliminates interferences resulting from the sample matrix, interferences from the Ar gas, from the sample solution introduced into the MC-ICPMS using a desolvating nebulizer, and from the N_2O^+ gas flow commonly used, produce their own set of challenges (Gussone et al., 2016). These interferences may be reduced or eliminated by analyzing in high mass resolution mode on the MC-ICPMS; use of high resolution mode, however, decreases the ion yields requiring samples be introduced at higher concentrations (Fantle and Tipper, 2014). It was found that the high Ca concentration of sample solutions resulted in faster degradation of machine sensitivity due to Ca depositing on the cones of the MC-ICPMS, necessitating extra cleaning and maintenance to maintain stability and necessary voltage to obtain precise results (Schiller et al., 2012).

The sample is introduced into the plasma chamber using a desolvating nebulizer which dries the solution to remove most of the water present, thus suppressing oxygen and hydrogen interference products and further enhancing the ion yields (Halicz et al., 1999). This is particularly important as measurements are conducted in high mass resolution mode. The desolvating system is a vital component of sample introduction in this study as high volumes of high concentration solutions were introduced into the plasma chamber for each measurement. N_2O^+ gas flow was not used in this study in order to eliminate any further induced interferences that may occur during sample introduction.

Ca-isotope measurements by MC-ICPMS require the introduction of sample and standard in dilute acid to keep ions stable in solution. In the present research, we use 2% HNO_3 at ~4ppm (of Ca). The precision and accuracy of the MC-ICPMS results further depend on the systematic removal of molecular interferences, which may be avoided by using a desolvating nebulizer, as described above, and correction for instrumental mass bias. Instrumental mass bias is defined as the deviation or drift of an isotope ratio overtime from the actual value of that element present in a given sample (Andr n et al., 2004; Rollion-Bard et al., 2007), commonly resulting from the changing conditions of the MC-ICPMS over the course of an analytical session. Andr n et al. (2004) noted that during extended analytical sessions the bias between first and last measurements can exceed 0.15%, which is significant relative to the size of the variations expected in this study. Instrument mass bias is corrected for by using sample-standard bracketing, which requires each sample be preceded and followed by measurement of a standard

(Sime et al., 2005; Fantle and Tipper, 2014; Hoefs, 2015). The standard used should have a similar chemical structure and therefore contain similar matrix elements as those in the present study.

2.4 Calcium in Low Temperature Systems

2.4.1 Continental Calcium System

The global calcium cycle can be used to describe the movement of Ca-isotopes through the major Earth systems (Fantle and Tipper, 2014). The calcium cycle acts as a major global sink for CO₂ through its sequestration from the atmosphere into carbonate minerals in marine and freshwater systems (Figure 2.4).

Oceans are one of the greatest sinks of calcium through the formation of CaCO₃. Major inputs of calcium into oceans include those from rivers, weathering and dissolution of carbonate and silicate minerals, hydrothermal fluids, and minor inputs from rain, dust and vegetation within the oceanic environment (Figure 2.4) (Fantle and Tipper, 2014). The major outputs of calcium from the oceans are through the crystallization of carbonates, calcium incorporation into animal shells and uptake by plants (Fantle and Tipper, 2014). Freshwater systems have similar inputs as oceans, except for minimal inputs from hydrothermal fluids and from rain and dust, the latter because of the vastly different terrestrial versus marine surface areas.

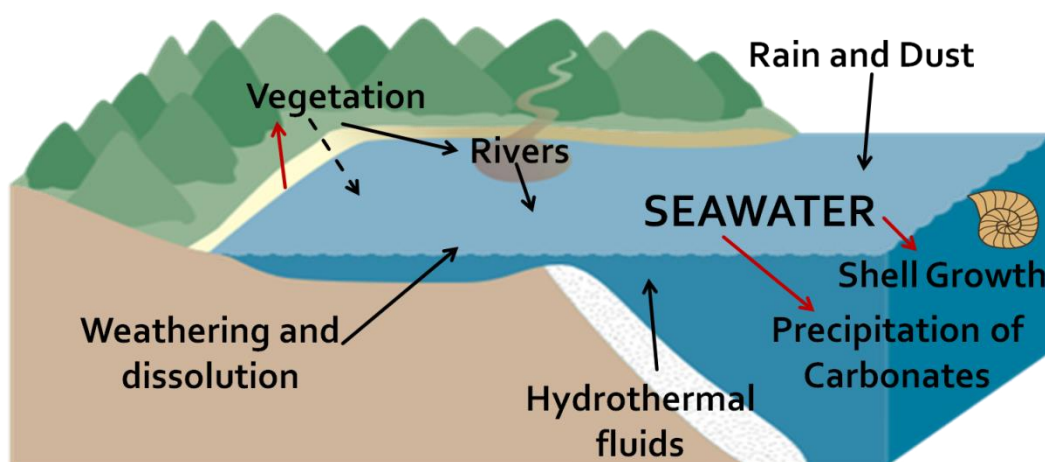


Figure 2.4: A depiction of the global calcium cycle, focusing on the marine system, showing the major inputs and outputs of Ca to the ocean. The red arrows indicate outputs of Ca, while black arrows indicate inputs of Ca, with vegetation having minor direct inputs into the marine system.

The chemical weathering of carbonates and silicates is a particularly important supplier of calcium to freshwater systems (Tipper et al., 2006; Fantle and Tipper, 2014). Moreover, carbonic

acid (H_2CO_3) is one of the common acids known to help dissolve rocks and minerals. The products of the acid reactions are carried by water and wind to bodies of water where new phases can precipitate under appropriate conditions. The chemical weathering factory liberates Ca^{2+} into solution held in pore spaces, lakes, rivers and streams. The weathering of fresh bedrock is the main supplier of Ca^{2+} to continental systems (Fantle and Tipper, 2014).

Calcium is cycled through continental systems primarily through mineral dissolution, mineral precipitation, biologic uptake and incorporation into shell species. These mechanisms may induce fractionations in Ca-isotopes; however, to date, no study has documented the preferential release of one isotope over another during mineral dissolution or weathering (Moore et al., 2013). A model of the Saint Agatha lake is shown in Figure 2.5, summarizing all of the information pertinent to the understanding of these deposits, including each of the dominant inputs and outputs, published Ca-isotope information, and the $\alpha(\text{calcite-water})$ and $\alpha(\text{aragonite-water})$ at 25°C . This provides an understanding of how each of the points discussed below influences our study site.

2.4.1a Mineral Crystallization

The crystallization of minerals from the dissolved constituents in freshwater systems can induce Ca-isotope fractionation. Unlike O-isotope system, in which the heavier isotope is preferred in the solid phase relative to the liquid phase, the opposite occurs in the Ca-isotope system (Skulan et al., 1997; Gussone et al., 2005; Baskaran, 2011; Fantle and Tipper, 2014). The magnitude of the Ca-isotope fraction is controlled by several factors, among which the rate of crystallization is extremely important (White, 2015).

Temperature and concentration of CO_3^{2-} are the major factors affecting crystallization rate (Inoue et al., 2015). Higher temperatures and concentrations have been shown to increase the crystallization rate, which in turn limits the magnitude of fractionation between the solid and liquid phase (Gussone et al., 2005; Gothmann et al., 2016). Conversely, mineral-water Ca-isotope fractionations are larger at lower temperatures and CO_3^{2-} concentrations (Gussone et al., 2015). The type of material crystallizing has also been shown to affect Ca-isotope fractionation. Gussone et al. (2005) noted that during the crystallization of aragonite and calcite in seawater, aragonite crystallizes about three times faster than calcite (Lemarchand et al., 2004). This

translates to a 0.05‰ smaller fractionation between ^{44}Ca and ^{42}Ca in aragonite crystallizing from seawater compared to calcite crystallizing from the same water (Gussone et al., 2005). Gussone et al. (2005), however, found that the observed systematic offset of 0.3‰ ($\delta^{44/42}\text{Ca}$) between inorganic aragonite and calcite was too large to be explained only by different crystallization rates as such an offset would correspond to a 20 to 25 times faster crystallization rate. Instead, they suggested that Ca-isotope fractionation in calcite and aragonite is also controlled by crystal structure.

2.4.1b Shell Growth

The biogenic growth of calcite and aragonite shells is very much species-specific. Generally, shell growth rate affects Ca-isotope fractionation in the same fashion as for inorganic precipitation, with smaller fractionations being associated with insufficient time for establishing isotopic equilibrium (Gussone et al., 2005). Gussone et al. (2005) also observed a temperature dependence of 0.2‰/°C associated with shell growth.

Gussone et al. (2005) explored calcium carbonate crystal growth in marine environments. They established that high $[\text{Ca}^{+2}]/[\text{CO}_3^{-2}]$ ratios in seawater caused the surface of calcite to become positively charged due to adsorption of Ca^{+2} ions to the crystals surface. Growth occurs by adsorption of CO_3^{-2} onto available Ca^{+2} sites. In short, crystal growth is controlled by the availability of Ca^{+2} sites and the concentration of CO_3^{-2} in the fluid from which the solid phase precipitates (Gussone et al., 2005). For the most part crystal growth is controlled by the concentration of CO_3^{2-} in the fluid as there is an abundance of available Ca^{+2} , particularly in seawater (Lyons et al., 2017). At higher temperatures carbonic acid dissociates into carbonate (CO_3^{2-}), therefore increasing its availability for incorporation into the shells of organisms. Whether a similar mechanism operates in freshwater systems remains unexplored.

2.4.1c Biologic Uptake

The biosphere has among the lowest Ca-isotope compositions of the global calcium cycle. Biologic uptake by plant species induces fractionation through the preferential uptake of light over heavy Ca-isotopes (Tipper et al., 2006; Baskaran, 2011; Fantle and Tipper, 2014), thus enriching pore waters and soils in the heavier isotopes (Tipper et al., 2010). Plants and vegetation exhibit the largest range of Ca-isotope compositions relative to the other systems, with an almost

4‰ variation in $\delta^{44/40}\text{Ca}$ (Fantle and Tipper, 2014). This equates to a 1.87 – 2.0‰ variation in $\delta^{44/42}\text{Ca}$ when converted using the expressions of Martin et al. (2015), White (2015) and Holmden (2009) (see 2.2.1 *Calcium Isotope Standards* for a full list of conversion equations). This leaves behind a reservoir of heavy Ca-isotopes in the inorganic fractions of sediments and soils and in surface and pore waters (Fantle and Tipper, 2014).

2.4.2 Calcium Carbonate Polymorphs

In low temperature systems calcium is predominately found in carbonate minerals particularly calcite and aragonite. Calcite and aragonite are two polymorphs of CaCO_3 that fractionate Ca-isotopes slightly differently. Fantle and Tipper (2014) summarized Ca-isotope data available to date illustrating that calcium carbonate minerals do not show Ca-isotope fractionations greater than a few ‰ relative to SRM 915a. The highest $\delta^{44/40}\text{Ca}$ values reported were for seawater, with values ranging from -2 to +2‰ (Fantle and Tipper, 2014). Gussone et al. (2005) reported a 0.6‰ offset in the $\delta^{44/40}\text{Ca}$ between inorganic calcite and aragonite co-precipitated from seawater at crystallization temperatures of 0 to 28°C under controlled laboratory conditions ($\delta^{44/42}\text{Ca} \approx 0.3\text{‰}$; converted using $\delta^{44/42}\text{Ca} \approx \delta^{44/40}\text{Ca} \times 0.488$, determined by Holmden (2009)). This reflects in part the constant 2⁺ oxidation state of Ca and the predominantly ionic nature of the bonds involving Ca (Gussone et al., 2005; Gussone et al., 2015). Calcite has a hexagonal structure, with a Ca coordination number of 6 while aragonite is orthorhombic and has a Ca coordination number of 9 (Colla et al., 2013). Any measured differences in Ca-isotope fractionation between inorganic calcite and aragonite may be linked to the differences and hence bond strengths between Ca^{2+} and CO_3^{2-} , depending on coordination number (Colla et al., 2013; Gussone et al., 2015).

Calcite is the most stable polymorph of calcium carbonate and typically exhibits a greater enrichment in ^{44}Ca than co-precipitated aragonite (Colla et al., 2013). Carbonates are generally more ionic in nature given the ionic character of the Ca-O bonds in the structure. The Ca-O bonds are 60% stronger in calcite than in aragonite which is a function of the difference in coordination number between each structure (Gussone et al., 2015). Heavier isotopes typically form a stronger bond which is consistent with enrichment in ^{44}Ca in calcite relative to aragonite. Within the above context, however, it must be explained why solid carbonates are more depleted of ^{44}Ca relative to the liquid phase from which they precipitate (Colla et al., 2013); in most

traditional isotopic systems heavier isotopes are concentrated in the solid phase relative to the liquid phase.

The proposed mechanism involves aqua complexes or aqua ions (Lemarchand et al., 2004; Colla et al., 2013). Aqua ions or aqua complexes are defined as cations dissolved in water that bond to water molecules through hydrogen bonding. The most common complexes found are those that bind metals and water. A solvation shell forms around the metal cation in water, with six or more water molecules bound to it via electrostatic forces and weak hydrogen bonding (Lemarchand et al., 2004). The strength of the bonds in aqua ions increases with increasing charge; hence a charge of 2⁺ on Ca results in a strong bond (Colla et al., 2013). Modelling by Lemarchand et al. (2004) indicated that the bonding of Ca in aqua ions is stronger than the bonding of Ca in calcite meaning that ⁴⁴Ca is preferentially held in the liquid phase relative to the solid phase (Colla et al., 2013; Lyons et al., 2017).

2.4.3 Ca-isotope Mineral-Water Geothermometers

Gussone et al. (2005) investigated the Ca-isotope fractionation between skeletal calcite and aragonite, and inorganic calcite crystallized from seawater in marine environments. Calcite and aragonite exhibit slightly different temperature-dependent Ca-isotope fractionations with seawater and the geothermometers are also somewhat different for entirely inorganic versus biologically precipitated carbonates (Gussone et al., 2005). Marl crystallization is believed to be facilitated by blue-green algae and therefore the biogenic calcite geothermometer is used in this thesis. The geothermometer for biogenic and inorganic calcite and aragonite are shown below.

Biogenic calcite:

$$1000\ln\alpha(\text{calcite-water}) = -1.39 \pm 0.17 + (0.026 \pm 0.01) \times T(^{\circ}\text{C}) \quad (8)$$

Biogenic aragonite:

$$1000\ln\alpha(\text{aragonite-water}) = -1.89 \pm 0.13 + (0.017 \pm 0.006) \times T(^{\circ}\text{C}) \quad (9)$$

Inorganic calcite:

$$1000\ln\alpha(\text{calcite-water}) = -1.02 \pm 0.25 + (0.015 \pm 0.013) \times T(^{\circ}\text{C}) \quad (10)$$

Inorganic aragonite:

$$1000\ln\alpha(\text{aragonite-water}) = -1.94 \pm 0.06 + (0.015 \pm 0.002) \times T(^{\circ}\text{C}) \quad (11)$$

(Gussone et al., 2005)

Assuming a crystallization temperature of 25°C for calcite, both biogenic and inorganic, and using the equations above, the following fractionation factors can be calculated; $\alpha(\text{calcite-water})$ for biogenic calcite 0.9993, and $\alpha(\text{calcite-water})$ for inorganic calcite 0.9985, a difference of 0.8‰. The values in this study are expected to range between -0.5 and 0.5‰ based on published literature, therefore making it useful to know whether the calcite was biogenic or inorganic.

However, note that equations 8 to 11 were determined in the laboratory under controlled environments. The calcite and aragonite species examined in this study are the product of a variety of mechanisms and processes operating simultaneous in the natural environment, which may influence the observed Ca-isotope discriminations.

2.4.4 Marl

Marl is a soft sediment, composed of calcium carbonate, plus minor quantities of organic matter, silt, sand and clay (Guillet, 1969; Vreeken, 1981). While marl is commonly white, its colour can vary based on minor elements incorporated during calcite precipitation, and its non-carbonate contents. Marl deposits are commonly found in spring-fed basins or depressions that contain abundant algal communities in areas of carbonate bedrock (Guillet, 1969; Vreeken, 1981). These water bodies are characteristic of southern Ontario, where the bedrock formations and glacial material are very calcareous, allowing for water to become enriched in Ca^{2+} and bicarbonate (HCO_3^{2-}) (Guillet, 1969; Vreeken, 1981; Macdonald, 1982). These basins or depressions commonly have limited outflows which allow Ca^{2+} to become enriched in the water during times of high evaporation (Guillet, 1969).

As noted earlier, marl crystallization can be facilitated by algae or cyanobacteria, and deposition occurs in whiting events, usually during warmer times when algal activity increases as a result of greater nutrient availability and increased light (Strong, 1978; Reynolds, 1984; Thompson et al., 1997). Cyanobacteria secrete calcium bicarbonate ($\text{Ca}(\text{HCO}_3)_2$). Calcium bicarbonate is held in the lake water to produce CaCO_3 , and is held in the water column by the partial pressure of dissolved CO_2 . Once the partial pressure of dissolved CO_2 decreases, $\text{Ca}(\text{HCO}_3)_2$ dissociates to produce CaCO_3 following equation 12. This releases CaCO_3 into the water column, and because of its low solubility, CaCO_3 crystallizes out as marl (Guillet, 1969).



An increase in algal activity in water bodies can cause a decrease in the partial pressure of dissolved CO₂ and trigger marl whitening events (Strong, 1978; Thompson et al., 1997). Increased algal activity is also associated with warmer (e.g. summer) conditions, and as algal blooms become more common in lake waters, consumption of dissolved CO₂ increases (Strong, 1978; Thompson et al., 1997). Warmer temperatures also contribute to an increase in surface evaporation and hence lower water levels, which concentrates solutes, such as CO₂, HCO₃⁻, Ca²⁺ and CO₃²⁻, in the water column which can also trigger marl crystallization.

Assumed temperature 25°C.

† Use Holmden (2009) to convert $\delta^{44/42}\text{Ca} = \delta^{44/40}\text{Ca} \times 0.488$

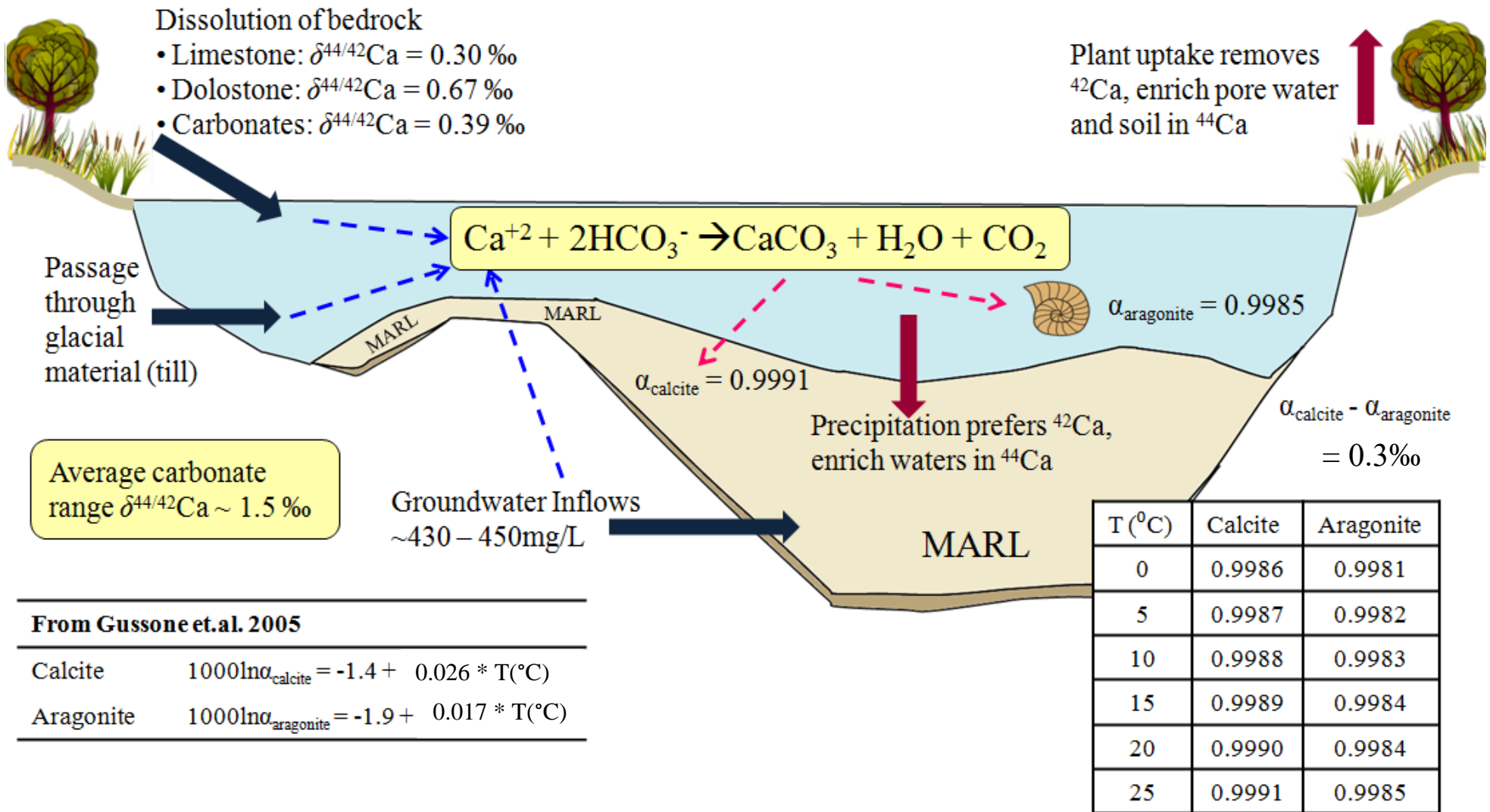


Figure 2.5: A summation of the continental Ca-isotope cycle as it specifically relates to the St. Agatha lake deposits and associated carbonate-water Ca-isotope fractionation factors.

Chapter 3

3 METHODOLOGY

3.1 Sample Collection

Calcium carbonate-rich (CaCO_3) marl and aragonite shells were obtained from the St. Agatha kettle lake deposits, from cores collected in 2004 by Paul Karrow and 2015 by Jacob Walker. Marl calcite samples containing coeval shelly fauna were of special interest to assess the variability in Ca-isotopes between calcite and aragonite, and to determine if there is Ca-isotope partitioning between these two materials. Groundwater samples were obtained from the Provincial Groundwater Monitoring Network (PGMN) within the Grand River Conservation Area (GRCA) to assess the Ca-isotope composition of the water flowing in this area. Bedrock material was obtained from cores located ~60km north of the St. Agatha kettle lake deposits to measure the Ca-isotope composition of bedrock in the region.

3.1.1 Marl Samples

The cores taken from the St. Agatha kettle lake deposits (2004 and 2015) were sampled every 0.5cm for the full ~5m of core for use in another study. They were then wet-sieved in order to remove any shells and organic material, and oven dried or freeze dried. Shells were separated from organic matter (OM), and both were stored separately in glass vials. This extraction method homogenized the full 0.5cm thickness of marl. From the material sampled every 0.5cm, a subsample of ~0.5g was collected in a glass vial and weighed for use in this study (see *Appendix B, Table B1* and *Table B2* for sample details). Then ~0.1g of CaCO_3 -rich marl was extracted and collected in a 15ml Teflon beaker for purification and further analyses.

Kulak (2005) completed Loss-On Ignition (LOI) measurements on the St. Agatha core taken in 2004 to determine the amount of moisture, and organic and inorganic carbon. Calculated weight loss percentages were determined at specific temperature increments (90°C, 550°C, and 1000°C), with the total weight lost used to estimate CaCO_3 content. Kulak (2005) reported that the marl comprises ~80 wt% CaCO_3 and ~20 wt% organic matter, silt and sand on average, with most samples containing ~73 to 97 wt% CaCO_3 .

3.1.2 Shell Samples

G. parvus, a freshwater snail commonly present in ponds and lakes in this region, was selected for investigation in the current study. This species is known to thrive in cool, clear, shallow, hard water (~1m depth) with abundant vegetation (Harman, 1972; Clarke, 1981; McKillop, 1985; Yang et al., 2000).

Kulak (2005) and Yang et al. (2000) reported an abundance of this species in cores from this locality (~85% of identified gastropods). Kulak (2005) noted that fewer *G. parvus* shells were found towards the top of the deposit, but their abundance still exceeded that of other shelly fauna. In the present study, however, the abundance of *G. parvus* decreased significantly below ~320cm, requiring other species present (*Valvata tricarinata*, *Pisidium sp.*) to be used. Two layers of marl (219.5 – 220.0cm; 309.0 – 309.5cm) that contained *G. parvus*, *V. tricarinata*, and *Pisidium sp.* were selected to test for inter-species variation in Ca-isotope composition.

Generally, the shells extracted were very small (~1mm or less in size), but those selected for analysis were large enough for at least one complete column separation protocol. The column protocol developed during this study was initially calibrated for ~200µg of Ca, but owing to the small size of some of the shells selected, ~50 or ~100µg of Ca was passed through the column instead (see *Appendix B, Table B2* and *Table B3* for sample details).

3.1.3 Groundwater samples

The Ontario PGMN provided water samples for two groundwater wells, one located to the northeast of the kettle lake deposits, and one to the southwest. Well 36 (W36) is located ~8km northeast of the St. Agatha kettle lake deposits, outside of the town of Saint Agatha, while Well 427 (W427) is located ~10km to the southwest outside of New Hamburg (Figure 3.1). Both samples were taken from overburden wells atop the Upper Silurian Salina formation. Based on the natural flow pattern of groundwater in Ontario (Carter and Fortner, 2010; Carter and Fortner, 2012), W36 may represent the approximate composition of water that once flowed into the kettle lake, while W427 may represent the composition of the water flowing from the kettle lake. This assumes that groundwater flow patterns have not changed over past ~13,500 years. W36 has an average Ca concentration of 438mg/L (sampled from 2003 to 2013 over irregular intervals),

while the water to the southwest at W427 has an average Ca concentration of 279mg/L (sampled from 2005 to 2013 over irregular intervals) (see *Appendix B, Table B6*).

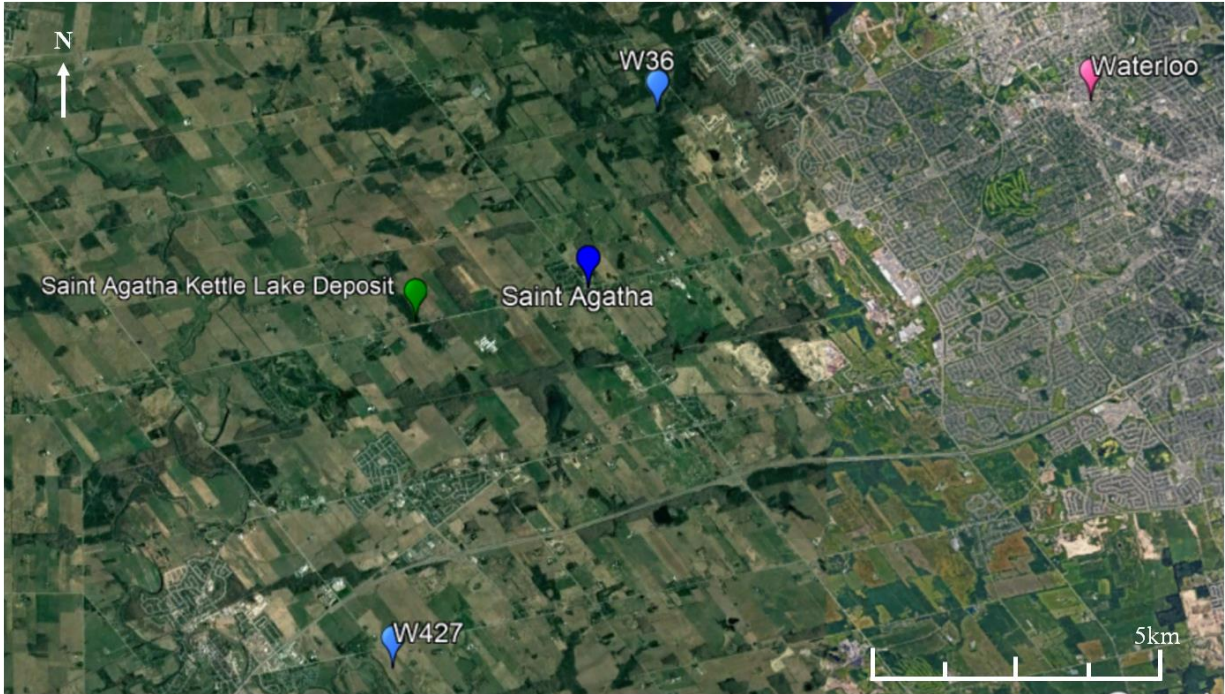


Figure 3.1: Map showing the locations of the two wells sampled by the GRCA. W36 is located to the northeast and W427 to the southwest. The location of the town of Saint Agatha is indicated by the dark blue marker, while the St. Agatha kettle lake deposit is indicated by the green marker (adapted from Google Earth, 2018 and the PGMN from the Government of Ontario).

Sampling of the wells was conducted on October 18, 2016 with the assistance of a GRCA well technician. Three full well volumes of water were purged before each water sample was taken. W427 was purged using a Redi-Flo Variable Frequency Drive which allows for control of the flow rate. The flow rate was obtained by timing how long it took to fill a 2L cylinder with water. It is important to monitor the flow rate to avoid running the well dry and to establish the time required to purge approximately three full well volumes. For W427, this required a purge of ~349L, which took 1 hour 10 minutes to complete. W427 is ~56.82m deep, and had an initial water level of 15.775m. During purging the water level dropped only by 0.72m, which indicates a good recharge rate.

W36 was purged using a Waterra Hydrolift, which employs a mechanical arm to help move the water up the well through a tube. The total purge time for ~410L of water was 2 hours 25

minutes. The well depth is ~76m and the initial and final water levels were 19.035m and 19.32m respectively, suggesting a very efficient recharge rate.

Once purging was complete ~125ml of well water was collected in an acid-washed polyethylene bottle, after thoroughly rinsing the bottle with the sample water. The water sampled was then filtered through a 0.45 μ m filter, and acidified using 10 drops of ~15.7M HNO₃ to a pH of <2. Each sample was labelled with the well site information and time of collection, and then placed in a cool box surrounded by ice, after which they were then stored in a refrigerator at 4°C. Once the necessary volume of water was removed from each bottle for analysis, the samples are to be stored at 4°C in a refrigerator located at the University of Western Ontario.

Prior to Ca-isotope and related analyses, two 20ml aliquots were removed from each 125ml bottle and transferred to two 30ml acid-washed Teflon beakers to be dried down on a hot plate at 120°C. Once dried down, the residue in one of the beakers was re-dissolved in 20ml of 2% HNO₃ while the other beaker was stored as a solid. An aliquot was taken from the beaker containing 20ml of 2% HNO₃ for analysis and quantification by ICPMS.

3.1.4 Bedrock Samples

The Oil, Gas and Salt Resource Library houses two bedrock cores, 1119 and 1120, which were drilled just outside Minto, Ontario (Figure 3.2), that span all units of interest in this study.



Figure 3.2: Cores 1119 (Latitude: 43° 58' 37.6" N, Longitude: 80° 53' 47.5" W) and 1120 (Latitude: 43° 58' 21.9" N, Longitude: 80° 56' 17.9" W) are the closest cored wells to the St. Agatha kettle lake deposits, indicated by the green marker, and which include most bedrock units of interest. They are located to the north near Minto, Ontario, indicated by the pink marker. (Image adapted from Google Earth, 2018, and the Oil, Gas and Salt Library, www.ogslibrary.com).

Ten samples in total, five from each core, were taken from the bedrock units suspected to underlie the St. Agatha kettle lake deposits, with a focus on the most permeable and hence most likely to have fed the former kettle lake. Samples were taken between the Salina E member and the Salina A-2 carbonate in each core with a focus on porous and vuggy carbonate and anhydrite.

3.2 Sample Preparation for Ca-isotope Analysis

Extraction and purification of Ca for isotopic analysis from the carbonate rock and sediment samples, marl calcite and shelly fauna were conducted in the GEOMETRIC Laboratory at the University of Western Ontario. This is a clean chemistry facility designed to minimize in-laboratory and external contamination of the samples during extraction of a high purity Ca sample used for quantification of elemental abundances by ICPMS at the University of Western Ontario and for Ca-isotope compositions by MC-ICPMS at Trent University.

All chemical reagents used in sample preparation and for column chromatography procedures were of ultra-trace purity (down to ppt for most metals). They were either single distilled in-

house from trace elemental grade acids (HCl, HNO₃), or purchased as such (acetic acid CH₃COOH, perchloric acid HClO₄, hydrogen peroxide H₂O₂ or HF Aristar Ultra). Ultrapure Milli-Q water with a resistivity of 18.2MΩ obtained from a Millipore Advantage A10 ion exchange filtering system coupled with a QPOD Element dispenser were used for all steps of the chemistry. The concentrations of the distilled acids were checked by acid-base titration using 1M NaOH and bromethyl blue solution as the indicator. Diluted acid solutions of concentrations >3M (15M HNO₃, 6M HNO₃ and 3M HNO₃) were stored in acid-washed Teflon bottles or beakers. Weaker acids (0.1M HNO₃, 0.01M HNO₃) were stored in acid-washed HDPE bottles. Acid washing was conducted using trace-metal grade 20% HCl, whose dilution was performed volumetrically inside a filtered fume hood, for several days before being rinsed 2 times using Milli-Q Element Ultrapure Water (~18.2 MΩ).

Teflon beaker cleaning procedure: Teflon beakers (Savillex® 7ml, 15ml and 30ml) used in sample preparation and column chromatography procedures were rinsed with Milli-Q water and then placed into a large 3L Teflon beaker. This 3L Teflon beaker was filled with reagent grade 50% HNO₃, whose dilution was determined volumetrically inside a filtered fume hood, before being placed on a hot plate for 24 hours at 120°C. The HNO₃ was allowed to cool before being replaced with Milli-Q water that was then boiled on a hot plate at 120°C for a minimum of 12 hours. The beakers were then air-dried in a laminar flow cabinet for several days, wrapped in plastic and stored until needed.

Plastic supplies (centrifuge tubes, pipette tips (50µl, 1000µl and 5000µl), tubes (10ml, 15ml and 50ml) were cleaned using a protocol requiring cold 20% HCl. These supplies were placed in 1L plastic containers and then submerged in cold trace-metal grade 20% HCl, the dilution for which was determined volumetrically in a filtered fume hood, for up to 24 hours before being rinsed 2 times using Milli-Q water. The 20% HCl bath was used up to 5 times for plastic supply cleaning before being discarded. Once acid-washed, the supplies were then left to air dry in a laminar flow cabinet for several days. Acid-washed plastic supplies, once dry, were wrapped in plastic, stored in Ziploc bags or in plastic boxes until needed.

3.2.1 Marl Sample Preparation

The presence of organic material was a major concern during processing of the marl calcite. Organic carbon needs to be removed from the sample prior to conducting column chromatography and analyses using the ICPMS and MC-ICPMS. There is no prescribed method or protocol for removing OM in the literature, and the protocol varies from laboratory to laboratory. When eliminating OM and impurities from carbonates, recommended treatments varied from H₂O₂-HNO₃ mixtures, to H₂O₂ treatments, to acetic acid (HAc) treatments and various leaching steps (Holcomb et al., 2015; Inoue et al., 2015; Gussone et al., 2016). Initially, a leaching method was used in which the marl was dissolved in 16M HNO₃ and allowed to react. The leachate was then removed via syringe and collected in a 15ml Teflon beaker, with the remaining fraction dried down on a hot plate at 120°C. This procedure, however, resulted in a significant loss of Ca to the leachate fraction (<20% of the estimated calcium content), which is not ideal for small sample sizes. Harouaka et al. (2016), however, recently reported success with methods for purifying gypsum samples, and so a similar protocol was then applied to this study to process the marl samples.

Ultrapure H₂O₂ was used to treat the marl (and shells), therefore, 1ml of 30-32% H₂O₂ was dried down in a 15ml acid-washed Teflon beaker on the hot plate at 120°C. Once fully evaporated the dried residue was then dissolved in 10ml 2% HNO₃ for further analysis (Table 3.1).

Table 3.1: Method for removal of OM and organic carbon from marl prior to column chromatography.

Step	Action
1	Weigh ~0.1g of marl into a 15ml acid washed Teflon beaker
2	Dissolve in 2ml 6N HNO ₃ , swirl the sample to dissolve
3	Cap and place on the hot plate at 110°C for 20 minutes,
4	Uncap and evaporate to dryness
5	Add 2ml of 30-32% ultrapure hydrogen peroxide (H ₂ O ₂)
6	Cap and place on the hot plate at 90°C for 30 minutes
7	Uncap and allow to evaporate to dryness
8	Complete Steps 2-6 again using the same protocol
9	Dissolve final residue in 1M HNO ₃ and put in 1.5ml centrifuge tube
10	Centrifuge for ~5 minutes prior to analysis at the ICPMS

(Harouaka et al., 2016)

3.2.2 Shell Sample Preparation

Shell samples were separated from the marl calcite and placed in a separate vial. The shells were then hand cleaned under a petrographic microscope using dental tools to ensure that all marl calcite and OM were removed from the shell interior. The shells were then identified and photographed. While all visible marl calcite and OM were removed during cleaning, further treatment was deemed necessary to ensure elimination of organic contamination. There is no universally accepted cleaning protocol for shells. Various publications recommend treatments ranging from H₂O₂-NaOH, to H₂O₂ alone, to NaClO (Inoue et al., 2015; Gussone et al., 2016). In the past, however, shells treated in these ways were commonly larger than those used in the present study, therefore, a similar protocol to that used for marl calcite purification was employed to treat the shells, using smaller volumes of H₂O₂ since there was significantly less shell material.

3.2.3 Bedrock Sample Purification and Treatment

As noted above, 10 bedrock samples were obtained from two cores located to the north of the St. Agatha kettle lake deposits. The samples were first cut and a representative portion then crushed using a stainless steel pulveriser in the rock preparation laboratory at the University of Western Ontario.

Once powdered, the samples were analyzed using the Rigaku powder diffractometer (pXRD) in the Experimental Mineralogy Laboratory at the University of Western Ontario. A small portion of powdered sample was added onto a glass plate, using an acetone-wiped scoop, was then wet with ethanol, allowed to dry and was then loaded into the pXRD machine. The samples were scanned from 5 to 90° in 2θ, with a step of 0.02 and a dwell time of 1.0s for ~1hr. The resulting XRD pattern was used to determine the mineralogy of each sample. Peak matching was conducted using EVA software in order to determine the most prominent phases in each core sample (see *Appendix B, Figure B1-B10*). With the mineralogy determined, it was then possible to define a protocol for extraction of all Ca-bearing phases (gypsum, carbonate, and silicate). The approach followed Moore et al. (2013) in which carbonate and silicate fractions were isolated using a leaching and digestion protocol, with amendments tailored to each sample's specific mineralogy.

Acetic acid plays a large role in the protocol developed for these samples. We used ultrapure glacial acetic acid Omni Trace® that had a Ca concentration about half that of the reagent grade acetic acid (ultrapure glacial 4.5ng/ml; reagent grade 8.9ng/ml), and was therefore used in the following protocol. The concentration of the ultrapure glacial acetic acid was checked volumetrically by titration in a filtered fume hood using 1M NaOH and bromethyl blue solution as the indicator. The 4M acetic acid solution was made using Milli-Q water and stored in an acid-washed 1L Teflon bottle.

Several bedrock samples contained multiple Ca-bearing phases, and so it was necessary to extract each phase individually. Each phase was collected in either a 15ml or 30ml acid-washed Teflon beaker, and dissolved in 2% HNO₃ for further analysis by ICPMS (Table 3.2).

Table 3.2: Purification process applied to bedrock samples to isolate the carbonate, sulphate and silicate fractions in preparation for column chemistry.

Step	Action
1	For samples containing gypsum, add Milli-Q H ₂ O and swirl repeatedly, pipetting off the liquid into a 15ml Teflon beaker
2	Dry down the remaining sample containing water and the pipetted liquid fraction on the hot plate at 120°C
3	For the remaining sample and samples devoid of gypsum, react ~1.0 g of powdered homogeneous sample with 10ml of 4M acetic acid (HAc) overnight
4	Centrifuge the supernatant
5	Pass supernatant through 0.45µm polypropylene syringe filter, and collect in 30ml Teflon beaker
6	Perform Steps 3-5 again, collecting in 30ml Teflon beaker
7	Dry down on the hot plate at 120°C and re-dissolve in 2% HNO ₃ for analysis
8	React residue with 10ml of cold 6M HNO ₃ overnight
9	Centrifuge and then pass the supernatant through 0.45µm syringe filters, collecting in 15ml Teflon beaker
10	Dry down supernatant on hot plate at 120°C and re-dissolve in 2% HNO ₃ for analysis
11	Digest remaining residue in 5:3 mixture of 29M HF and 16M HNO ₃ , and place capped on hot plate at 120°C. Uncap and evaporate to dryness
12	Repeat Step 9 again
13	Dissolve residue in HClO ₄ . Uncap and evaporate to dryness
14	Dissolve in 15M HNO ₃ , place on hot plate at 120°C for 2-3 days, ultrasonicate the sample and then uncap and evaporate to dryness
15	Re-dissolve in 10ml of 1M HNO ₃

Once the samples had been fully treated for the removal of any OM, sulphate and silicate materials, they were analyzed at the ICPMS to determine the elemental compositions and the concentrations necessary to proceed using Ca column chemistry. During the necessary purification protocol, multiple samples did not fully dissolve, notably those rich in sulphates. Once separated successfully from the heterogeneous sample, the sulphates were to be dissolved in 2% HNO₃ for further analyses; this proved challenging, however, as part of the sample remained suspended in the acid solution. For fear of inducing artificial isotopic fractionations, these samples were not processed through Ca column chemistry. The silicate materials were also separated from the dominant Ca-bearing phases, however, the complex silicate matrices and minor and trace element compositions necessitated less than 200µg of Ca be loaded during column chemistry. For each element found in the silicate matrices, it was necessary to calculate the Eichrom DGA resin capacity to ensure each element was effectively removed from the Ca fraction. To avoid overloading the column with minor and trace elements during the purification process, and to ensure a pure Ca fraction at the end of the protocol, substantially less than the calibrated 200µg of Ca would have been loaded on each column. This resulted in a less than ideal column yield and a Ca fraction that still contained unwanted minor and trace elements. In order to effectively analyze the silicate fraction, it would have been necessary to develop a further protocol which time did not permit. As a result of the challenges faced during sample preparation, only the Ca-bearing carbonates were analyzed at the MC-ICPMS.

3.3 Column Chromatography

3.3.1 Calcium

High precision column chromatography was used to purify Ca for isotope analysis. Bulk samples equivalent to 200µg of calcium were passed through a BioRad polypropylene column filled with 1ml of Eichrom DGA resin. Due to the relatively simple sample matrices, and the low concentrations of trace elements, it was found that a resin bed packed with 1ml of Eichrom DGA resin was sufficient to purify the Ca fraction, and resulted in the collection of a sample of Ca devoid of matrix elements and interference elements. Nitric acid, in various molarities, was the main acid used in this process. During column chromatography, it is necessary to collect >98% of the Ca initially added to avoid isotopic fractionations during the purification process.

The method used to purify the Ca fraction in the present study followed Valdes et al. (2014) and is summarized in Table 3.3. Column calibrations were conducted using a pure calcite sample obtained from the DANA mineral collection at the University of Western Ontario, and marl samples from the St. Agatha kettle lake deposits. The column calibrations were designed to assess the optimal amount of Ca to load and load volumes and kinds of acid solutions to add to a column in order to collect the full Ca fraction, while removing matrix elements, especially those that might cause interference during isotopic analysis.

Table 3.3: Protocol to separate the Ca fraction from matrix and interference elements using Eichrom DGA resin packed into a polypropylene Bio-Rad column, as adapted from Valdes et al. (2014).

Acid/Liquid	Volume (ml)	What is Eluted
H ₂ O	Full reservoir	Rinse column
2M HF	Full reservoir	Cleaning column
H ₂ O	Full reservoir	Rinse column
15 M HNO ₃	5	Cleaning resin + column
1 M HNO ₃	6	Conditioning column
Load Sample 1 M HNO ₃	1	200µg sample equivalent of Ca
1 M HNO ₃	5	Elute matrix elements
15 M HNO ₃	20	Collect Ca, Sr and matrix elements
15 M HNO ₃	5	Rinsing/cleaning column
0.1M HNO ₃	5	Wash out nitric acid
H ₂ O	Full reservoir	Wash column then store in acid bath

The molarities of acids used was determined following Pourmand and Dauphas (2010) and Horwitz et al. (2005), who report the distribution coefficients of each element relative to the molarity of HNO₃. The distribution coefficient dictates which elements have greater retention and adsorption on the resin bed, and therefore which molarities are best for isolating the calcium fraction. Pourmand and Dauphas (2010) showed that 1M HNO₃ had the greatest distribution coefficient for both Ca and strontium (Sr), two elements of interest in this study, but had little to no adsorption for elements such as Na, Mg, K, Al, Rb, Ba and Zn. These latter elements do not stick to the resin bed when loaded onto a column in 1M HNO₃ and are therefore eluted into the “matrix” cut. At molarities >12M both Ca and Sr are not adsorbed onto the resin, therefore, 15M HNO₃ was selected to elute the Ca and Sr fractions from the column in the “Ca cut”.

The volume of 15M HNO₃ used was calibrated to the specific matrices and samples used in this study, starting with the pure calcite sample. Once a sufficient volume was established for the

“matrix cut” the calibrations were completed using a processed marl sample. To wash the column after sample purification occurred, 0.1M HNO₃ was used followed by a full column reservoir (~12ml) of Milli-Q water; no element is retained on the resin bed at such low molarities and hence any residual matrix elements are eluted from the column. Once the columns were fully washed, they were stored in an acid-washed bottle containing ~450ml of Milli-Q water and ~5 drops of concentrated HNO₃ (~16M HNO₃). The Bio-Rad DGA columns were used 10 times before being replaced with a fresh acid-washed column and resin bed; early tests indicated that the column and resin bed could degrade due to the high volume of concentrated acids used in the protocol.

Once the Ca and Sr fraction was collected from the Ca column protocol, it was dried down, re-dissolved in 1ml of 3M HNO₃ and centrifuged in preparation for a second (Sr) column protocol. The overall average yield of the whole procedure was calculated at >97%.

3.3.2 Strontium

The DGA resin can separate the Ca fraction from many elements, but it is unable to isolate Ca from Sr. This step requires a second column protocol. Sr-specific resin packed columns were used to process the Ca fraction after the BioRad column protocol was complete. Molded columns were made from shrinkable Teflon to achieve a ~0.18ml resin bed that was packed with ~200µl of Eichrom Sr-specific resin with a 100-150µm mesh sized beads. The protocol laid out in Valdes et al. (2014) was the foundation for the method used in this study, with adaptations from Torres et al. (2000) and Jakopič et al. (2005). The protocol was test-calibrated for calcite, marl calcite and shell aragonite using both 3M and 4M HNO₃ (Fietzke and Eisenhauer, 2006; Simon et al., 2009). Column yields were greater using 3M HNO₃, and hence use of this acid was adopted. Table 3.4 summarizes the steps taken to remove Sr from each Ca fraction.

Table 3.4: Protocol used to separate the Ca fraction from Sr using a Sr-specific resin after purification using Eichrom DGA resin, adapted from Valdes et al. (2014).

Acid/Liquid	Volume (ml)	What is Eluted
3 M HNO ₃	5	Cleaning resin + column
3 M HNO ₃	5	Conditioning
Load Sample 3M HNO ₃	1	Load sample equivalent 200µg Ca from DGA
3 M HNO ₃	5	Ca
0.01 M HNO ₃	5	Sr

Store resin packed column in 20% HNO₃ for 3 column passes, then discard.

3.3.3 Calcium Column Blanks

Blanks are used to measure the amount of Ca added to a sample from external sources during its purification and isolation. Controlling the Ca blanks during column protocols is important to obtain reliable isotopic data (Wieser et al., 2004). Most Ca blanks are introduced during column procedures and loading protocols and originate from the environment, supplies, or the technician (Holmden, 2009). Blanks during column chromatography procedures commonly range from ~80 – 130ng, but may be as low as 30ng in some instances (Holmden, 2009; Martin et al., 2015). Generally, if the blank is <1% of the sample there is no need to apply blank corrections to sample isotope compositions.

To monitor Ca blanks during column procedures, one column was set aside for processing the Ca blank for each set of samples (8) processed (Figure 3.3). This column is loaded with acid alone, allowing for the environmental conditions at that time to be tracked and monitored. Through all column protocols completed in this study, the Ca blank measured was 79ng. This represents 0.04 – 0.15% of the total Ca loaded into a column if 50 - 200µg of Ca is processed. The average blank across all column protocols performed was $33 \pm 18\text{ng}$ (1SD). Thus blank corrections to sample Ca-isotope compositions were unnecessary.

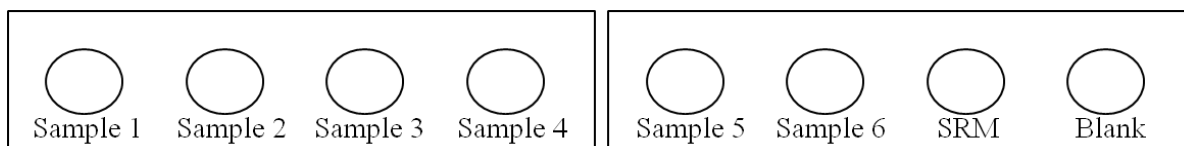


Figure 3.3: Bird's eye view of the Ca chromatographic column protocol, with each batch of samples accompanied by SRM 915b and a blank sample to ensure the consistency between sample batches.

A SRM 915b carbonate standard, equivalent to 200µg of Ca, was also processed together with each batch of 8 samples to check column yields and accuracy of Ca-isotope compositions measured for the samples (Figure 3.3), and to test for changes in Ca-isotope composition relative to unprocessed SRM 915b.

3.4 Analytical Procedures

3.4.1 ICPMS

Samples were analyzed for major and some trace element abundances and concentrations using the ThermoFisher iCap Q ICPMS located in the GEOMETRIC Lab at the University of Western Ontario. The purified marl calcite and shell aragonite samples, as described earlier, were diluted 100-10,000 times in 2% HNO₃ depending on the anticipated concentrations. A suite of standards for the specific series of elements desired were created to form a six-point calibration curve against which all marl and shell samples were measured to quantify their elemental compositions. The elements incorporated into this suite of standards followed previous studies of trace elements in marine calcium carbonates (Rosenthal and Katz, 1989; Vander Putten et al., 2000; Ravera et al., 2003; Carré et al., 2006) and included Na, Mg, K, Ca, Cr, Mn, Fe, Zn, Sr, and Ba. The standards were prepared at varying concentrations in 2% HNO₃ by volumetric dilution in a filtered cabinet (Table 3.5).

A challenge faced was that most samples, especially marl, lost mass after they were initially weighed because of OM removal. Measured abundances for these samples are therefore not reliable. To mitigate this problem elemental concentrations were normalized to the amount of Ca expected in CaCO₃ (~40% of the initial mass dissolved), and a focus was placed on interpreting changes in element ratios rather than absolute elemental abundances.

Compared to the marl calcite and shell aragonite samples, the bedrock samples offered a more complex matrix that required element quantification using multi-element ICPMS standard QCS-26 at various concentrations. QCS-26 is a high purity standard containing 26 elements (Al, Sb, As, Ba, Be, C, Ca, Cr, Cu, Fe, Pb, Mg, Mn, Mo, Ni, K, Se, Si, Ag, Na, Tl, Ti, V and Zn) dissolved in 5% HNO₃ + Trace HF, with all elements at a concentration of 100µg/ml (QCS-26-R ICP 26 Element Quality Control Standard, High Purity Standards) . Ca and Sr in this standard however, occur in the same concentration, and Ca counts are affected by double charged Sr production during ionization. In order to accurately quantify Ca, therefore, a separate session in which a pure Ca standard was used is also performed.

Table 3.5: Elemental standards for ICPMS analysis of carbonates.

Element	Element Concentration (ppb)					
	S1	S2	S3	S4	S5	S6
Na	10	5	2.5	0.5	0.25	0.05
Mg	2000	1000	500	100	50	10
K	10	5	2.5	0.5	0.25	0.05
Ca	20000	10000	5000	1000	500	100
Cr	1	0.5	0.25	0.05	0.025	0.005
Mn	200	100	50	10	5	1
Fe	1000	500	250	50	25	5
Zn	200	100	50	10	5	1
Sr	200	100	50	10	5	1
Ba	500	250	125	25	12.5	2.5

A pure Ca ICPMS standard prepared at a variety of concentrations in 2% HNO₃, was used to test that column yields were sufficient and that the solutions subsequently analyzed using the MC-ICPMS at Trent University were within 10% of the SRM 915b standard solution concentration (Sime et al., 2005; Morgan et al., 2011; Tacail et al., 2014). As described above, Sr produces a strong interference during measurement of Ca. For minor Sr concentrations, application of a Sr interference correction factor to the ICPMS data commonly resulted in over correction, leading to higher than actual Ca concentrations. This became apparent for the marl calcite, where samples typically contained 30,000-40,000ppm Ca, and ~200ppm Sr. As a result, Sr interference corrections were not applied to the data reported in this thesis.

3.4.2 Ca-Isotope Measurements

A Thermo Neptune Multi- Collector ICPMS (MC-ICPMS) located at the Trent University Water Quality Center was used to conduct high precision isotopic analyses of the purified Ca samples. A sample-standard bracketing technique was used with the processed SRM 915b employed as the bracketing standard. This allows for correction of instrument drift during individual analyses. Each sample was measured at least 3-4 times (Fantle and Tipper, 2014). The equation used to calculate the $\delta^{44/42}\text{Ca}$ value is:

$$\delta^{44/42}\text{Ca} = \frac{((^{44}\text{Ca}/^{42}\text{Ca})_{\text{sample}})}{(((^{44}\text{Ca}/^{42}\text{Ca})_{\text{standard1}} * (^{44}\text{Ca}/^{42}\text{Ca})_{\text{standard2}})/2)} \times 10^3 \quad (13)$$

The sample solutions were prepared at 4ppm Ca in 2% HNO₃, with solution concentrations verified by ICPMS. Samples were introduced to the MC-ICPMS as a wet aerosol from the Apex Q desolvating nebulizer with the intent of increasing the sensitivity. A 4ppm Ca ICPMS standard solution was used to tune and calibrate the MC-ICPMS prior to sample analysis. In order to assess the stability and reproducibility of the MC-ICPMS, the Ca ICPMS standard solution was analyzed against itself to ensure that the average $\delta^{44/42}\text{Ca}$ was 0‰ with 2 standard deviations also close to 0. Each sample was bracketed with a SRM 915b standard solution, also at 4ppm, with extra care taken to ensure the sample concentration was within 10% of the standard solution (Sime et al., 2005; Morgan et al., 2011; Tacail et al., 2014). The sample uptake time was 100s, with a wash out time of 2 minutes over a 25 cycle block of analyses, with ~5-6ml of sample solution consumed for a full sample run. Voltages from 2 - 8V were obtained for ⁴⁴Ca and 2 – 4V for ⁴²Ca, with ~1.3-1.4V on ⁴⁴Ca and ~0.35-0.4V on ⁴²Ca being the lowest limits in obtaining reliable results. Sr double charge interference on Ca was monitored using a mass of 43.5 (⁸⁷Sr m/z = 43.5u) on one of the Faraday cups to test whether a double charge correction to the Ca-isotope measurements was required (Tipper et al., 2006). The cup configuration used during all analyses was L4 – ⁴²Ca, L2 – ⁴³Ca, L1 – ⁴⁴Ca, H1 – ⁴⁶Ca, H2 – ⁴⁷Ti, and H3 – ⁴⁸Ca, with the subsequent isotopic ratios calculated from L4|L1, L2|L1 and H3|L1.

When voltages dropped below acceptable limits or the stability began to deteriorate, this commonly signalled a need to clean the cones, replace some sample introduction tubing and/or to wash the nebulizer. The high solution concentrations required to record sufficient voltages commonly caused a build up of Ca on the cones, or within the nebulizer. Cones were cleaned using an abrasive powder and then rinsed with Milli-Q water before being re-inserted into the MC-ICPMS. In several instances the MC-ICPMS required almost 24 hours to regain an acceptable level of performance and stability, likely because the cones needed to build up a sufficient layer of the Ca used for conditioning. Conditioning consisted of sample-standard bracketing a Sr-resin purified 4ppm solution of SRM 915b with itself until the MC-ICPMS re-established optimal performance conditions for sample analysis.

Replicate analyses of SRM 915b processed through the full column protocol gave $\delta^{44/42}\text{Ca} = -0.002 \pm 0.08\text{‰}$ (2SD; n=11). To compare sample results obtained in this study with $\delta^{44/42}\text{Ca}$

values reported relative to the now-exhausted SRM 915a, +0.35‰ can be added to each value, as described earlier.

3.4.3 Sr Isotope Measurements

Solutions at 50ppb (40ppb in 1ml if the amount of Sr available was not sufficient) dissolved in 1.5ml of 2% HNO₃ were analyzed using the Nu Instrument Plasma II MC-ICPMS at Trent University. The samples were introduced using a desolvating nebulizer much as for Ca isotope analyses and were bracketed using the National Bureau of Standards (NBS) 987 Sr standard (Tipper et al., 2006). During the analyses it was determined that no correction was required based on the measured composition of SRM 987 Sr $^{87}\text{Sr}/^{86}\text{Sr} = 0.710246 \pm 14$ (2SD; n=17), which compares well with its certified value of $^{87}\text{Sr}/^{86}\text{Sr} = 0.710248$. In addition, results obtained in the present study for basalt standard USGS BCR-2 ($^{87}\text{Sr}/^{86}\text{Sr} = 0.705025 \pm 0.000003$) are in agreement. SRM 987 normalized values reported by Weis et al. (2006), vary from 0.705005 to 0.705024, with an average of $^{87}\text{Sr}/^{86}\text{Sr} = 0.705013 \pm 0.000010$, as measured using thermo-ionization mass spectrometry (TIMS).

Chapter 4

4 RESULTS

This chapter details the elemental compositions and ratios and Ca- and Sr-isotope results for marl calcite and aragonite shells, as well as groundwater and bedrock samples, obtained at the University of Western Ontario and the Trent University Water Quality Center.

4.1 Elemental Concentrations

4.1.1 Marl

As reported in Chapter 3, Kulak (2005) determined from loss-on ignition (LOI), on average, each marl calcite sample contained ~80 wt% CaCO₃ (range 73 wt% to 97 wt%). The elemental concentrations obtained in the present study are consistent with the LOI measurements (see *Appendix B, Table B4*). On average ~15% of the initial mass (the mass of marl calcite prior to any applied purification protocols) was lost during preparation for Ca-isotope analysis, mostly through removal of organic matter, silt and sand, although this amount varied substantially along the core (~2.7 wt% to ~29 wt%, calculated using the amount of Ca expected minus what was actually measured using ICPMS).

A full list of the normalized element concentrations are listed in Appendix B, Table B6. The measured Ca concentration of each sample ranged between ~26 and ~45%, excluding one anomalous measurement of ~51%. These values assume no change in mass occurred during purification, and result in an average measured Ca concentration of 34.7% (347,000ppm) (see *Appendix B, Table B4*). It is unknown why values exceeding 40% Ca were recorded. After normalization and assuming no mass change during purification, minor and trace element concentrations (Mg, Fe, Mn, Ba, Sr, Cr, Zn) account for ~8400 to ~26,000ppm, or 0.8 to 2.7% of the initial sample (see *Appendix B, Table B5*). Cr and Zn account for ~11 to ~646ppm, and are minor in comparison to Mg, Fe, Mn, Ba and Sr (Figure 4.1a to d). Mg accounts for ~0.6 to 1.2% and Fe accounts for ~0.05 to ~1.3% (Figure 4.1a and b). A sharp rise (by ~0.5%) in the Fe concentration occurs from the base of the marl calcite to its peak, followed by a decrease of ~1% moving further up the core (Figure 4.1b); Mn exhibits a similar pattern, albeit at lower concentrations moving up the core, however, not of the same magnitude (Figure 4.1c). Na and K were present in amounts too low to quantify.

Figure 4.1a to d illustrates the depth-dependent variation in Ca-normalized concentrations in marl calcite of each minor or trace element of interest (ppm). The amount of Ca measured in each sample was normalized to the amount of Ca expected (~40% of the mass of CaCO₃, assuming a pure CaCO₃ sample). Figure 4.2 focuses on the depth-related relationships among Ba, Mg and Fe in the marl, with Mg and Fe normalized concentrations shown divided by a factor of 10 for graphing purposes. Mg and Fe contents are highest in the lowermost 50cm of the marl; Mg and Fe also covary in relative abundance throughout the section. Mn follows a similar trend to both Mg and Fe, with an observable peak in the lowermost ~50cm of the marl; however the normalized concentrations measured are ~1.5x lower by comparison. In contrast, Ba concentrations are lowest near the base of the marl section and increase gradually upwards to ~300cm, above which they fluctuate about a more or less constant concentration; any covariance with Fe and Mg concentrations is inconsistent. Excluding the lowermost ~50cm of the marl, the curves of Mn and Ba covary, with an average difference of ~400ppm between a high in Mn concentration and the associated low in Ba concentration.

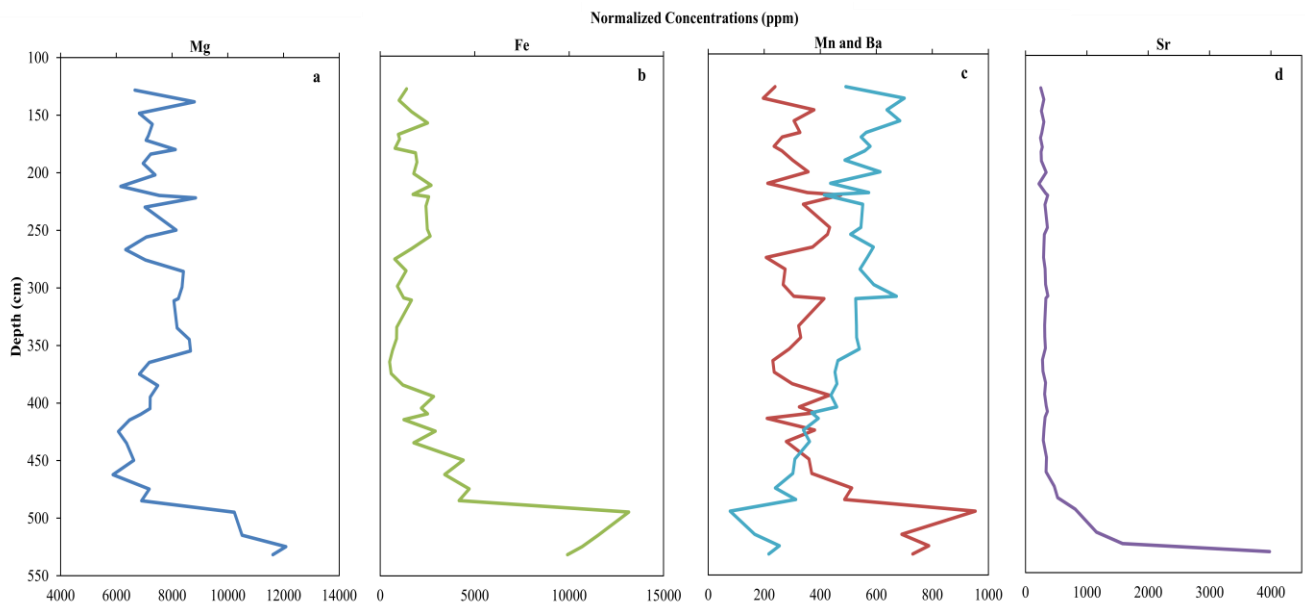


Figure 4.1: Depth versus Ca-normalized concentrations (ppm) of St Agatha marl; with (a) Mg (dark blue), (b) Fe (green), (c) Mn (red) and Ba (light blue), and (d) Sr (purple).

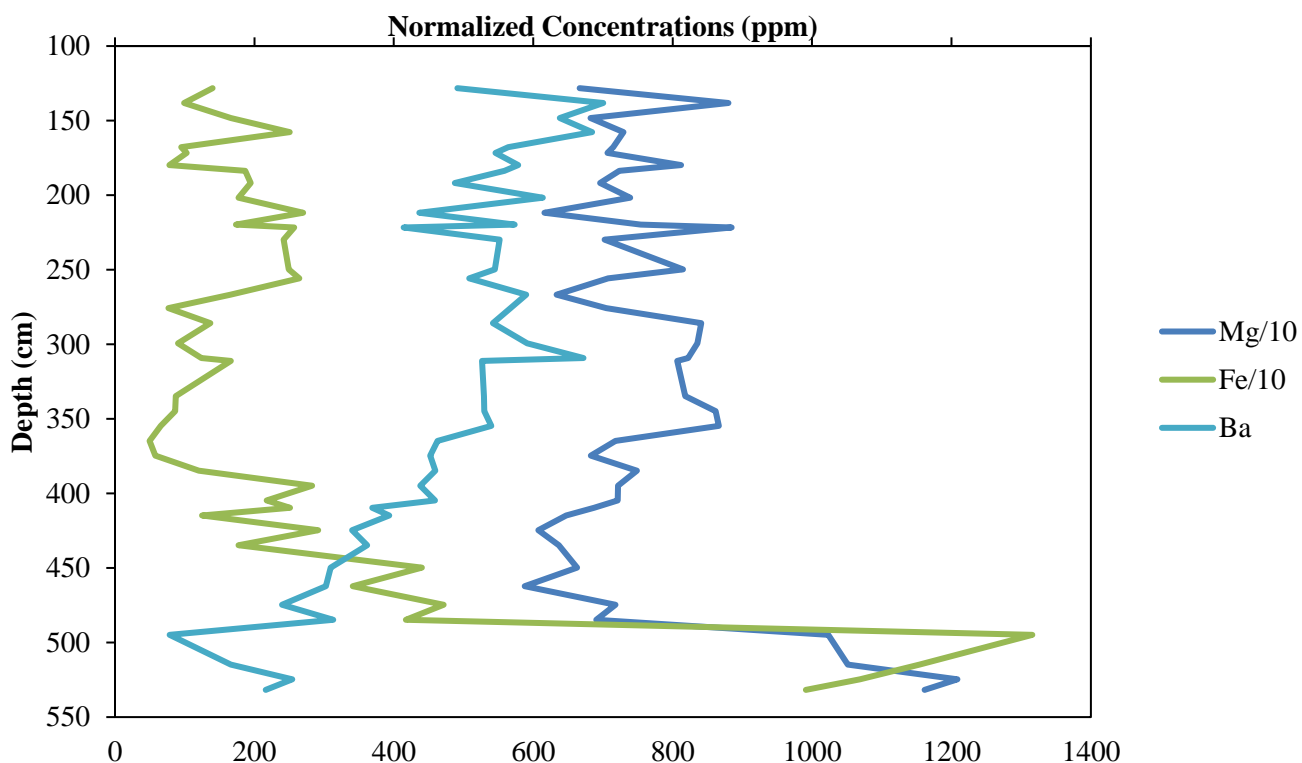


Figure 4.2: Depth versus Ca-normalized concentrations of barium (Ba), magnesium (Mg) and iron (Fe) in marl calcite. Fe and Ba concentrations have been divided by a factor of 10.

A list of the elemental ratios illustrated in Figure 4.3 can be found in Appendix B, Table B6. Like the Fe and Mg normalized contents, the Mg/Ca and Fe/Ca ratios also show a sharp increase to >0.03 in the bottom 50cm of the core, with the upper portions having much lower values (Mg/Ca, ~ 0.015 to ~ 0.030 ; Fe/Ca ~ 0.002 to ~ 0.033) (Figure 4.3). Ba/Ca ratios vary between ~ 0.0002 and ~ 0.002 , and gradually increase upcore.

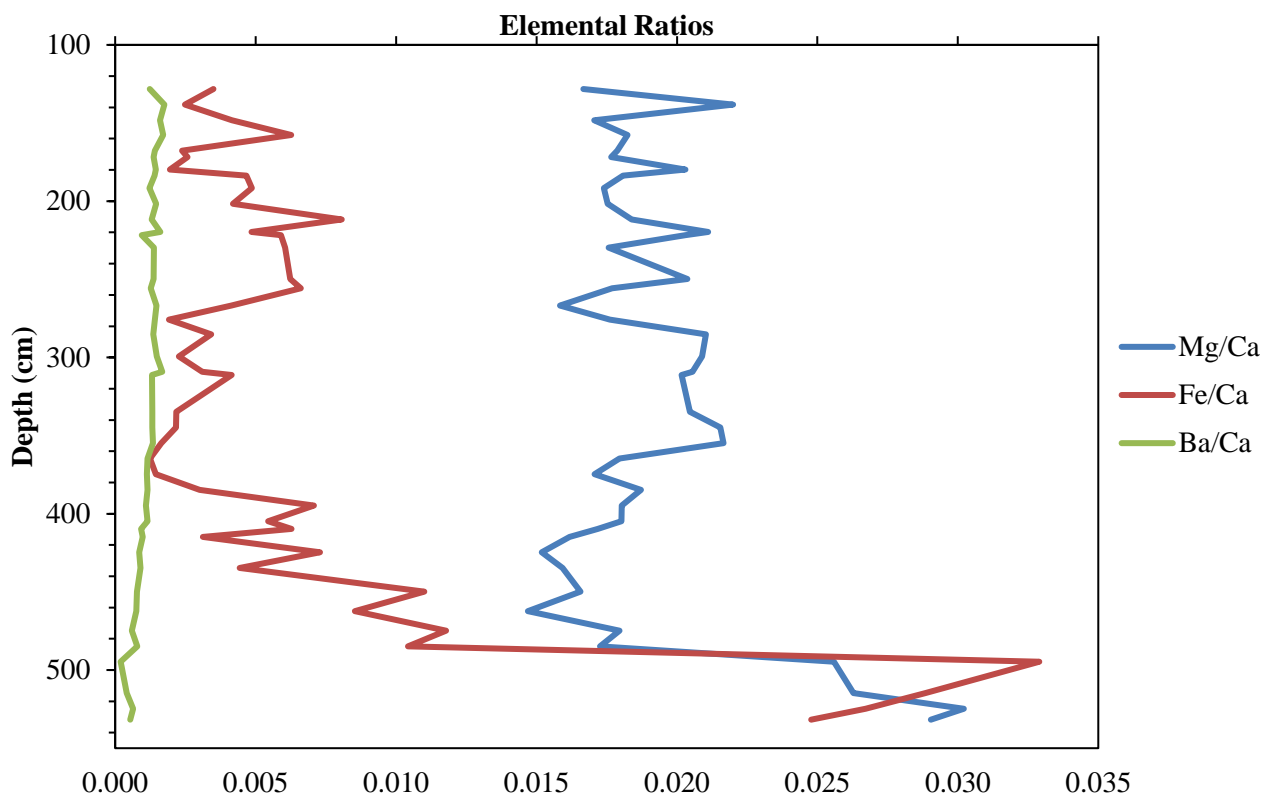


Figure 4.3: Depth versus Mg/Ca, Fe/Ca and Ba/Ca ratios.

4.1.2 Aragonite Shells

The shells analyzed in this study are predominantly *G. parvus*, a freshwater bivalve, composed of aragonite. Below a depth of ~300cm the abundance of *G. parvus* shells was greatly diminished, and only 4 samples could be analyzed. Unlike the other samples, these 4 shells were not from exactly the same interval as analyzed marl samples but were situated nearby (within 2cm). The elemental results are illustrated in Figure 4.4 and listed in Appendix B, Table B7.

As for the marl samples, there is an apparent loss of Ca in the aragonite shells (see Appendix B, Table B8). Each shell, however, was carefully cleaned and was therefore devoid of OM, silt, sand and clay (see 3.2.2 Shell Sample Preparation for information on the cleaning procedure used). Hence, the process used to purify each carbonate sample likely resulted in this loss. The expected amount of Ca in each of the aragonite shells was ~40% (~400,000ppm) of the initial mass dissolved, which ranged from ~0.00007g to ~0.0012g. The measured Ca contents of the *G. parvus* shells ranged from ~250,000ppm to ~650,000ppm, with an anomalous Ca concentration of ~1,020,000ppm in shell V1, which may reflect contamination, a weighing error or other unknown

analytical artefacts. Several elements had concentrations below the background detection limit of the ICPMS, including Na, K, Cr and Fe. Leaching of Na, and K during dissolution of aragonite may have contributed to the low concentrations (Rosenthal and Katz, 1989).

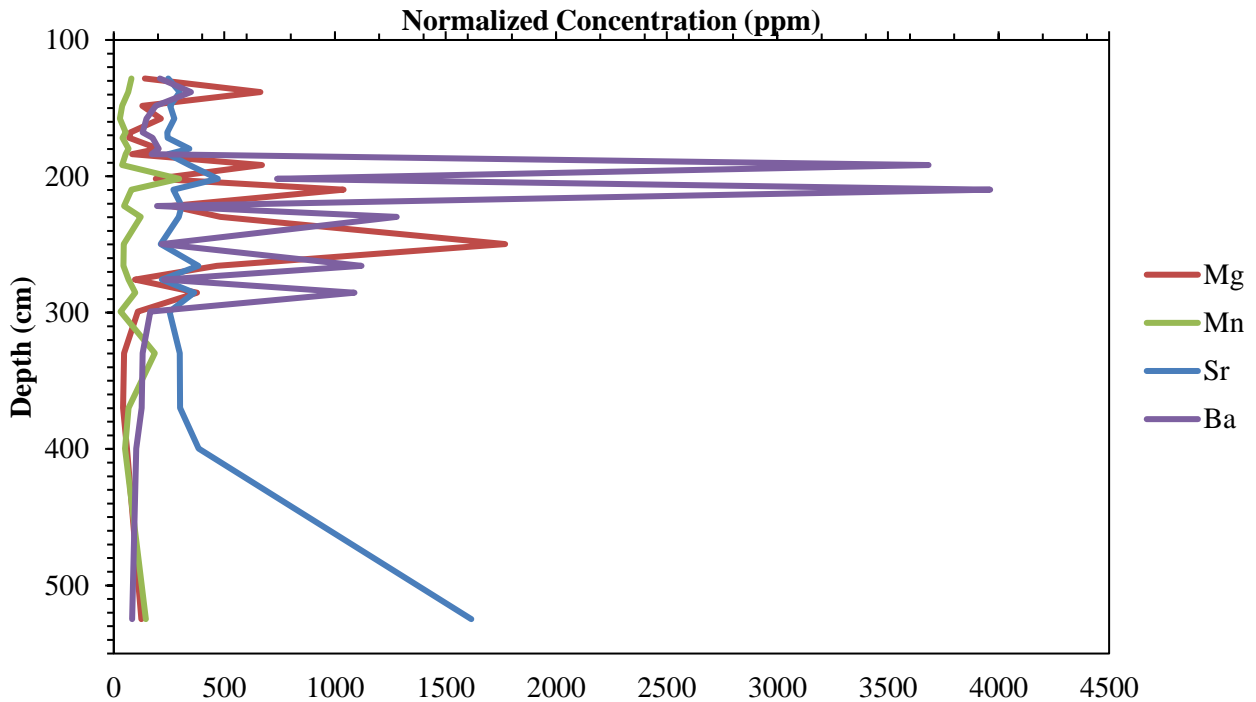


Figure 4.4: Depth versus normalized minor and trace element concentrations (ppm) for *G. parvus*.

As was the case for the marl, the concentrations of the minor and trace elements measured for the *G. parvus* shells were normalized to the expected Ca concentration (~40% of the original mass dissolved). Mg and Ba have the greatest concentration in the shells above ~300cm ranging from ~69 to ~1700ppm, and ~102 to ~3900ppm, respectively. Ba has the greatest range as well as the highest concentration (shell R9; see *Appendix B, Table B7*). These two elements display the greatest variability between 191.5 and 299.5cm, an almost 1m section in the middle of the core, where they covary with depth. Within this ~1m section, Mn also appears to covary with Mg and Ba. The Sr concentrations remain the most consistent along the core with values ranging from ~212 to ~470ppm, and an anomalous value of ~1600ppm occurring at the very base of the core. No other minor or trace element experiences a similar spike in concentration at this depth. Below ~300cm the minor and trace element concentrations decrease substantially.

Figure 4.5a compares the normalized Mg concentrations in marl calcite and shell aragonite for *G. parvus* across the core. Above ~300cm there is greater sample resolution, with the marl calcite and aragonite shell displaying a negative linear relationship ($r^2=0.38$) in the ~1m section that was noted earlier (Figure 4.5b).

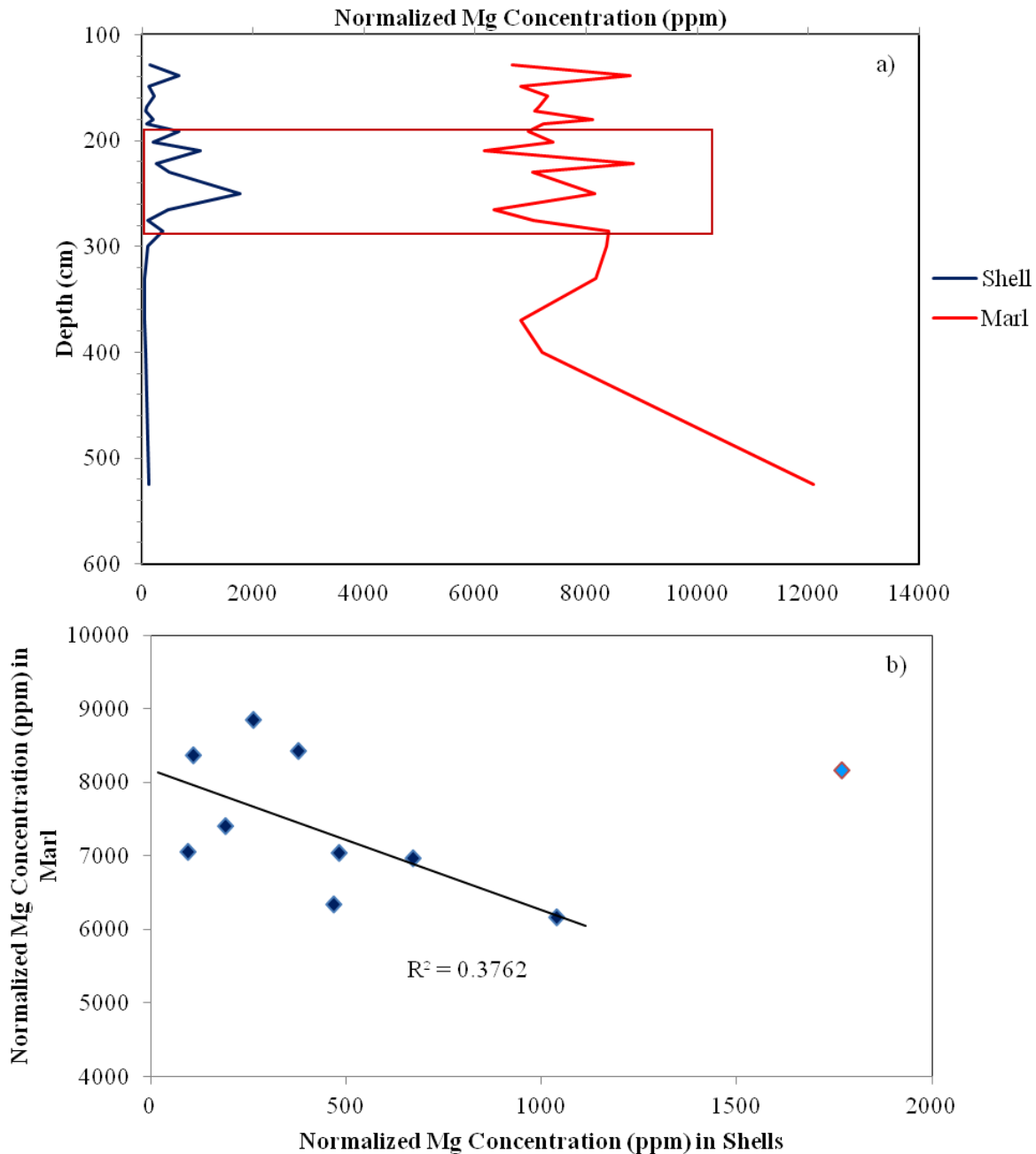


Figure 4.5: (a) Depth versus normalized Mg concentration of marl calcite and shell aragonite *G. parvus*. The ~1m section of covariance is highlighted in the red box, (b) Normalized Mg concentration of marl calcite versus shell aragonite *G. parvus* for depths 191.5-299.5cm.

Figure 4.5b plots the normalized Mg concentrations between depths 191.5 to 299.5cm of marl calcite versus shell aragonite. Shell V1, established above to an anomalous Ca concentration, is shown in light blue. For this ~1m section, marl calcite normalized Mg concentrations are clustered between ~6100 and ~8800ppm, while shell aragonite normalized Mg concentrations range from ~95 and ~1000ppm. Excluding shell V1, from 191.5 to 299.5cm the data shows a negative linear relationship, whereby a high Mg concentration in shell aragonite is associated with a low Mg concentration in marl calcite (Figure 4.5b). Outside of this ~1m section, there is no covariation between marl calcite and shell aragonite normalized Mg concentrations (Figure 4.6). Approximately 80% of normalized aragonite shell Mg concentrations are <~500ppm, and excluding the anomalously high marl calcite value at ~12,000ppm (see *Appendix B, Table B5*), all the values are in the range noted above.

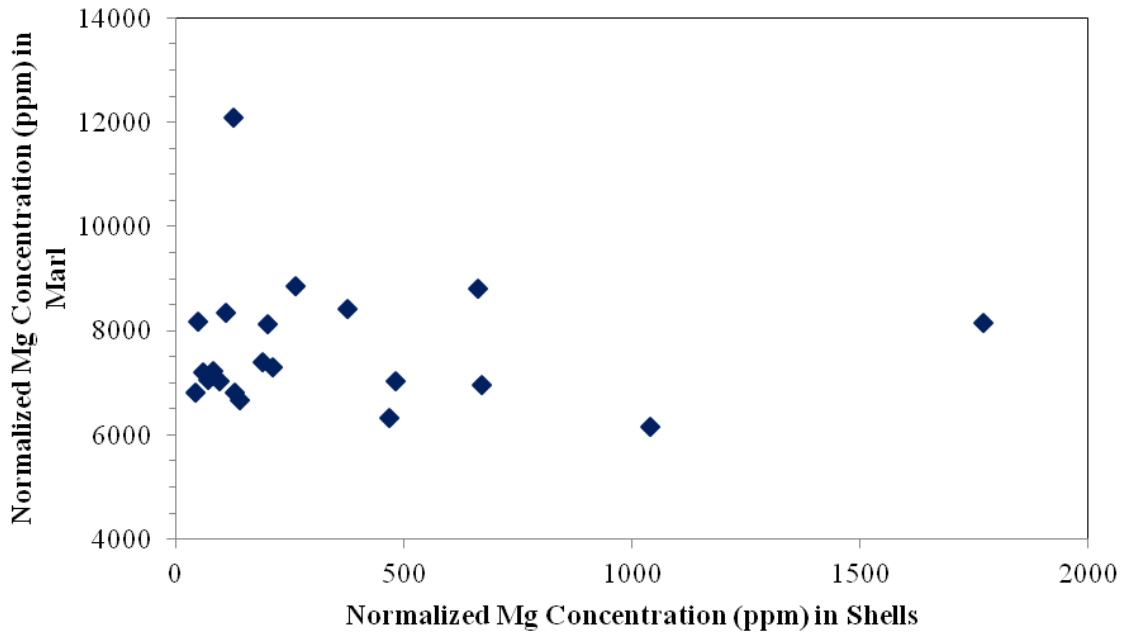


Figure 4.6: Normalized Mg concentrations of shell aragonite (*G. parvus*) versus marl calcite for all depths.

At two depths it was possible to analyze at least one shell of *G. parvus*, *V. tricarinata* and *Pisidium sp* (see *Appendix B, Table B3* and *Table B7*) to test for chemical and isotopic differences in different species within a common lake. Those results are summarized in Table 4.1. This comparison highlights not only the variability between species but also between shells. This variability is most pronounced for Mg and Ba. Mg concentrations for *V. tricarinata* range from ~61 to ~475ppm, for *G. parvus* from ~83 to ~278ppm and *Pisidium sp.* from ~176 to 2314ppm, while Ba concentrations for *V. tricarinata* range from ~302 to ~2247ppm, for *G.*

parvus from ~589 to ~4819ppm and *Pisidium sp.* ~33 to ~47ppm. Ba shows the greatest relative intra-species variability as well as spatial variability along the core, with *Pisidium sp.* having considerably lower concentrations compared to both *V. tricarinata* and *G. parvus*. Mg, Mn, Zn and Sr contents are comparable between the same species of shell at each depth. The Mg concentration of *Pisidium sp.*, however, is markedly different between each depth, with a ~2200ppm difference between the two values. The Mn concentrations are the lowest measured, ranging from ~6 to ~36ppm and show the smallest intra-species and spatial variability, with the *Pisidium sp.* at 219.5 – 220cm being anomalously low relative to other measured values. The Zn content of *V. tricarinata* and *G. parvus*, however, varies greatly between depths, with concentrations ranging from ~58 to 126ppm and ~67 to ~528ppm respectively. Zn contents, however, were below the detection limits for *Pisidium sp.* The Sr contents of each shell are consistent at ~200ppm, with *G. parvus* shells sampled at 309.5- 310.0cm ranging from ~470 to ~711ppm. These values are anomalously high compared with the other *G. parvus* shells measured in this study, which range from ~200 to ~300ppm (see Appendix B, Table B7 to compare with other *G. parvus* shells).

Table 4.1: Elemental data for *G. parvus*, *V. tricarinata* and *Pisidium sp.* for two depths.

Depth (cm)	Shell Species	Concentration (ppm)				
		Mg	Mn	Zn	Sr	Ba
219.5 - 220.0	<i>V. tricarinata</i>	126	26	91	264	302
	<i>V. tricarinata</i>	475	24	126	224	2247
	<i>G. parvus</i>	83	20	161	172	589
	<i>G. parvus</i>	264	13	67	267	622
	<i>Pisidium Sp.</i>	176	6	/	259	33
309.0 - 309.5	<i>V. tricarinata</i>	61	17	58	287	413
	<i>V. tricarinata</i>	172	21	105	289	621
	<i>G. parvus</i>	186	16	376	470	1732
	<i>G. parvus</i>	278	36	528	711	4819
	<i>Pisidium Sp.</i>	2314	25	/	286	47

4.1.3 Groundwater

The elemental concentrations for the two groundwater samples are summarized in Table 4.2, along with the average values reported by the Provincial Groundwater Monitoring Network (PGMN) Well Chemistry Reports. The values for site W36, located to the northeast of the Saint

Agatha deposits, fall within the reported range of previous years, but those for site W427, located to the southwest of the Saint Agatha deposits are higher (see *Appendix B, Table B7a and b*).

Table 4.2: Elemental concentrations of groundwater site W36 and W427.

Sample Site	Concentration (ppm)								
	Na	Mg	K	Ca	Mn	Fe	Zn	Sr	Ba
W36	5	73	1	471	0.1	2.3	0	9.2	0
Average (2002-2015)	22	72	2	437	0.1	2.3	0	9.4	0
W427	5	69	1	343	0.1	1.5	0	9.3	0
Average (2005-2015)	20	62	2	278	0.1	1.4	0	8.7	0

4.1.4 Bedrock

Table 4.3 summarizes the elemental abundance of the leachate and filtered products collected during the protocol outlined in Table 3.2, and discussed in section 3.2.4 (Bedrock Sample Purification and Treatment). Only seven of the ten original bedrock samples collected were analyzed for elemental concentrations and isotope ratios, due to complex sample matrices and difficulties in completing the necessary purification protocols. The leachate and filtered products yielded low Ca-concentrations and abundant minor and trace elements, when compared with the silicate fraction (Table 4.4).

Overall, Ca-concentrations range ~2.3 to 15.5ppm, and Mg concentrations range ~122 to 788ppm; however, the concentration of elements measured in the filtered fraction was lower than that of the leachate fraction in steps 8 to 10. Steps 3 to 7 had Ca concentrations ranging from ~2.3 to ~5.7ppm, Mg concentrations ranging from ~122 to ~272ppm, and Fe concentrations from ~2.1 to ~15.5ppm, with Na and K ranging from ~0.3 to ~8ppm. The values of Ti, Zn and Ba were just above the background detection limit of the ICPMS. Steps 8 to 10 has Ca concentrations ranging from ~6 to ~15.5ppm, Mg concentrations ranging from ~300 to ~788ppm, and Fe concentrations from ~9.7 to ~75ppm, with Na and K ranging from ~0.1 to ~13ppm.

Table 4.3 illustrates that the leachate fraction (steps 8 to 10) has higher concentrations across all elements measured, most notably Ca and Mg, compared with the filtered fraction (Steps 3 to 7).

Table 4.3: The abundance of various elements in the filtered (steps 3 to 7) and leachate (steps 8 to 10) fractions from the carbonate bedrock samples.

Sample Name	Concentration (ppm)										
	Na	Mg	Al	K	Ca	Ti	Mn	Fe	Zn	Sr	Ba
Steps 3 to 7											
CS1_1119	0.7	125	1.8	1.7	5.7	0.4	0.2	2.2	0.0	0.8	0.0
CS2_1119	1.3	263	0.6	0.9	5.1	0.4	0.4	2.1	0.0	0.3	0.0
CS3_1119	0.5	268	0.8	0.6	5.3	0.4	0.3	2.5	0.0	0.1	0.0
CS1_1120	1.0	266	0.5	0.4	5.5	0.4	0.3	2.2	0.0	0.5	0.02
CS2_1120	0.6	156	0.5	0.4	3.2	0.2	0.2	5.0	0.0	0.2	0.0
CS3_1120	0.8	122	7.3	8.0	2.3	0.2	0.8	15.5	0.01	0.2	0.02
CS5_1120	1.0	272	0.7	0.3	5.2	0.4	0.2	2.3	0.0	2.0	0.0
Steps 8 to 10											
CS1_1119	1.2	704	1.3	1.4	13.0	1.0	0.6	16.5	0.0	0.6	0.1
CS2_1119	0.7	639	0.3	0.4	11.2	0.9	1.0	10.0	0.0	0.5	0.0
CS3_1119	0.7	788	0.9	0.7	15.5	1.3	0.7	18.0	0.0	0.4	0.0
CS1_1120	0.5	737	0.1	0.2	13.0	1.1	0.8	9.7	0.0	0.4	0.6
CS2_1120	0.5	576	0.2	0.3	10.7	0.8	0.7	11.0	0.0	0.3	0.0
CS3_1120	0.9	300	13	8.9	6.0	0.7	1.7	75	0.04	0.5	0.1
CS5_1120	1.8	693	0.4	0.4	13.5	1.0	0.4	15.5	0.0	22.4	0.1

Table 4.4 summarizes the element abundances of the silicate mineral component found within the carbonate bedrock. Due to a misunderstanding of the protocol employed, it was thought that this fraction was the carbonate fraction; upon later inspection, however, it was realized that this was the silicate fraction. While, the goal in developing and using this protocol was to identify and isolate the carbonate fraction from the sulphate and silicate fractions, the Ca-isotope and Sr-isotope ratios were collected for the silicate fraction only.

Ca concentrations range ~81 to ~900ppm and Mg concentrations range ~93 to ~380ppm, with both having the highest concentrations measured. The highest concentrations of Mn, Ba, and Sr, are ~2.1, ~4.2 and ~36ppm, respectively. Na and K range from ~0.6 to ~8.3ppm and ~5 to ~450ppm.

Table 4.4: The abundance of various elements in the carbonate bedrock arising from the silicate mineral content.

Sample Name	Concentration (ppm)												
	Na	Mg	Al	K	Ca	Ti	Cr	Mn	Fe	Zn	Sr	Ba	Pb
CS1_1119	2.1	94	125	105	129	8	0.1	0.4	60	0.1	0.1	0.8	0.1
CS2_1119	0.8	325	18	15	658	1.1	0.0	0.4	15	0	0.2	0.1	0.02
CS3_1119	0.8	263	28	22	560	1.8	0.0	0.3	13	0.3	0.1	0.1	0.02
CS1_1120	0.7	382	7.5	5.6	678	0.9	0.0	0.3	8.1	0.4	0.2	0.4	0.0
CS2_1120	0.6	397	11	8.4	757	1	0.0	0.4	11	0.4	0.2	0.1	0.0
CS3_1120	8.3	196	662	450	81	3	0.6	2.1	267	1.1	0.4	4.2	0.03
CS5_1120	1.2	363	4.2	2.2	919	0.2	0.0	0.2	3.1	0.6	36	0.2	0.0

4.2 Calcium-Isotope Ratios

4.2.1 SRM 915b

As described earlier, NIST SRM 915b, a pure carbonate standard, was processed through the Ca and Sr chromatographic column protocols to check for yields and the accuracy of the Ca-isotope compositions. The Ca-isotope composition of the processed SRM 915b was sample-standard bracketed by SRM 915b. The average $\delta^{44/42}\text{Ca}$ of SRM 915b is $-0.02 \pm 0.07\%$ (2SD, n=13), which shows that the protocol used to purify samples of matrix elements that interfere with accurate data collection is acceptable. The goal was to obtain a result as close to 0‰ with 2SD <0.1‰.

Table 4.5: Ca-isotope composition of each SRM 915b purified through the full column chromatography protocol.

Batch #	$\delta^{44/42}\text{Ca}$ (‰)	2SD	2SE*
1	0.06	0.07	0.05
2	-0.01	0.07	0.04
3	0.07	0.08	0.04
4	-0.06	0.05	0.04
5	0.03	0.08	0.05
6	-0.05	0.13	0.08
7	-0.05	0.07	0.04
8	-0.03	0.05	0.03
9	-0.01	0.09	0.05
10	0.04	0.05	0.03
11	-0.07	0.05	0.03
12	-0.09	0.07	0.04
15	-0.05	0.05	0.03
Average	-0.02	0.07	0.05

$$*2SE = \frac{(2SD)}{\sqrt{n}}$$

Table 4.6 lists results for an unprocessed SRM 915b **not** passed through the Sr-resin protocol, bracketed against SRM 915b that had been processed through the Sr-resin protocol. As described earlier, Sr interferes with accurate measurement of Ca-isotope compositions, and it was necessary to test if the small amount of Sr found in a ~4ppm Ca solution of unprocessed SRM 915b made a significant difference in the isotopic results. Table 4.6 shows that even a small amount of Sr in the sample analyzed has a large effect on the Ca-isotope values measured, thus demonstrating the need to purify SRM 915b using the Sr-resin protocol.

Table 4.6: Ca-isotope value of unprocessed SRM 915b sample-standard bracketed against purified SRM 915b.

	$\delta^{44/42}\text{Ca}$ (‰)	2SD	2SE*
Unprocessed	+1.05	0.33	0.17
Processed (average)	-0.02	0.07	0.05

$$*2SE = \frac{(2SD)}{\sqrt{n}}$$

4.2.2 Marl

The marl Ca-isotope data are listed in Table 4.7 and illustrated in Figure 4.7. The results generally represent ~10cm intervals, with some samples reflecting an interval of ~5cm and others ~15cm. Samples were drawn from a homogenized ~0.5cm thickness of marl. The presence of coeval shell samples dictated the location at which marl was sampled, except below ~320.0cm when the abundance of *G. parvus* decreased, as described earlier. The highest $\delta^{44/42}\text{Ca}$ value obtained was $-0.11 \pm 0.06\text{‰}$ (2SD, n=3), and the lowest value $-0.61 \pm 0.10\text{‰}$ (2SD, n=3), thus defining a range of ~0.5‰. The average $\delta^{44/42}\text{Ca}$ of the marl calcite measured was -0.33‰ (n=40) with an average error on the $\delta^{44/42}\text{Ca}$ values of 0.08‰.

Results for two samples have a 2SD higher than the desired 0.10‰ but overall the values obtained have 2SD <0.10‰ and 2SE <0.05‰. All but four values measured for marl fall within the range of the average Ca-isotope value ($\delta^{44/42}\text{Ca} = -0.33\text{‰}$, and average error 0.08‰).

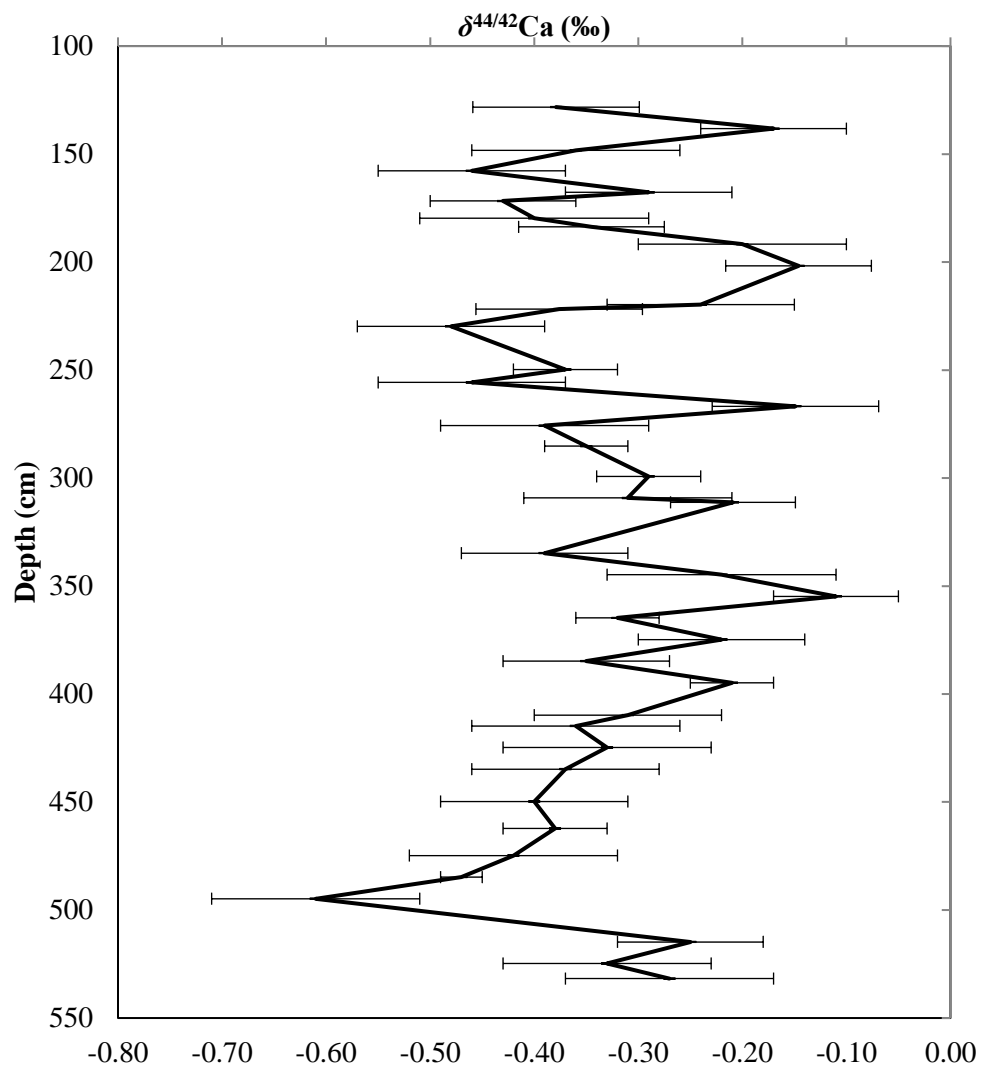


Figure 4.7: Depth versus $\delta^{44/42}\text{Ca}$ (‰) obtained for marl calcite.

Table 4.7: Marl calcite $\delta^{44/42}\text{Ca}$ (‰) with 2SD and 2SE* relative to SRM 915b, all measured at ~4ppm.

Depth (cm)	$\delta^{44/42}\text{Ca}$ (‰)	2SD	2SE*	n
128.0 – 128.5	-0.38	0.08	0.04	4
138.0 – 138.5	-0.17	0.07	0.04	3
148.0 – 148.5	-0.36	0.10	0.05	4
157.5 – 158.0	-0.46	0.09	0.05	3
167.5 – 168.0	-0.29	0.08	0.04	4
171.5 – 172.0	-0.43	0.07	0.04	4
179.5 – 180.0	-0.40	0.11	0.06	3
183.5 – 184.0	-0.35	0.07	0.04	3
191.5 – 192.0	-0.20	0.10	0.06	3
201.5 – 202.0	-0.15	0.07	0.04	3
219.5 – 220.0	-0.24	0.09	0.05	3
221.5 – 222.0	-0.38	0.08	0.04	4
229.5 – 230.0	-0.48	0.09	0.05	4
249.5 – 250.0	-0.37	0.05	0.03	4
255.5 – 256.0	-0.46	0.09	0.05	4
266.5 – 267.0	-0.15	0.08	0.04	4
275.5 – 276.0	-0.39	0.10	0.05	4
285.5 – 286.0	-0.35	0.04	0.02	3
299.0 – 299.5	-0.29	0.05	0.03	4
309.0 – 309.5	-0.31	0.10	0.05	4
311.0 – 311.5	-0.21	0.06	0.03	4
334.5 – 335.0	-0.39	0.08	0.05	3
344.5 – 345.0	-0.22	0.11	0.08	2
354.5 – 355.0	-0.11	0.06	0.03	3
364.5 – 365.0	-0.32	0.04	0.02	4
374.5 – 375.0	-0.22	0.08	0.06	2
384.5 – 385.0	-0.35	0.08	0.05	3
394.5 – 395.0	-0.21	0.04	0.02	4
409.5 – 410.0	-0.31	0.09	0.06	2
414.5 – 415.0	-0.36	0.10	0.06	3
424.5 – 425.0	-0.33	0.10	0.05	4
434.5 – 435.0	-0.37	0.09	0.05	3
449.5 – 445.0	-0.40	0.09	0.05	4
462.0 – 462.5	-0.38	0.05	0.03	4
474.5 – 475.0	-0.42	0.10	0.06	3
484.5 – 485.0	-0.47	0.02	0.01	4
494.5 – 495.0	-0.61	0.10	0.06	3
514.5 – 515.0	-0.25	0.07	0.04	4
524.5 – 525.0	-0.33	0.10	0.05	4
531.5 – 532.0	-0.27	0.10	0.06	3

$$*2SE = \frac{(2SD)}{\sqrt{n}}$$

4.2.3 Aragonite Shells

The shell aragonite Ca-isotope data are listed in Table 4.8 and illustrated in Figure 4.8. The highest $\delta^{44/42}\text{Ca}$ measured was $-0.25 \pm 0.06\text{‰}$ (n=4, 2SD) and the lowest value $-0.56 \pm 0.05\text{‰}$ (n=3, 2SD), a range of $\sim 0.3\text{‰}$.

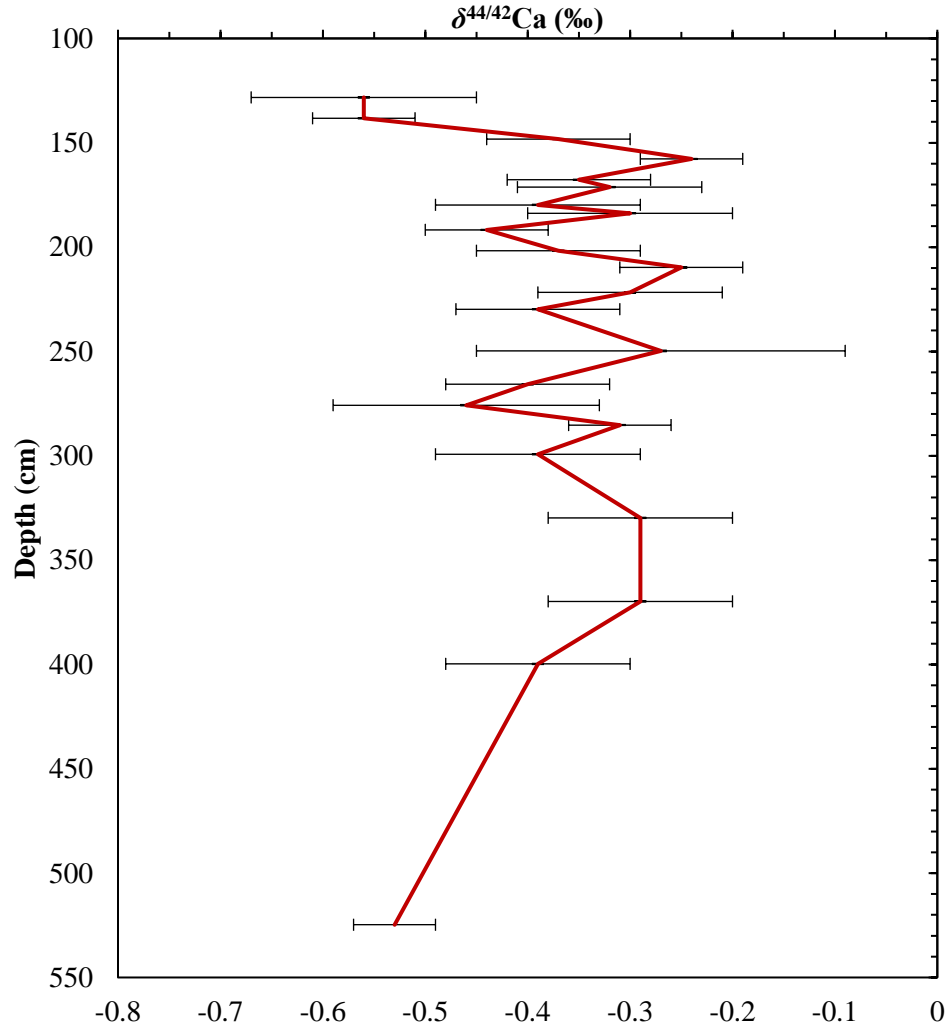


Figure 4.8: Depth versus $\delta^{44/42}\text{Ca}$ (‰) of aragonite shell samples (*G. parvus*).

Table 4.8: Shell aragonite $\delta^{44/42}\text{Ca}$ (‰) with 2SD and 2SE* relative to SRM 915b, all measured at ~4ppm.

Depth (cm)	$\delta^{44/42}\text{Ca}$ (‰)	2SD	2SE*	n
128.0 – 128.5	-0.56	0.11	0.08	2
138.0 – 138.5	-0.56	0.05	0.03	3
148.0 – 148.5	-0.37	0.07	0.04	3
157.5 – 158.0	-0.24	0.05	0.03	4
167.5 – 168.0	-0.35	0.07	0.04	4
171.5 – 172.0	-0.32	0.09	0.05	4
179.5 – 180.0	-0.39	0.10	0.05	4
183.5 – 184.0	-0.30	0.10	0.06	3
191.5 – 192.0	-0.44	0.06	0.03	4
201.5 – 202.0	-0.37	0.08	0.04	4
209.5 – 210.0	-0.25	0.06	0.03	4
221.5 – 222.0	-0.30	0.09	0.05	4
229.5 – 230.0	-0.39	0.08	0.04	4
249.5 – 250.0	-0.27	0.18	0.10	3
265.5 – 266.0	-0.40	0.08	0.04	4
275.5 – 276.0	-0.46	0.13	0.08	3
285.0 – 285.5	-0.31	0.05	0.03	4
299.0 – 299.5	-0.39	0.10	0.06	3
329.5 – 330.0	-0.29	0.09	0.05	3
369.5 – 370.0	-0.29	0.09	0.05	3
399.5 – 400.0	-0.39	0.09	0.05	3
524.5 – 525.0	-0.53	0.04	0.02	4

$$*2SE = \frac{(2SD)}{\sqrt{n}}$$

A comparison of Ca-isotope values for coexisting *G. parvus*, *V. tricarinata*, and *Pisidium sp.* shells at depths of 219.5 – 220.0cm and 309.0 – 309.5cm, respectively, is provided in Table 4.9 along with the coeval marl calcite for each depth.

Table 4.9: Ca-isotope results at two depths for coexisting *V. tricarinata*, *G. parvus*, and *Pisidium sp.* aragonite shells and coeval marl calcite.

Depth (cm)		$\delta^{44/42}\text{Ca}$ (‰)	2SD	2SE*	Shell Species	$\delta^{44/42}\text{Ca}$ (‰)	2SD	2SE*
219.5 - 220.0	Marl	-0.24	0.09	0.05				
219.5 - 220.0					<i>V. tricarinata</i>	-0.17	0.04	0.02
219.5 - 220.0					<i>V. tricarinata</i>	-0.21	0.09	0.05
219.5 - 220.0					<i>G. parvus</i>	-0.21	0.07	0.02
219.5 - 220.0					<i>G. parvus</i>	-0.08	0.03	0.02
219.5 - 220.0					<i>Pisidium sp.</i>	-0.40	0.07	0.04
309.0 - 309.5	Marl	-0.31	0.10	0.05				
309.0 - 309.5					<i>V. tricarinata</i>	-0.30	0.04	0.02
309.0 - 309.5					<i>V. tricarinata</i>	-0.26	0.08	0.04
309.0 - 309.5					<i>G. parvus</i>	-0.12	0.02	0.01
309.0 - 309.5					<i>G. parvus</i>	+0.03	0.05	0.03
309.0 - 309.5					<i>Pisidium sp.</i>	-0.46	0.02	0.01

$$*2SE = \frac{(2SD)}{\sqrt{n}}$$

The freshwater clams (*Pisidium sp.*) have more negative $\delta^{44/42}\text{Ca}$ values than the freshwater snails. At a given depth, greater variability exists in the $\delta^{44/42}\text{Ca}$ values among *G. parvus* shells than *V. tricarinata*.

4.2.4 Comparison of Marl Calcite and Aragonite Shells

Figure 4.9 illustrates the depth verses $\delta^{44/42}\text{Ca}$ values of marl calcite (black) and the shell aragonite (*G. parvus*; red). There is no obvious correlation between the data sets, however, the shell aragonite, in general has lower $\delta^{44/42}\text{Ca}$ values than the marl calcite. The literature notes a systematic offset of $\sim 0.3\%$ in the $\delta^{44/42}\text{Ca}$ of calcite and aragonite, with aragonite generally having lower values (Gussone et al., 2005). The difference between $\delta^{44/42}\text{Ca}$ of calcite and aragonite averages 0.05% , with $\sim 40\%$ of aragonite shell $\delta^{44/42}\text{Ca}$ values being higher than the $\delta^{44/42}\text{Ca}$ of marl calcite. The lowest aragonite shell $\delta^{44/42}\text{Ca}$ is -0.61% and the lowest marl $\delta^{44/42}\text{Ca}$ is -0.61% , while the highest aragonite shell $\delta^{44/42}\text{Ca}$ is -0.56% and the highest marl $\delta^{44/42}\text{Ca}$ is -0.24% . There is greater variability in the $\delta^{44/42}\text{Ca}$ values of marl calcite than of the aragonite shells, with the average marl calcite value being $\sim 0.03\%$ higher than the aragonite shells average value.

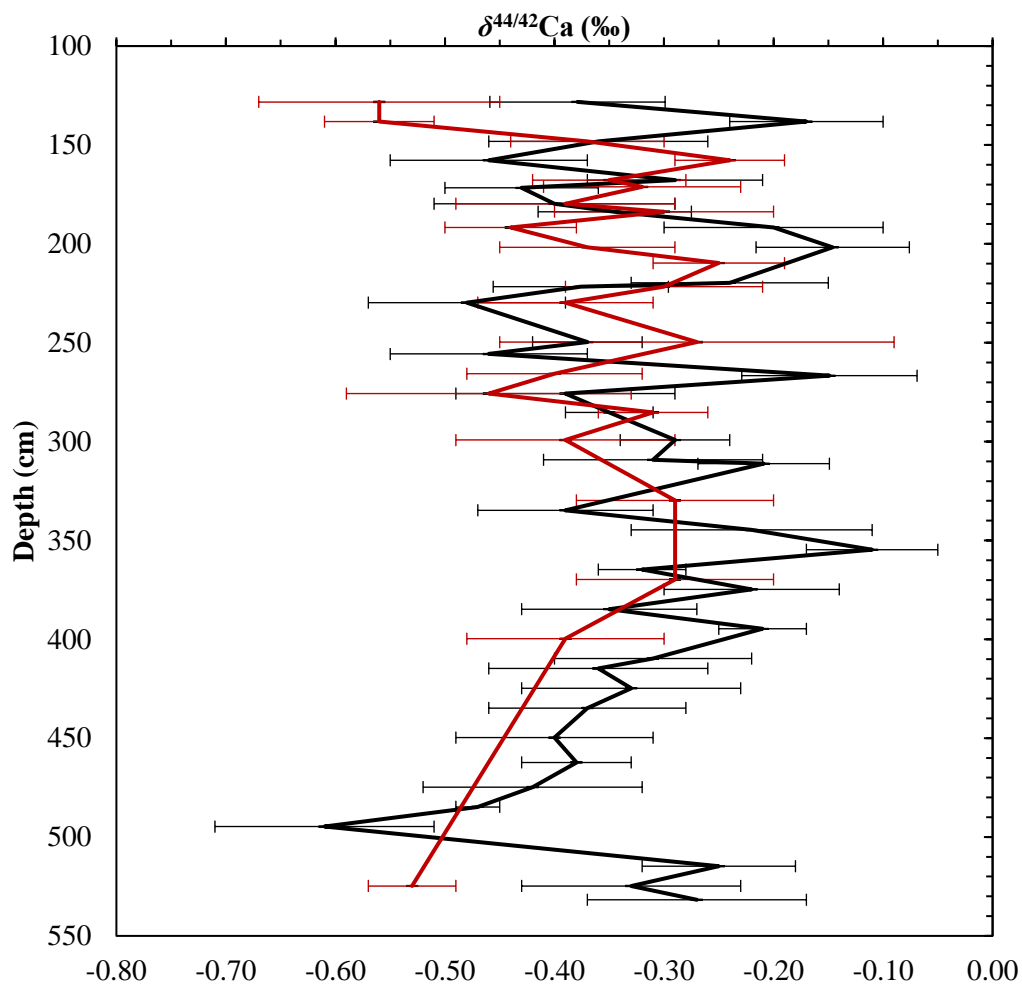


Figure 4.9: Depth versus $\delta^{44/42}\text{Ca}$ (‰) for marl calcite (black) and aragonite shells (*G. parvus*) (red).

4.2.5 Groundwater

The average $\delta^{44/42}\text{Ca}$ value of groundwater sample W36 is $+0.94 \pm 0.11\text{‰}$, and W427 is $+1.15 \pm 0.08\text{‰}$ (Table 4.10), comprising an average for the overburden groundwater flowing in the area $\sim 1\text{‰}$.

Table 4.10: Ca-isotope values for groundwater.

Well Site Label	$\delta^{44/42}\text{Ca}$ (‰)	2SD	2SE*
W36	+0.95	0.14	0.08
	+0.92	0.07	0.04
W427	+1.11	0.12	0.07
	+1.19	0.03	0.02

$$*2SE = \frac{(2SD)}{\sqrt{n}}$$

This value is higher on average by ~1.7‰ than those obtained for marl calcite and aragonite shells and is higher than most values published in the literature for the Ca-isotope compositions of carbonate bedrock (Figure 2.5) (Fantle and Tipper, 2014).

4.2.6 Silicate Fraction from the Carbonate Bedrock Samples

The Ca-isotope results arising from the silicate fraction of the carbonate bedrock samples are listed in Table 4.11. The pXRD patterns show that of the ten original samples, two contained only gypsum (CS5_1119 and CS4_1120), and three contained dolostone and gypsum together (CS3_1119, CS4_1119, CS5_1120) (see *Appendix B, Figures B1-B10*). Seven, rather than ten, samples were analyzed as a consequence of complications with the methodology (see 2.4 *Bedrock Sample Purification and Treatment* for more information). The seven samples analyzed were primarily dolostone, but contained minor quartz and mica, along with orthoclase and fluorite. The $\delta^{44/42}\text{Ca}$ of the silicate fraction of the Salina E formation ranges from +0.06 to +0.30‰, while the Salina C ranges from -0.24 to +0.22‰ and the Salina A2 carbonate has a value of +0.72‰.

Table 4.11: $\delta^{44/42}\text{Ca}$ (‰) of the silicate fraction from the carbonate bedrock samples.

Sample Name	Formation	$\delta^{44/42}\text{Ca}$ (‰)	2SD	2SE*
CS1_1119	Salina E	+0.06	0.04	0.02
CS2_1119	Salina E	+0.30	0.04	0.02
CS3_1119	Salina C	+0.22	0.07	0.04
CS1_1120	Salina E	+0.17	0.07	0.04
CS2_1120	Salina E	+0.11	0.06	0.03
CS3_1120	Salina C	-0.24	0.04	0.02
CS5_1120	Salina A2	+0.72	0.06	0.03

$$*2SE = \frac{(2SD)}{\sqrt{n}}$$

4.3 Strontium Isotope Ratios

Samples of marl, groundwater, bedrock, and NIST SRM 915b purified for Ca-isotope measurements contained sufficient Sr to determine their $^{87}\text{Sr}/^{86}\text{Sr}$ ratio.

4.3.1 SRM 915b Sr-Isotope Ratios

The $^{87}\text{Sr}/^{86}\text{Sr}$ ratios obtained for SRM 915b during this study are listed in Appendix A, Table A2. As described earlier, SRM 915b was not only processed through the full chromatographic protocol as a check on each individual batch, but also was passed through the Sr-resin protocol in

order to be used as the bracketing standard, given that each gram (g) of SRM 915b contains 150µg of Sr. An internationally accepted Sr-isotope ratio for SRM 915b is not yet available. The average $^{87}\text{Sr}/^{86}\text{Sr}$ ratio of 14 column protocols is 0.707994 ± 0.000051 (2SD), and is consistent between samples (see *Appendix A, Table A2*). This confirms that the Sr-resin protocol is an acceptable method for removing Sr from carbonate samples, and that the methodology provides consistent precise results from sample to sample.

4.3.2 Marl Sr-Isotope Ratios

The Sr-isotope compositions of the marl calcite are listed in Table 4.12 and illustrated in Figure 4.10. The lowest $^{87}\text{Sr}/^{86}\text{Sr}$ ratio, 0.708547 ± 0.000002 (2SD) occurs at 531.5 – 532.0cm, and corresponds to a Sr concentration of ~2825ppm, whereas the highest ratio, 0.709636 ± 0.000002 (2SD), was measured for a sample from 409.5 – 410.0cm. The average $^{87}\text{Sr}/^{86}\text{Sr}$ ratio over the analyzed marl section is 0.709333 ± 0.000003 (2SD; n=40). As illustrated in Figure 4.10, the lowest $^{87}\text{Sr}/^{86}\text{Sr}$ ratio occurs at the base of the marl section, reaching a maximum at 409.5 – 410.0cm, before generally but variably declining upwards in the marl section. The deeper marl calcite samples (between ~450.0 and 532.0cm), have lower $^{87}\text{Sr}/^{86}\text{Sr}$ ratios and higher Sr concentrations, while samples with higher $^{87}\text{Sr}/^{86}\text{Sr}$ ratios trended towards lower Sr concentrations.

Table 4.12: Sr-isotope compositions of marl calcite.

Core	Depth (cm)	$^{87}\text{Sr}/^{86}\text{Sr}$	2SD	2SE*
1B	128.0 – 128.5	0.709243	0.000002	0.000007
1B	138.0 – 138.5	0.709265	0.000002	0.000007
1B	148.0 – 148.5	0.709308	0.000003	0.000009
1C	157.5 – 158.0	0.709316	0.000003	0.000009
1C	171.5 – 172.0	0.709456	0.000002	0.000007
1C	179.5 – 180.0	0.709487	0.000002	0.000005
1C	183.5 – 184.0	0.709342	0.000002	0.000006
1C	191.5 – 192.0	0.709281	0.000064	0.000005
1C	201.5 – 202.0	0.709308	0.000002	0.000006
1D	211.5 – 212.0	0.709336	0.000068	0.000005
1D	219.5 – 220.0	0.709251	0.000002	0.000006
1C	221.5 – 222.0	0.709305	0.000002	0.000007
1C	229.5 – 230.0	0.709292	0.000052	0.000004
1D	249.5 – 250.0	0.709291	0.000002	0.000005
1D	255.5 – 256.0	0.709319	0.000058	0.000004
1D	266.5 – 267.0	0.709321	0.000002	0.000007
1E	275.5 – 276.0	0.709352	0.000002	0.000007
1D	285.5 – 286.0	0.709301	0.000064	0.000005
1D	299.0 – 299.5	0.709348	0.000002	0.000008
1D	309.0 – 309.5	0.709315	0.000058	0.000004
1E	311.0 – 311.5	0.709311	0.000002	0.000005
1E	334.5 – 335.0	0.709384	0.000060	0.000004
B7	344.5 – 345.0	0.709288	0.000002	0.000008
B7	354.5 – 355.0	0.709441	0.000052	0.000004
B7	364.5 – 365.0	0.709429	0.000002	0.000006
B7	374.5 – 375.0	0.709494	0.000076	0.000005
B7	384.5 – 385.0	0.709506	0.000002	0.000006
B8	394.5 – 395.0	0.709566	0.000070	0.000005
B8	409.5 – 410.0	0.709636	0.000002	0.000006
B8	414.5 – 415.0	0.709573	0.000058	0.000004
B8	424.5 – 425.0	0.709506	0.000001	0.000004
B8	434.5 – 435.0	0.709569	0.000060	0.000004
B9	449.5 – 445.0	0.709242	0.000002	0.000005
B9	462.0 – 462.5	0.709412	0.000050	0.000004
B9	474.5 – 475.0	0.709446	0.000052	0.000004
B10	484.5 – 485.0	0.709339	0.000058	0.000004
B10	494.5 – 495.0	0.709499	0.000070	0.000005
B10	514.5 – 515.0	0.708919	0.000118	0.000008
B10	524.5 – 525.0	0.708790	0.000002	0.000007
B10	531.5 – 532.0	0.708547	0.000074	0.000005

$$*2SE = \frac{(2SD)}{\sqrt{n}}$$

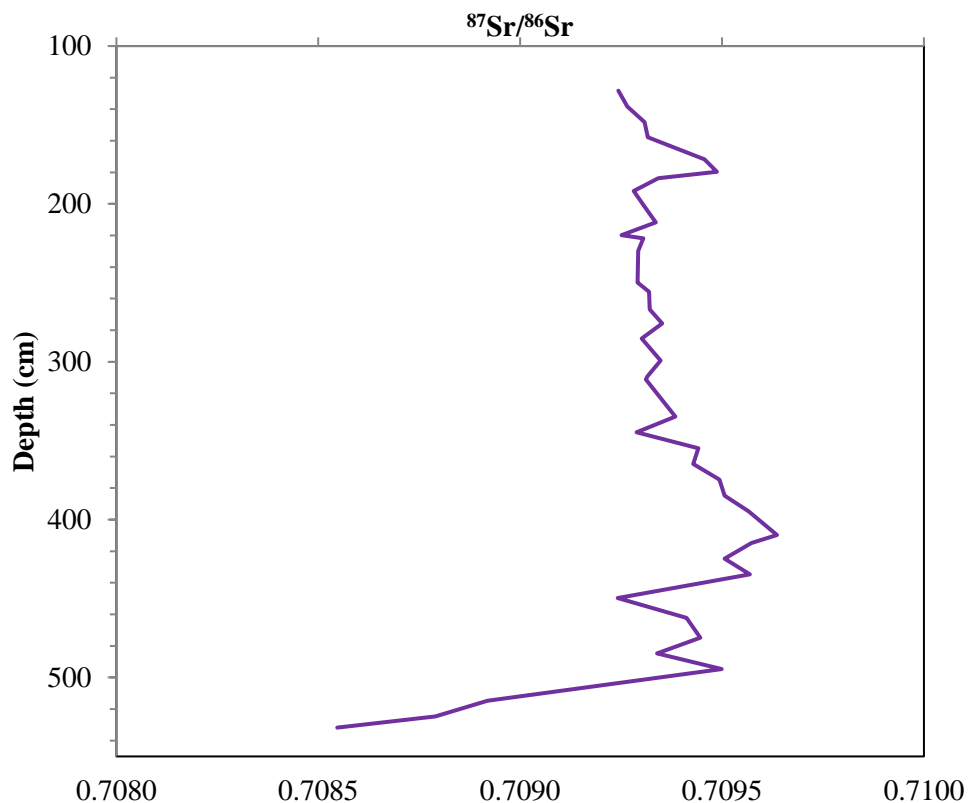


Figure 4.10: Depth versus marl calcite $^{87}\text{Sr}/^{86}\text{Sr}$.

4.3.3 Groundwater Sr-Isotope Ratios

The $^{87}\text{Sr}/^{86}\text{Sr}$ ratios of the two groundwater samples are listed in Table 4.13. These Sr-isotope ratios are lower than measured for the marl calcite, albeit close to the ratios obtained at the very base of the marl section (Figure 4.10).

Table 4.13: $^{87}\text{Sr}/^{86}\text{Sr}$ ratios of water from overburden wells W36 and W427.

Site	$^{87}\text{Sr}/^{86}\text{Sr}$	2SD	2SE*
W36	0.708337	0.000089	0.000013
W427	0.708437	0.000065	0.000009

$$*2SE = \frac{(2SD)}{\sqrt{n}}$$

4.3.4 Sr-Isotope Ratios of the Silicate Fraction from the Carbonate Bedrock Samples

The $^{87}\text{Sr}/^{86}\text{Sr}$ ratios of the silicate fraction from the carbonate bedrock samples are listed in Table 4.14. Most of the ratios are extremely high, typical of origin from Precambrian felsic basement rocks (see *Appendix A*).

Table 4.14: $^{87}\text{Sr}/^{86}\text{Sr}$ ratios of bedrock samples.

Sample Name	Formation	$^{87}\text{Sr}/^{86}\text{Sr}$	2SD	2SE*
CS1_1119	Salina E	0.744121	0.000067	0.000009
CS2_1119	Salina E	0.711601	0.000073	0.000010
CS3_1119	Salina C	0.714919	0.000084	0.000012
CS1_1120	Salina E	0.709997	0.000088	0.000012
CS2_1120	Salina E	0.710188	0.000095	0.000013
CS3_1120	Salina C	0.768947	0.000108	0.000015
CS5_1120	Salina A2	0.708529	0.000120	0.000017

$$*2SE = \frac{(2SD)}{\sqrt{n}}$$

Chapter 5

5 DISCUSSION

The following chapter discusses the results for the isotope systems (Ca, Sr) analyzed in this study, in order to determine the dominant controls on the Ca-isotope variability measured for freshwater marl calcite and aragonite shells from the St. Agatha deposit. To assist with this discussion, oxygen- (O)- and carbon (C)-isotope data previously collected for the marl samples by Walker and Longstaffe (personal communication, 2017) are also summarized and described here. These additional data provide a larger context for interpreting the elemental and Ca- and Sr-isotope data collected in the present study. In particular, the O- and C-isotope data are used in conjunction with Ca- and Sr-isotope ratios to explore water source and isotopic composition through the use of isotope paleothermometers and to evaluate the environmental history of the St. Agatha kettle lake system. The carbonate $\delta^{18}\text{O}$ and $\delta^{13}\text{C}$ data were measured by J.Walker (personal communication, 2017) as part of his ongoing PhD dissertation research.

5.1 Lake Water Composition

5.1.1 Paleothermometers

The O-isotope calcite-water and aragonite-water systems have been extensively investigated in the past. The O-isotope geothermometer developed by Kim and O'Neil (1997), in particular, provides a means to investigate paleotemperature and paleo-lake water $\delta^{18}\text{O}$ using natural proxies, which in this study are marl calcite and shell aragonite deposited during much of the lifetime of the former St. Agatha kettle lake:

$$1000\ln\alpha (\text{calcite-H}_2\text{O}) = 18.03(10^3\text{T}^{-1}) - 32.24; \text{T in Kelvin (K)} \quad (14)$$

(Kim and O'Neil, 1997)

The challenge with such geothermometers is that they require temperature to be known if water $\delta^{18}\text{O}$ is to be calculated and *vice versa*. For biologically mediated marl calcite precipitation, the optimal growth temperature of algae ranges between 16 and 27°C (Lavens and Sorgeloos, 1996), with temperatures below 16°C slowing growth rates and warmer temperatures becoming toxic for algal communities (Sorokin and Krauss, 1962; Lavens and Sorgeloos, 1996; Cassidy, 2011).

Liu (2016) conducted a study of a modern, till-hosted, southern Ontario lake crystallizing marl calcite. An average temperature of 21°C was determined using the $\delta^{18}\text{O}_{\text{calcite}}$ and the $\delta^{18}\text{O}_{\text{water}}$ of marl calcite deposited within the last 2 to 4 years at the time of the study. While the conditions within this modern lake may not be mirrored exactly in the St. Agatha kettle lake system, this result provides a reasonable first estimate for the summer temperatures that trigger marl calcite precipitation. Assuming a similar crystallization temperature for the St. Agatha kettle lake, it is possible to calculate the $\delta^{18}\text{O}_{\text{water}}$ using equation 14.

Using equation 13 and the assumed crystallization temperature of 21°C, the average $\delta^{18}\text{O}_{\text{water}}$ is calculated to be $-9.2 \pm 0.7\text{‰}$ (VSMOW; 1SD) for the St. Agatha kettle lake system. Leng and Marshall (2004) noted that for lakes with short residence times and a limited catchment area, such as was likely the case for St. Agatha, marl calcite crystallization occurs when surface water temperatures are approximately the same each year. This is the current working assumption for the St. Agatha kettle lake deposits.

Using an average temperature of 21°C and the calcite Ca-isotope geothermometer proposed by Gussone et al. (2005), the Ca-isotope composition of the water in the St. Agatha lake system during marl precipitation can also be calculated (see 2.4.3 *Ca-isotope Mineral-Water Geothermometers*). The calculated average $\delta^{44/42}\text{Ca}_{\text{water}}$ is calculated to be $+0.51 \pm 0.21\text{‰}$ (2SD) with possible values ranging from +0.34 to +0.89. This $\sim 0.55\text{‰}$ range could suggest some variability in lake water sources. These values are lower than the average value of the two groundwater samples, $\delta^{44/42}\text{Ca} \approx +1.04 \pm 0.09\text{‰}$ (2SD). These geothermometers, however, presume that Ca-isotope equilibrium was established between the precipitating phase and water, whereas Jacobson and Holmden (2008), Holmden (2009), Steefel et al. (2014) and Oelkers et al. (2019) posit that there is no Ca-isotope fractionation between water and authigenic carbonates when sufficient time has been allowed for equilibrium to be established.

The water in the St. Agatha lake system was the main supplier of Ca to the kettle lake and hence its marl. There is no known Ca-isotope fractionation effect from the weathering or dissolution of carbonate materials (Moore et al., 2013). Therefore, assuming equilibrium, source waters more enriched in ^{44}Ca require interaction with solids that have a higher $\delta^{44/42}\text{Ca}$ value. The $\delta^{44/42}\text{Ca}$ of water found in the subsurface reflects water-rock interactions with local bedrock formations

(Frape et al., 1984). Values for carbonate bedrock $\delta^{44/42}\text{Ca}$ from around the St. Agatha marl are currently not available. Paleozoic dolomites and limestones from the Williston Basin, Saskatchewan, measured by Holmden (2009), however, have $\delta^{44/42}\text{Ca}$ of $\sim +0.14$ to $+0.40\text{‰}$; water-rock interactions with such carbonate bedrock would impart similar Ca-isotope compositions to groundwater.

Figure 5.1 compares the range in St. Agatha lakewater $\delta^{44/42}\text{Ca}$ calculated using the geothermometer of Gussone et al. (2005), with the measured $\delta^{44/42}\text{Ca}$ of groundwater samples near St. Agatha (W36 and W427) and the $\delta^{44/42}\text{Ca}_{\text{water}}$ of measured *G. parvus* shells.

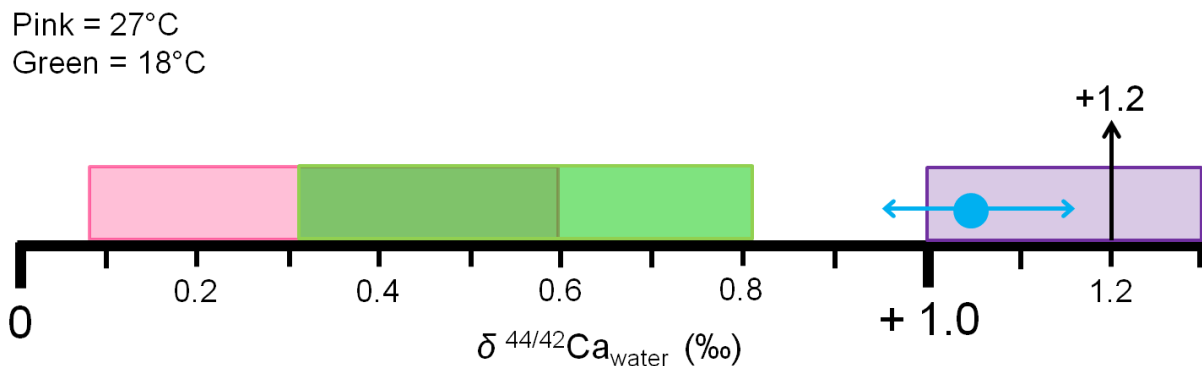


Figure 5.1: The calculated Ca-isotope composition of St. Agatha lake water, using Gussone et al. (2005) assuming a water temperature of 18°C and 27°C. The pink box outlines the range of $\delta^{44/42}\text{Ca}_{\text{water}} (\text{‰})$ at 27°C and the green box outlines the range of $\delta^{44/42}\text{Ca}_{\text{water}} (\text{‰})$ at 18°C. The purple box outlines the $\delta^{44/42}\text{Ca}_{\text{water}} (\text{‰})$ of measured *G. parvus* using a temperature of 18°C with the average $\delta^{44/42}\text{Ca}_{\text{water}}$ of *G. parvus* indicated by the black arrow (+1.2‰). The blue dot indicates the average $\delta^{44/42}\text{Ca} (\text{‰})$ of groundwater measured in this study, with the range in values shown by the blue arrows.

Fossil shells: The average $\delta^{18}\text{O}_{\text{water}}$ calculated for each depth in the St. Agatha cores can be used to estimate the temperature of fossil aragonite shell formation, assuming the shells formed from the same water as the marl calcite. The aragonite-water oxygen isotope geothermometer of Böhm et al. (2000) is used here for this purpose:

$$1000\ln\alpha (\text{aragonite-H}_2\text{O}) = 18.45 \times 10^3\text{T}^{-1} - 32.54 \text{ (temperature in K)} \quad (15)$$

(Böhm et al., 2000)

Wilson (2016) noted that *G. parvus* is associated with warmer waters and are known to exist alongside *Pisidium sp. G. parvus*, along with *V. tricarinata*, forms its shells from spring to fall and has a life cycle typically spanning one year (McKillop, 1985). *G. parvus* is known to live closer to the lake surface in permanent or temporary water bodies among abundant macrophyte vegetation (Harman, 1972; Clarke, 1981; Yang et al., 2000). *V. tricarinata*, much like *G. parvus*,

is found among abundant vegetation in perennial lakes and water bodies (Clarke, 1981).

Pisidium sp. are epifaunal or infaunal that are found in muddy or sandy lake bottoms (Clarke, 1981).

Pisidium sp. have a known growth range of 14 - 22°C, the average of which is 18°C. The average $\delta^{18}\text{O}_{\text{water}}$ calculated using a temperature of 18°C is $-10.1 \pm 0.8\text{‰}$. This can be compared with the average $\delta^{18}\text{O}_{\text{water}}$ of $-9.2 \pm 0.7\text{‰}$ calculated earlier using the Kim and O'Neil (1997) calcite-water geothermometer and the $\delta^{18}\text{O}_{\text{marl}}$ at each depth. If the $\delta^{18}\text{O}_{\text{water}}$ of $-9.2 \pm 0.7\text{‰}$ is used in equation 14, the calculated aragonite shell formation temperature of *G. parvus* is 23°C (range 18 to 28°C). Liu (2016) found that nearby Barry Lake in southern Ontario had a mean summer whole lake temperature of $21 \pm 4^\circ\text{C}$ and a euphotic water temperature of $23 \pm 3^\circ\text{C}$. McKillop (1985) found that water temperatures reached 20°C by early May in southeastern Manitoba (near the geographical center of Canada), and remained above this temperature until September.

The calculated average $\delta^{44/42}\text{Ca}$ of the water from which *G. parvus* shells precipitated was $+1.2 \pm 0.2\text{‰}$ (2SD) (range +1.0 to +1.3‰), assuming an average formation temperature of 18°C. This $\sim 0.3\text{‰}$ range is smaller than that calculated for the marl calcite $\delta^{44/42}\text{Ca}$, which could arise from differences in lakewater $\delta^{44/42}\text{Ca}$, the assumption of an average temperature of shell formation, and/or the extent of Ca-isotope equilibrium established during aragonite shell versus marl calcite precipitation.

Shells of two other species (*V. tricarinata* and *Pisidium sp.*) were collected at two core depths (219.5 – 220.0cm and 309.0 – 309.5cm) alongside *G. parvus*. This allows for a comparison of the $\delta^{18}\text{O}_{\text{water}}$ of the ecological niche that each species likely occupied at St. Agatha. *V. tricarinata* typically occupies a similar ecological niche as *G. parvus* and has a similar growing season. Hence, it is expected that the average aragonite shell formation temperatures of each species would be similar. *Pisidium sp.*, however, is primarily found on or in the benthic substrate in lakes and occupy an ecological niche that is vastly different from both *G. parvus* and *V. tricarinata*, contributing to the differences in isotope compositions measured. Using the $\delta^{18}\text{O}_{\text{water}}$ calculated with Kim and O'Neil (1997), an average temperature of aragonite shell formation was estimated for each of *V. tricarinata* and *Pisidium sp.* For depth 219.5 – 220.0cm, the calculated *V. tricarinata* average formation temperature was 19.8°C (range 15 to 24°C), and *Pisidium sp.* was

20.6°C (range 20 to 21°C), while at 309.5 – 310cm depth, *V. tricarinata* was 23.5°C (range 23 to 24°C) and *Pisidium sp.* was 22.8°C.

These temperatures are higher than commonly reported for each species. Macdonald (2012) reported shell formation temperatures ranging from ~11 and 17°C for *V. tricarinata* from Lake Huron. Using an average temperature of ~14°C is used; the calculated average $\delta^{18}\text{O}_{\text{water}}$ for *V. tricarinata* becomes $-9.6 \pm 1.4\text{‰}$ (1SD) at 219.5 – 220.0cm, ~1.3‰ lower than coeval marl calcite $\delta^{18}\text{O}_{\text{water}}$ at the same depth, and $-10.5 \pm 0.1\text{‰}$ (1SD) at 309.0 – 309.5cm, ~1.8‰ lower than coeval marl calcite $\delta^{18}\text{O}_{\text{water}}$ at the same depth. Liu (2016) calculated an average *Pisidium sp.* shell formation temperature of $15 \pm 5^\circ\text{C}$ for ancient species found at Barry Lake, and Macdonald (2012) measured $17 \pm 3^\circ\text{C}$ for *Pisidium sp.* found near the shores of Lake Huron, without a vital effect correction (see 5.3.1b *Shell Aragonite Oxygen* and 5.3.2b *Shell Aragonite Carbon* for information on vital effects). In the present study, a temperature of 17°C was used to estimate the isotope composition of the paleo-lake water during *Pisidium sp.* shell formation, which produced average $\delta^{18}\text{O}_{\text{water}}$ of $-9.1 \pm 0.1\text{‰}$ (1SD), at a depth of 219.5 – 220.0cm, ~0.8‰ lower than coeval marl calcite $\delta^{18}\text{O}_{\text{water}}$ at the same depth, and ~9.8‰ at a depth of 309.0 – 309.5cm, ~1.1‰ lower than the marl calcite $\delta^{18}\text{O}_{\text{water}}$ at the same depth, assuming marl calcite precipitation occurred at 21°C. This is generally consistent with Liu's (2016) observation that surface water at the modern-day Barry Lake analogue to St. Agatha was ~0.6‰ higher than bottom water during the summer months.

5.2 Water History

The O- and Ca-isotope water compositions estimated above are used conjunction with the Sr-isotope and elemental data to explore possible histories for the water that supplied the St. Agatha lake system. This approach helps to understand the local Ca cycle for the St. Agatha kettle lake and evaluate whether changes in the relative source contributions or other processes are reflected in the marl Ca-isotope record.

The normalized concentrations of Mg, Ba and Fe in marl calcite indicate a major change from the bottom ~50cm to higher in the core (see Figure 4.1). In the core's bottom ~50cm Mg and Fe concentrations covary and are much higher than in the rest of the marl sequence. These results suggest a significant change in lake water composition from the interval reflected by the core's

lowermost 50cm to above that point. The first lake water recorded by the marl (~13,500 yrs BP; Guillet, 1969; Thompson et al., 1997; Kulak, 2005; J. Walker and F. Longstaffe, personal communication, 2017) may have had greater access to Mg, Mn and labile Fe from leaching of fine-grained glacial rock flour comprising dolomite, gypsum/anhydrite, soluble Fe-bearing phases and organic matter. Alternatively, this water may have had a different source than later in the lake's history.

Sr-isotope ratios (Figure 5.2) can be a very good indicator of a change in water source (Matthews, 2014) (see *Appendix A* for additional information). In the St. Agatha core, there is only a small increase in $^{87}\text{Sr}/^{86}\text{Sr}$ (0.709243 to 0.709569) in marl calcite from ~128 to ~475cm depth, but below ~475cm $^{87}\text{Sr}/^{86}\text{Sr}$ peaks at 0.709446 before decreasing to 0.708547, the lowest Sr-isotope ratio measured (Figure 4.10). Below ~475cm the Sr-isotope ratios are typical of Silurian to lower Devonian carbonate rocks in the region, while above ~475cm the higher Sr-isotope ratios are more comparable to those observed in Cambrian units (see *Appendix A, Figure A1*). If marl calcite precipitated from water that acquired its Sr from the same bedrock or till throughout the history of marl precipitation, then the $^{87}\text{Sr}/^{86}\text{Sr}$ ratios should be very similar along the core (Veizer, 1989). The deepest marl (below ~450cm) was deposited ~13,500 years ago (J. Walker and F. Longstaffe, personal communication, 2017) but has $^{87}\text{Sr}/^{86}\text{Sr}$ ratios similar to modern groundwater (samples W427 and W36). The Sr-isotope data therefore hint at a groundwater supply to the St. Agatha kettle lake system at ~13,500 years ago that was similar to shallow groundwater still active in the region today, at least based on Sr-isotope ratios. The higher $^{87}\text{Sr}/^{86}\text{Sr}$ ratios (>0.709243) above the base of the marl section, however, suggest involvement of another or at least an additional source. Further confounding the origin of the water from which the deepest portion of the marl crystallized is that its calculated $\delta^{44/42}\text{Ca}_{\text{water}}$ is ~1.4‰ lower than modern groundwater, a point to which we return later.

Figure 5.2 compares the $^{87}\text{Sr}/^{86}\text{Sr}$ versus Sr concentration of St. Agatha marl calcite (blue) and the two modern groundwater (red and orange) samples with data reported by Skuce (2014) and Skuce et al. (2015) for shallow groundwater and deeper brines from the Paleozoic aquifers of southwestern Ontario. McNutt et al. (1987) reported similar results.

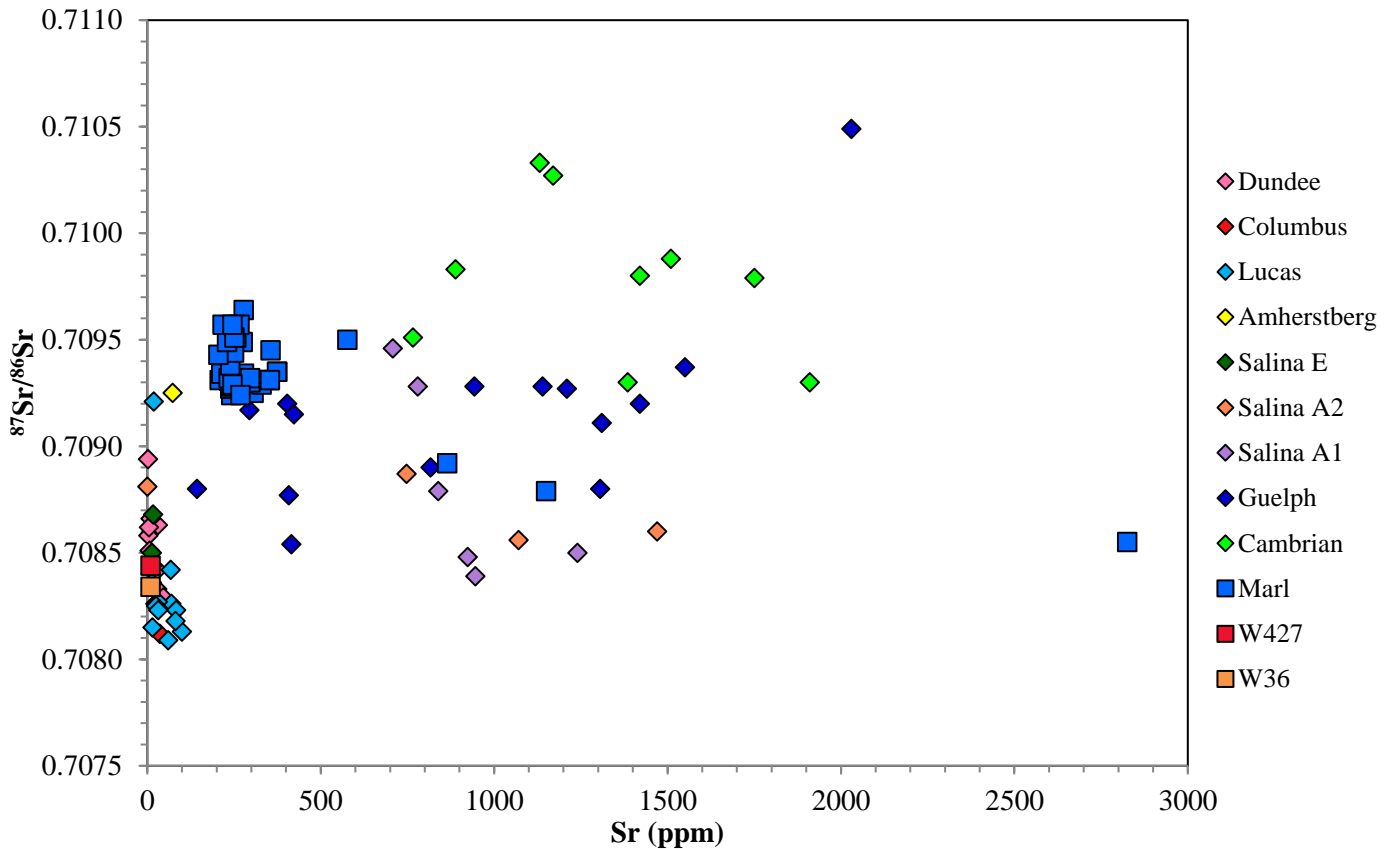


Figure 5.2: $^{87}\text{Sr}/^{86}\text{Sr}$ versus Sr concentration (ppm) of southwestern Ontario shallow and deep groundwater (diamonds) from Skuce (2014) and Skuce et al. (2015) compared with the results for St. Agatha marl calcite and two modern groundwater samples (squares).

The majority of the marl calcite samples have $^{87}\text{Sr}/^{86}\text{Sr}$ and Sr concentrations consistent with mixing between shallow groundwater like that present in the Middle Devonian Amherstberg Formation or lower salinity portions of the Silurian Guelph Formation of southwestern Ontario and more Sr-rich brines from the Guelph Formation and Cambrian units. The Cambrian units, in particular, have the higher $^{87}\text{Sr}/^{86}\text{Sr}$ needed to explain the ratios obtained for some marl. The three samples from the lowermost portion of the marl sequence have $^{87}\text{Sr}/^{86}\text{Sr}$ ratios and Sr concentrations more typical of the Salina A1 and A2 units, and trend towards the still lower $^{87}\text{Sr}/^{86}\text{Sr}$ measured for the modern groundwater samples, ratios that are typical of the Middle Devonian Lucas Formation.

Modern shallow groundwater in the area of the St. Agatha marl deposits has $\delta^{18}\text{O}$ ranging from ~ -13 to -11‰ (Skuce, 2014; Skuce et al., 2015), whereas the average calculated $\delta^{18}\text{O}_{\text{water}}$ for the St. Agatha marl is $-9.2 \pm 0.8\text{‰}$ (1SD). For the lowermost marl samples, however, the calculated

average $\delta^{18}\text{O}_{\text{water}}$ is lower, -10.0‰ , than the rest of the marl sequence ($\sim -9.0\text{‰}$). Lakewater is typically enriched in ^{18}O relative to its sources, including groundwater, because of evaporation. The lower $\delta^{18}\text{O}_{\text{water}}$ inferred for the lake at the base of the marl sequence could reflect a period of lower evaporation (higher humidity), and/or a change in source water O-isotope composition. Cooler temperatures, higher relative humidity and lower source water $\delta^{18}\text{O}$, both of precipitation and groundwater, are self-consistent variables that could produce this $\sim 1\text{‰}$ decrease associated with the lowermost marl, given that the region was only just beginning to undergo the warming associated with the retreat of the Laurentide Ice Sheet.

Values of $^{87}\text{Sr}/^{86}\text{Sr}$ are plotted versus Ca/Sr and Mg/Ca ratios in Figure 5.3a and b, respectively, following Holmden (2009). Figure 5.3a shows that the lowermost three marl samples (514.5 to 532.0cm) describe a very different trend than the samples from higher up in the marl section. The intersection of the two trends occurs at 474.5 – 475.0cm, consistent with previous estimates of the depth at which a significant change in fluid composition occurred. Figure 5.3b illustrates distinct clustering between the lowermost three marl samples at higher Mg/Ca and lower $^{87}\text{Sr}/^{86}\text{Sr}$ and the rest of the marl data at lower Mg/Ca and higher $^{87}\text{Sr}/^{86}\text{Sr}$, again consistent with different fluid sources and/or geochemical evolution. The anomalous point at 494.5 – 495.0cm represents the lowest $\delta^{44/42}\text{Ca}$ and highest Mg/Ca ratio measured.

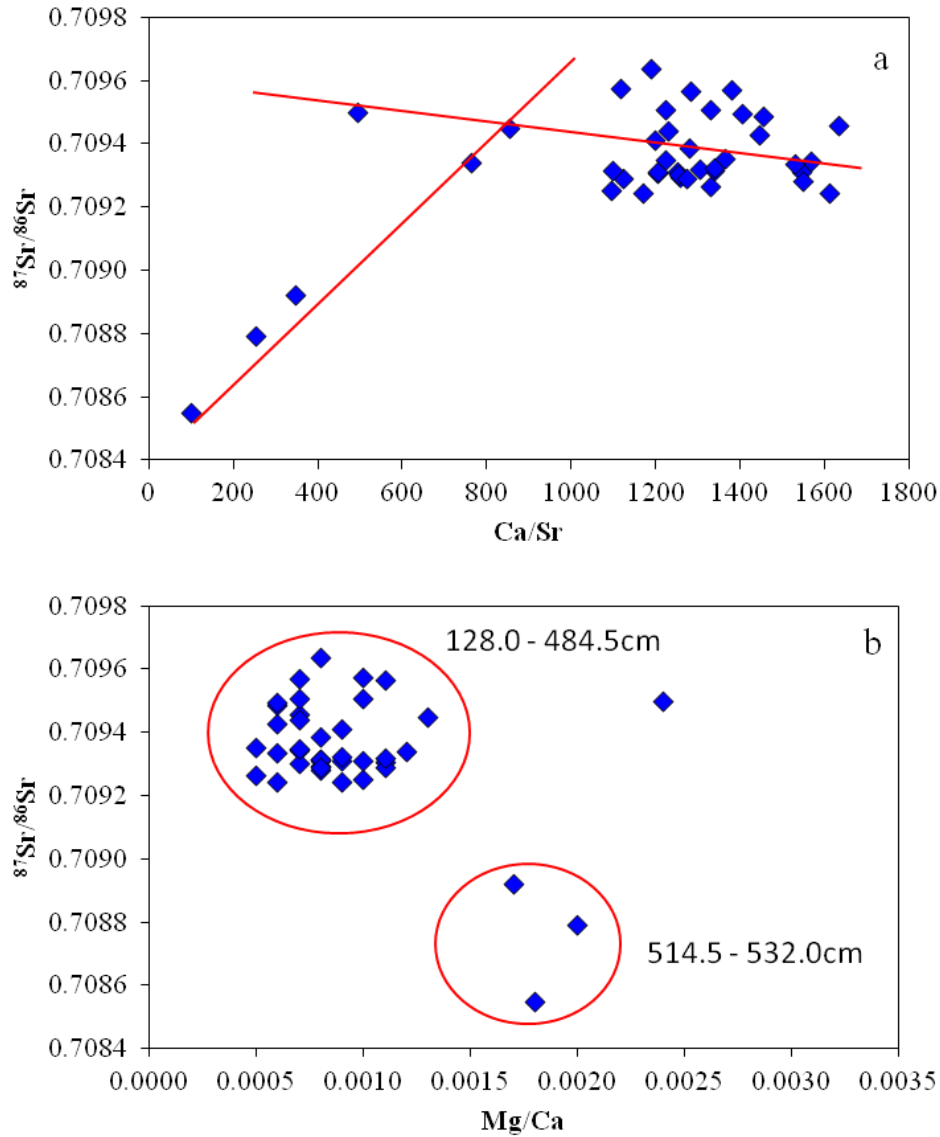


Figure 5.3: $^{87}\text{Sr}/^{86}\text{Sr}$ ratios versus (a) Ca/Sr and (b) Mg/Ca for St. Agatha marl calcite.

5.2.1 Open or Closed Lake

Talbot (1990) found that $\delta^{18}\text{O}$ and $\delta^{13}\text{C}$ of authigenic carbonates in lacustrine environments tend to covary, with the strength of the correlation indicating more open versus more closed lake systems. Strong covariance indicates a closed-lake system whereas weak covariance indicates an open-lake system (Talbot 1990; Li and Ku, 1997).

Evaporative effects become more pronounced in closed bodies of water, as they commonly have longer residence times, which allows for a greater enrichment in ^{18}O and ^{13}C (Stuiver, 1970; Talbot, 1990; Li and Ku, 1997; Leng and Marshall, 2004; Sharp, 2007). These enrichments are reflected in the endogenic and biogenic carbonates that crystallize from the lake water. In closed lakes, the water may enter the system from a variety of sources, such as precipitation, surface runoff, or groundwater but there are few to no outflows. Water leaves the lake primarily by evaporation, which leaves diagnostic isotopic and chemical signatures on the lakewater that remains. Open lakes typically have multiple inputs, outflows, and a shorter water residence time and hence typically exhibit lower evaporative enrichments of lakewater ^{18}O , ^{13}C and other dissolved components. Open lakes are more influenced by the $\delta^{18}\text{O}$ of source waters entering the system than by evaporation. The primary source of $\delta^{13}\text{C}$ in lake waters is the dissolution of bedrock and glacial material.

Figure 5.4 illustrates the trends in marl calcite $\delta^{18}\text{O}$ and $\delta^{13}\text{C}$ for the St. Agatha kettle lake system. The data in blue diamonds indicates the O-isotope and C-isotope data for marl depths above 435.0cm, while the data in red diamonds represent depths between 450.0 and 532.0cm. Data shown in green diamonds are for the depths between 449.5 and 463.0cm. Talbot (1990) noted that a linear relationship in $\delta^{13}\text{C}$ and $\delta^{18}\text{O}$ space with an $r^2 \geq 0.64$ is generally representative of a closed lake, while an $r^2 \leq 0.49$ is diagnostic of an open lake. The marl data above 435.0cm suggest a lake system that was more closed than open ($r^2 = 0.65$), consistent with our earlier suggestions – based solely on $\delta^{18}\text{O}$ – of greater evaporative enrichment. The data below 450.0cm represent a weaker correlation than the marl data above 435.0cm ($r^2 = 0.19$). The marl data for 449.5 and 435.0cm, however, does not appear to follow the trends of either data clusters, suggesting that this was a period of transition from an open lake system with lower $\delta^{18}\text{O}$ and higher $\delta^{13}\text{C}$, to a more closed system with higher $\delta^{18}\text{O}$ and lower $\delta^{13}\text{C}$ (Figure 5.4). The data point at $\delta^{13}\text{C} = -0.89\text{‰}$ and $\delta^{18}\text{O} = +20.5\text{‰}$ (Figure 5.4) is anomalous and currently unexplained. It is located at the very base of the marl succession (531.5 – 532.0cm).

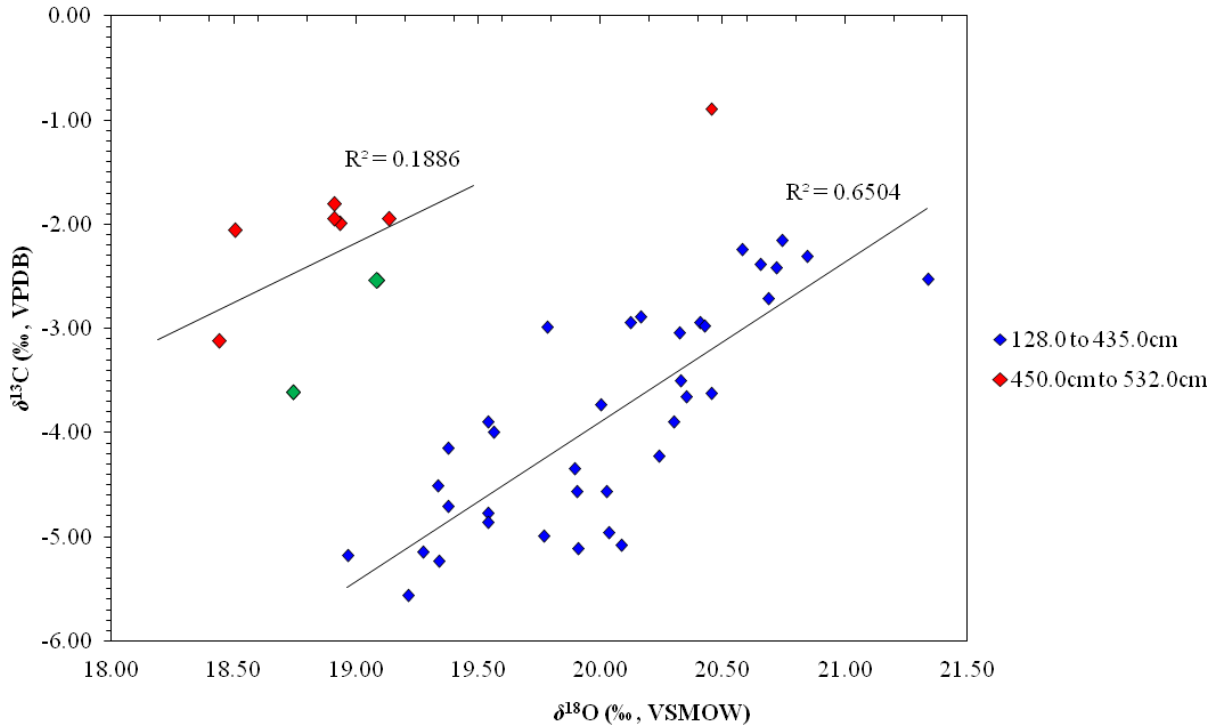


Figure 5.4: $\delta^{18}\text{O}$ (‰) versus $\delta^{13}\text{C}$ (‰) of marl calcite illustrating the covariance between the two isotope systems.

5.3 Controls on the Isotopic Composition of St. Agatha Marl Calcite and Shell Aragonite

This section further explores the controls on the $\delta^{18}\text{O}$, $\delta^{13}\text{C}$, $\delta^{44/42}\text{Ca}$, and $^{87}\text{Sr}/^{86}\text{Sr}$ of the St. Agatha kettle lake as inferred from marl calcite and shell aragonite. The $\delta^{18}\text{O}$ and $\delta^{13}\text{C}$ results for the marl and aragonite are summarized in Table 5.1 and 5.2 and illustrated versus depth in Figure 5.5a ($\delta^{18}\text{O}$) and 5.5b ($\delta^{13}\text{C}$), respectively.

Table 5.1: Marl calcite $\delta^{18}\text{O}$ (‰, VSMOW) and $\delta^{13}\text{C}$ (‰, VPDB) with depth (cm).

Depth (cm)	$\delta^{18}\text{O}_{\text{marl}}$ (‰)	$\delta^{13}\text{C}_{\text{marl}}$ (‰)
128.0 – 128.5	+20.3	-3.9
138.0 – 138.5	+21.4	-2.5
148.0 – 148.5	+19.3	-5.2
157.5 – 158.0	+19.9	-5.1
167.5 – 168.0	+19.3	-5.1
171.5 – 172.0	+19.0	-5.2
179.5 – 180.0	+20.0	-3.7
183.5 – 184.0	+20.1	-5.1
191.5 – 192.0	+20.0	-5.0
201.5 – 202.0	+19.5	-4.8
219.5 – 220.0	+20.8	-2.3
219.5 – 220.0	+20.7	-2.4
221.5 – 222.0	+19.8	-5.0
229.5 – 230.0	+19.5	-4.9
249.5 – 250.0	+20.7	-2.4
255.5 – 256.0	+19.3	-4.5
266.5 – 267.0	+19.2	-5.6
275.5 – 276.0	+19.4	-4.7
285.0 – 285.5	+20.4	-3.7
299.0 – 299.5	+20.5	-3.6
299.0 – 299.5	+20.3	-3.5
309.0 – 309.5	+20.4	-2.9
311.0 – 311.5	+20.7	-2.2
334.5 – 335.0	+20.3	-3.0
344.5 – 345.0	+20.4	-3.0
354.5 – 355.0	+20.7	-2.7
364.5 – 365.0	+20.0	-4.6
374.5 – 375.0	+19.9	-4.6
374.5 – 375.0	+19.9	-4.4
384.5 – 385.0	+20.6	-2.2
394.5 – 395.0	+20.1	-2.9
394.5 – 395.0	+20.2	-2.9
409.5 – 410.0	+19.8	-3.0
414.5 – 415.0	+19.5	-3.9
424.5 – 425.0	+19.6	-4.0
434.5 – 435.0	+19.4	-4.2
449.5 – 445.0	+18.7	-3.6
462.0 – 462.5	+19.1	-2.5
474.5 – 475.0	+18.9	-2.0
484.5 – 485.0	+18.9	-1.8
494.5 – 495.0	+18.9	-1.9
514.5 – 515.0	+18.4	-3.1
524.5 – 525.0	+18.5	-2.0
524.5 – 525.0	+19.1	-2.0

531.5 – 532.0	+20.5	-0.9
----------------------	-------	------

*Data provided by J. Walker and F. Longstaffe, personal communication (2017)

Table 5.2: *G. parvus* shell aragonite $\delta^{18}\text{O}$ (‰, VSMOW) and $\delta^{13}\text{C}$ (‰, VPDB) with depth (cm).

Depth (cm)	$\delta^{18}\text{O}_{\text{shell}}$ (‰)	$\delta^{13}\text{C}_{\text{shell}}$ (‰)
128.0 – 128.5	+21.8	-10.1
138.0 – 138.5	+22.2	-9.2
148.0 – 148.5	+20.7	-10.6
157.5 – 158.0	+20.6	-10.8
167.5 – 168.0	+19.6	-12.4
171.5 – 172.0	+18.8	-11.5
179.5 – 180.0	+21.1	-8.1
191.5 – 192.0	+20.6	-10.2
191.5 – 192.0	+21.4	-10.4
201.5 – 202.0	+21.4	-7.1
209.5 – 210.0	+21.9	-6.9
221.5 – 222.0	+20.2	-8.3
229.5 – 230.0	+20.5	-10.2
249.5 – 250.0	+21.4	-6.6
265.5 – 266.0	+20.1	-9.5
275.5 – 276.0	+20.8	-10.0
285.0 – 285.5	+20.1	-8.8
299.0 – 299.5	+21.2	-9.2
299.0 – 299.5	+21.5	-9.3
329.5 – 330.0	+22.0	-7.2
329.5 – 330.0	+22.2	-7.2
369.5 – 370.0	+20.8	-9.8
369.5 – 370.0	+20.7	-9.5
399.5 – 400.0	+21.3	-7.1
399.5 – 400.0	+21.5	-7.3
524.5 – 525.0	+20.2	-7.8

*Data provided by J. Walker and F. Longstaffe, personal communication (2017)

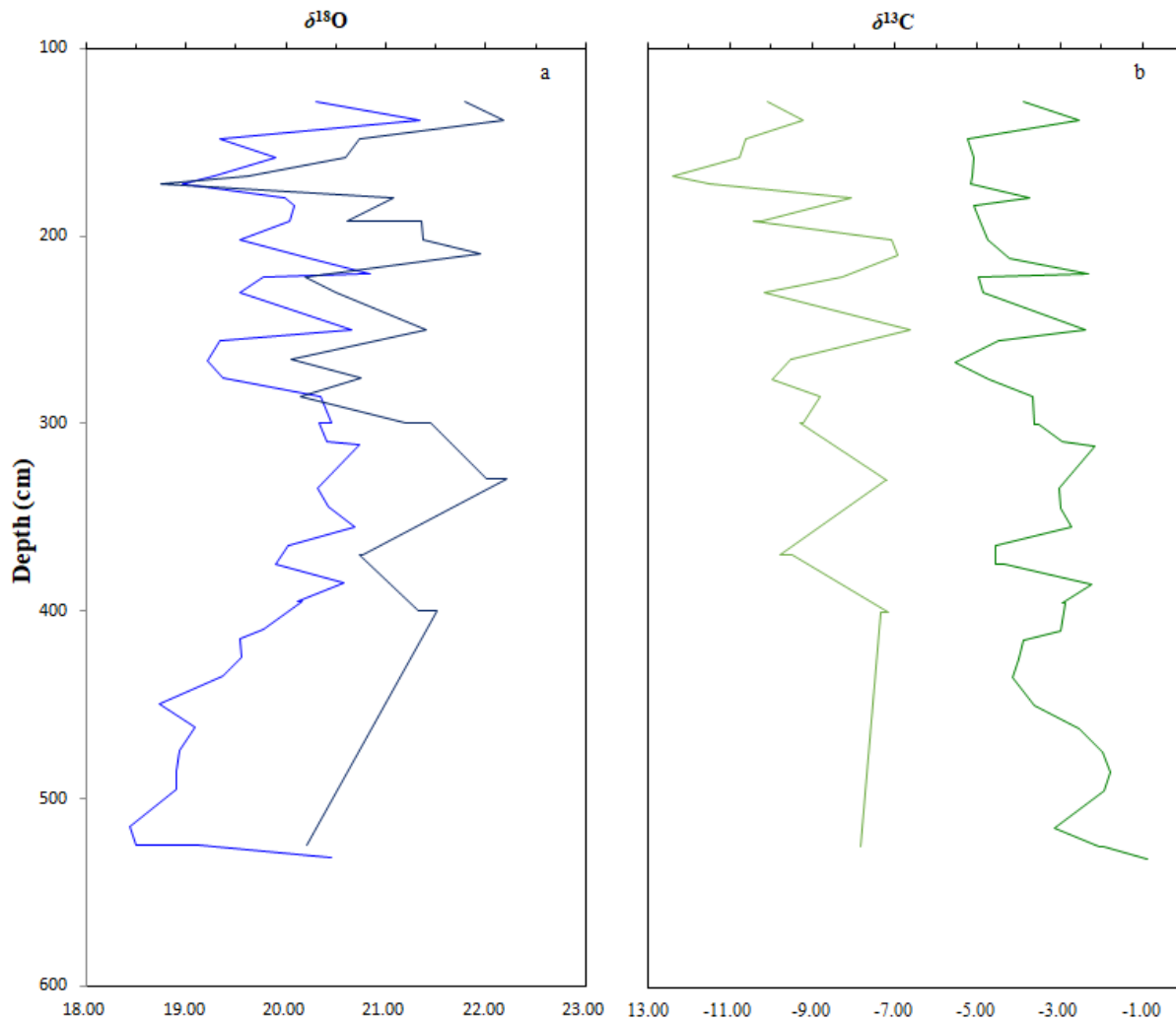


Figure 5.5: Depth versus (a) $\delta^{18}\text{O}_{\text{marl}}$ (light blue) and $\delta^{18}\text{O}_{\text{shell}}$ (dark blue), and (b) $\delta^{13}\text{C}_{\text{marl}}$ (dark green) and $\delta^{13}\text{C}_{\text{shell}}$ (light green). Data courtesy J. Walker and F. Longstaffe (personal communication, 2017).

5.3.1 Oxygen Isotopes

Leng and Marshall (2004) summarize the dominant controls on the $\delta^{18}\text{O}$ of carbonate precipitated in lakes, which includes temperature, evaporation, $\delta^{18}\text{O}_{\text{water}}$, and the extent of isotopic equilibrium attained (Figure 5.6). Equilibrium carbonate precipitation $\delta^{18}\text{O}$ is controlled by temperature and by the isotopic composition of lakewater; any change in either causes a shift in the equilibrium O-isotope composition of the carbonate formed. Climate variability, however, confounds interpretation of endogenic and biogenic oxygen isotope compositions as both temperature and lakewater isotopic compositions can vary at the same time. In addition, kinetic (rate-dependent) and vital (metabolic) effects during carbonate precipitation can both cause

isotopic disequilibrium that can be unique to any individual lake systems. Such isotopic disequilibrium can be triggered by factors such as a change in pH and rate of precipitation, which cause changes in the isotope composition. For oxygen, disequilibrium effects are not considered to be a factor in the St. Agatha lake system, as the O-isotope composition of marl calcite is generally controlled primarily by temperature and lakewater composition (Leng and Marshall, 2004). Variability in marl $\delta^{18}\text{O}$ can therefore signal a change in lakewater sources or – more likely – climate-related variations (temperature, humidity) that can affect the lake’s O-isotope composition by driving changes in input signals and the extent of evaporation.

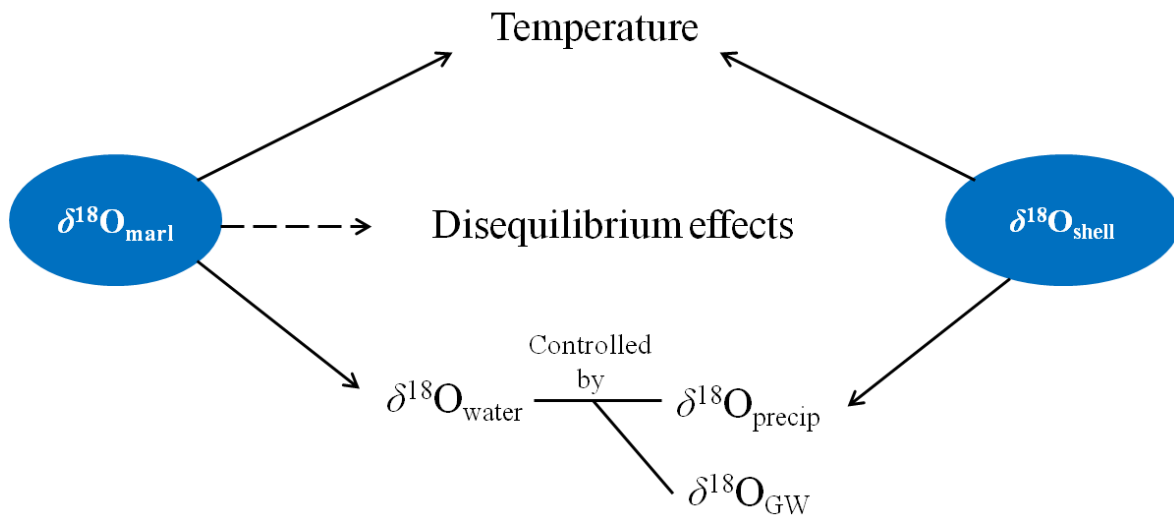


Figure 5.6: Dominant controls on the O-isotope composition of freshwater endogenic and biogenic carbonates (after Leng and Marshall, 2004).

5.3.1a Marl Calcite Oxygen

Temperature plays a large role in determining the O-isotope composition of marl calcite. First, evaporation from a standing body of water preferentially moves water molecules enriched in ^{16}O into the vapour phase causing ^{18}O enrichment in the remaining lakewater (Stuiver, 1970; Li and Ku, 1997; Sharp, 2007). If this is the only factor at play, higher marl $\delta^{18}\text{O}$ would indicate an increase in temperature-related evaporation, and lower values, a decrease. Second, temperature also influences the O-isotope composition of rain and snow, another direct and indirect source of water for the St. Agatha lake system, with higher precipitation $\delta^{18}\text{O}$ typically associated with warmer temperatures (Dansgaard, 1964). Third, temperature affects the size of the O-isotope fractionation between marl calcite and the water from which it crystallizes, with larger fractionations (and hence higher marl $\delta^{18}\text{O}$) occurring at lower temperatures.

Assuming that $\delta^{18}\text{O}_{\text{water}}$ remains unchanged across the seasons (unlikely in a small lake), temperature increases during the summer months should cause a decrease in marl $\delta^{18}\text{O}$ formed then relative to spring crystallization (Stuiver, 1970). Marl crystallization during cooler seasons, however, is unlikely. Marl calcite typically crystallizes in, or very close to, O-isotope equilibrium during whitening events that occur in the summer months within a temperature range of 18 to 27°C; the marl crystallization is triggered by the rising productivity of blue-green algae that function and live within a temperature range of 18 to 27°C (Grabau, 1920; Strong, 1978; Reynolds, 1984; Lavens and Sorgeloos, 1996; Thompson et al., 1997; Liu, 2016).

At St. Agatha, the $\delta^{18}\text{O}$ of water that entered the lake was controlled by groundwater and precipitation. Presently in the region groundwater $\delta^{18}\text{O}$ is ~ -13 to -11‰ (Skuce, 2014; Skuce et al., 2015) whereas precipitation is $\sim 9\text{‰}$ (F. Longstaffe, personal communication, 2019). These input values of $\delta^{18}\text{O}_{\text{water}}$ undoubtedly changed over the latest Pleistocene to early Holocene time period of marl precipitation, but the general condition of $\sim 2\text{‰}$ lower values for groundwater than precipitation inputs likely was preserved.

5.3.1b Shell Aragonite Oxygen

The controls on aragonite shell O-isotope composition are similar to marl calcite, assuming isotopic equilibrium (Figure 5.6) (Abell and Williams, 1989). Leng and Marshall (2004) found that most shell species, including those genera (snails, clams) examined in the present study, form their shells at or near O-isotope equilibrium with the surrounding water. Different genera and species living in the same body of water can exhibit O-isotope variability as a result of habitat differences (Leng and Marshall, 2004). Such variability likely existed at St. Agatha, as *G. Parvus* typically lives on submerged vegetation in cool, shallow ($\sim 1\text{m}$) water bodies (Harman 1972; Clarke, 1981; Yang et al., 2000), *V. tricarinata* lives among abundant vegetation to depths $> 9\text{m}$ (Clarke, 1981; McKillop, 1985) and *Pisidium sp.* are epifaunal or infaunal lake bottom dwellers (Clarke, 1981; von Grafenstein, 1998; Apolarinska and Hammerlund, 2009).

Vital effects can lead to non-equilibrium enrichment of ^{16}O during carbonate formation (Abell, 1985; von Grafenstein et al., 1999). Light isotopes (^{16}O and ^{12}C) diffuse faster than heavy isotopes, and participate more rapidly in reactions (McConnaughey, 1989). As was noted above,

however, most shell species form their shells at or near O-isotope equilibrium with surrounding water, with negligible vital effects (Fritz and Poplawsky, 1974; Leng and Marshall, 2004).

The $\delta^{18}\text{O}$ of the *G.parvus* shells shows an average enrichment of $\sim 1.1\text{‰}$ relative to coexisting marl (Figure 5.5a). Stuiver (1970) reported a similar offset of $\sim +1.3\text{‰}$ between coexisting aragonite shells and marl calcite. The species examined in this study crystallize shell aragonite from spring until fall. The higher $\delta^{18}\text{O}$ of the shells reflects conditions within the lake during the period of time, and in particular, the lower average temperature of shell formation (18°C) compared to the marl calcite, which forms at higher temperatures only during the summer months (21°C).

5.3.2 Carbon Isotopes

5.3.2a Marl Calcite Carbon

The C-isotope fractionation between marl and the DIC is largely invariant at surface temperatures, and hence variation in $\delta^{13}\text{C}_{\text{marl}}$ more directly reflects other processes (Stuiver, 1970; Romanek et al., 1992). In particular, changes in $\delta^{13}\text{C}_{\text{marl}}$ can be used to infer changes arising from the primary productivity of freshwater lakes. Marl carbon is supplied by carbonate (CO_3^{2-}), which is precipitated from a water column containing bicarbonate (HCO_3^-). The original C-isotope composition of lake bicarbonate supplied by inflow is modified by lake processes and productivity (photosynthesis, organic matter decay and respiration). Marl crystallization, facilitated by blue-green algae is fueled by the amount of CO_2 dissolved in the water column (see 2.3.4 Marl) (and potentially also the supply of Ca^{2+} ; see below). Dissolved CO_2 enters the water column through exchange with the atmosphere, which is one major control on $\delta^{13}\text{C}_{\text{DIC}}$. The value of $\delta^{13}\text{C}_{\text{DIC}}$ also depends on other factors including; (1) the degree of equilibrium established with atmospheric CO_2 , (2) the rates and amounts (e.g. primary productivity) of photosynthesis within the water column, (3) decomposition of terrestrial organic matter in the lake, and (4) input water composition (Figure 5.7) (Boutton, 1991). Input water $\delta^{13}\text{C}$ is controlled by (1) particulate and dissolved C-species in rain and snow, (2) dissolution of carbonates in overburden and bedrock, and (3) soil zone processes. Skuce (2014) and Skuce et al. (2015) reported the $\delta^{13}\text{C}_{\text{DIC}}$ of major bedrock aquifers in southwestern Ontario, including: Salina A2 carbonate unit, -3.0 to -1.9‰ ; Salina A1 carbonate unit, $+0.9$ to $+14.2\text{‰}$, and Guelph Formation -6.5 to $+3.5\text{‰}$.

The $\delta^{13}\text{C}$ of atmospheric CO_2 during the lifetime of the St. Agatha kettle lake ranged from $\sim -6.5\text{‰}$ (VPDB) prior to the Industrial Revolution to the present value of -8.4‰ . Water bodies with longer residence times, such as lakes, have more time to equilibrate with the atmosphere (Macdonald, 2012). Typically, freshwater lakes have $\delta^{13}\text{C}_{\text{DIC}}$ ranging between -15 to 0‰ , with the lower values reflecting contributions from oxidative decay of terrestrial organic matter, which preferentially releases ^{12}C into the water column (Boutton, 1991). Another contributor to $\delta^{13}\text{C}_{\text{DIC}}$ is the dissolution of marine carbonate rock from the region, which has $\delta^{13}\text{C}$ closer to 0‰ (Macdonald, 2012), similar to most Paleozoic carbonates ($\delta^{13}\text{C}$ of ~ -1 to $+4\text{‰}$; Lohmann and Walker, 1989).

Lake primary productivity is a strong control on $\delta^{13}\text{C}_{\text{marl}}$. Photosynthetic activity removes ^{12}C from the water column. As blue-green algae flourish from $18 - 27^\circ\text{C}$, the remaining ^{13}C -enriched DIC is used in marl precipitation. Hence, during times of higher algal productivity, $\delta^{13}\text{C}_{\text{marl}}$ will be higher, and during times of decreased algal productivity, $\delta^{13}\text{C}_{\text{marl}}$ will be lower. Periods of high productivity are also commonly associated with increased lake-bottom organic decay and increased production of ^{12}C -rich DIC. Marl, however, crystallizes just below the lake surface, thus limiting immediate negative feedback from this potential reservoir.

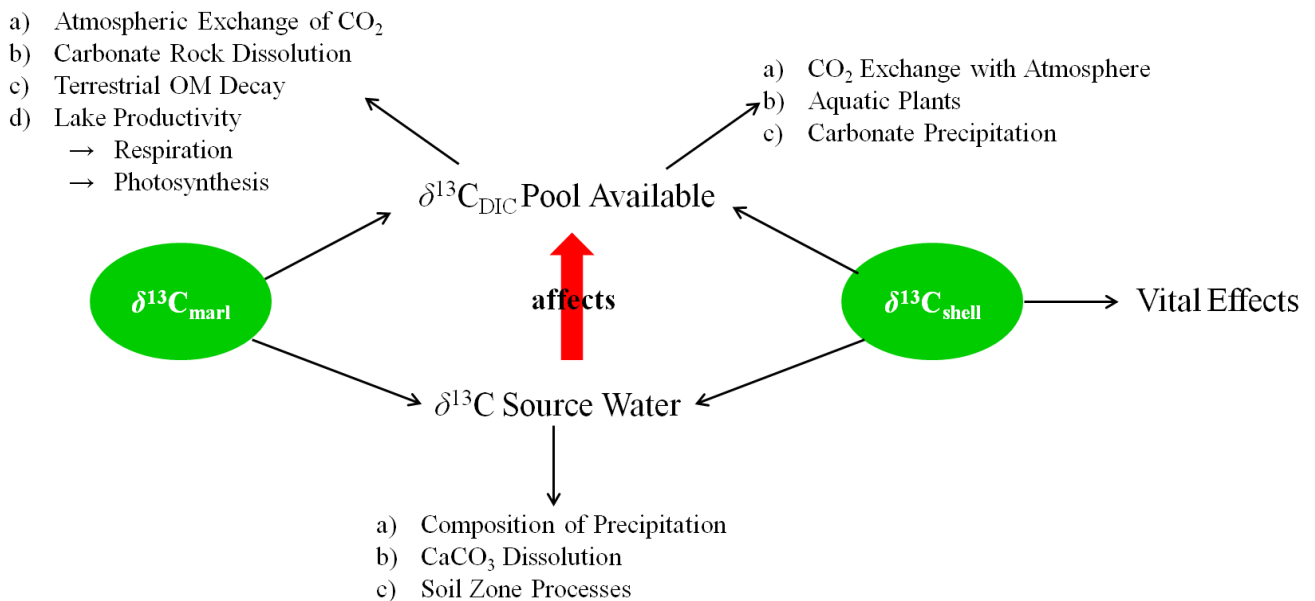


Figure 5.7: Dominant controls on the C-isotope composition of freshwater endogenic (marl) calcite and biogenic (shells) aragonite.

5.3.2b Shell Aragonite Carbon

Like marl calcite, the $\delta^{13}\text{C}$ of aragonite shells in the St. Agatha deposits is largely independent of shell formation temperature (Cespuglio et al., 1999; Grossman and Ku, 1986). Instead, the C-isotope composition is strongly controlled by the $\delta^{13}\text{C}_{\text{DIC}}$ pool, and vital effects during shell formation (Figure 5.7). Shell C-isotope vital effects are caused by (1) rapid shell formation that preferentially incorporates ^{12}C , (2) exchange with low ^{12}C respired aqueous CO_2 or bicarbonate, and (3) species-specific metabolic effects that preferentially incorporate ^{12}C during shell formation (Spero et al., 1991; McConnaughey et al., 1997). In the case of St. Agatha, however, *G. parvus* and *V. tricarinata* are not known to exhibit C-isotope vital effects. Gill-breathing snails, like those examined in the present study, form shells with $\delta^{13}\text{C}$ close to that of DIC, whereas lung-breathing snails incorporate greater amounts of metabolic carbon and as a result have lower $\delta^{13}\text{C}$ (McConnaughey et al., 1997).

The *G. Parvus* shells measured in this study are more depleted of ^{13}C than marl calcite analyzed from the same depth (Figure 5.5b); the difference of $\sim 5\text{‰}$ on average was also noted by Stuiver (1970). Thus, the DIC pool during available crystallization was more depleted of ^{13}C than that utilized during marl precipitation. There are at least two explanations for this difference. First, *G. parvus* lives in or on abundant macrophyte vegetation, which would be actively respiring causing the gastropod to have access to a local DIC pool depleted of ^{13}C during shell formation. Second, shell aragonite forms more or less continuously from spring to fall, whereas marl calcite is precipitates in summer at the height of blue-green algal productivity (Stuiver, 1970), a period during which the DIC pool remaining for marl formation is particularly enriched in ^{13}C .

5.3.3 Calcium Isotopes

The freshwater Ca-isotope system is not nearly as well understood as the O-, C- and Sr-isotope systems. Figure 5.9 illustrates several of the factors that may control the $\delta^{44/42}\text{Ca}$ of freshwater and marl calcite and shell aragonite that crystallizes from it, but many have not yet been fully investigated.

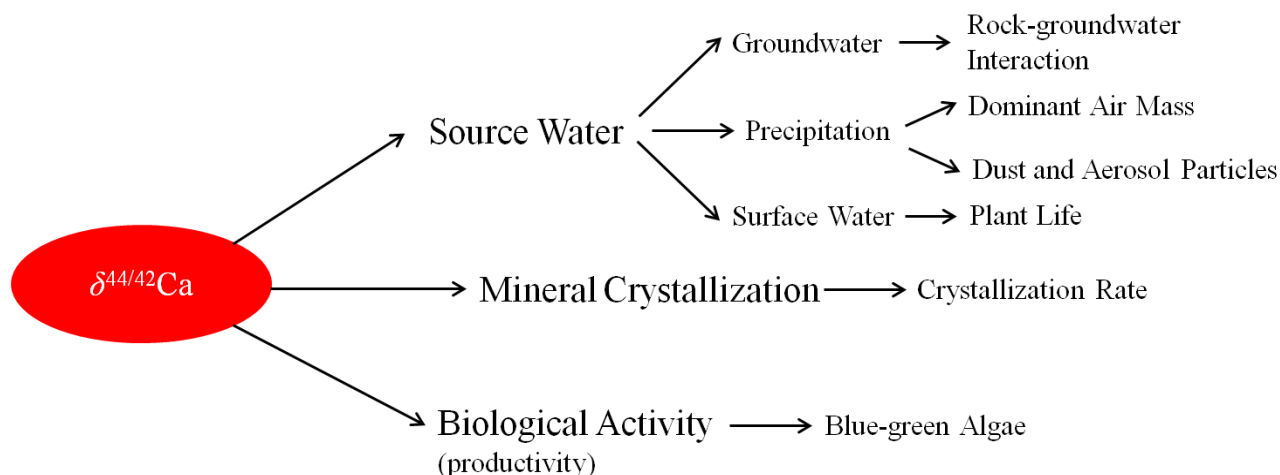


Figure 5.8: Potential controls on the $\delta^{44/42}\text{Ca}$ of freshwater in the St. Agatha kettle lake system.

As discussed earlier, marl calcite crystallization is facilitated by blue-green algae and likely occurs at about the same summer-time temperatures from year to year. Variability in $\delta^{44/42}\text{Ca}_{\text{marl}}$, therefore, likely reflects other factors such as changes in lake water compositions or the extent of Ca-isotope disequilibrium. As noted earlier, groundwater Ca-isotope inputs from groundwater are believed to reflect the dominant carbonate formations in the area (Fantle and Tipper, 2004). The elemental and Sr-, O- and C-isotope results presented earlier suggest a change in water chemistry and perhaps source/history from the base of the marl section upwards, particularly between the lowermost 20cm (532.0 to 513.5cm) and above. The Sr-isotope record, which is the most diagnostic of changes in water inputs, however, shows only modest changes above 475.0cm, whereas significant fluctuations in the $\delta^{44/42}\text{Ca}_{\text{marl}}$ record continue (Figure 5.10). This suggests that the changes in the $\delta^{44/42}\text{Ca}_{\text{marl}}$ record are heavily affected by additional factors.

Marl crystallization rate could be a dominant control on $\delta^{44/42}\text{Ca}_{\text{marl}}$ variation (see 2.4.1a *Mineral Crystallization*). This rate is controlled by the availability of ions in solution, and commonly considered to be controlled by HCO_3^- , most notably in marine systems (Gussone et al., 2015). Changes in the source and fluxes of water affect the concentration of HCO_3^- and hence could affect the Ca-isotope composition of precipitating marl calcite. A more rapid crystallization rate, due to increased concentration of ions in solution – arising from increased evaporation and associated with lower water levels – should cause a decrease in $\delta^{44/42}\text{Ca}_{\text{marl}}$ relative to equilibrium. A slower crystallization rate, perhaps reflecting lower ionic concentration in a lake

– associated with less evaporation and higher water levels – should result in higher $\delta^{44/42}\text{Ca}_{\text{marl}}$ as a closer approach to isotopic equilibrium might be anticipated. Whether any marl (or shelly carbonate) crystallizes in Ca-isotope equilibrium with water, however, is unclear. Based on analysis of calcite crystallized in aquifers with very long residence times for water, Jacobson and Holmden (2008) and Holmden (2009) posited that achieving Ca-isotope equilibrium between authigenic carbonate and water can take a very long time, rather than the hours to days associated with marl formation. They further suggest that the Ca-isotope fractionation between authigenic calcite and water disappears given sufficiently slow crystallization rates. Still other mechanisms may therefore be needed to explain the Ca-isotope variations in the St. Agatha marl calcite (see below).

The controls on $\delta^{44/42}\text{Ca}_{\text{shell}}$ are similar to those affecting marl calcite with the notable differences that *G. parvus* and *V. tricarinata* shells crystallize shell aragonite from spring to fall, over one year generally at generally lower temperatures than marl, and *Pisidium sp.*, forms its shell in the summer months over several years, and the rate of shell formation is slower than that of marl crystallization (see Table 4.8 for $\delta^{44/42}\text{Ca}_{\text{shell}}$ of each species) (Leng and Marshall, 2004). As described earlier, (see 2.4.1a *Mineral Crystallization*) lower temperatures are believed to result in larger Ca-isotope fractionations, following the premise that Ca-isotope equilibrium is established. An increase or decrease in temperature should also be mirrored in marl $\delta^{44/42}\text{Ca}$, provided that Ca-isotope equilibrium is established during mineral formation. This scenario should produce shells that have lower $\delta^{44/42}\text{Ca}$ than coexisting marl calcite, assuming no seasonal change in $\delta^{44/42}\text{Ca}_{\text{water}}$. For *G. parvus*, however, only 57% of the samples have $\delta^{44/42}\text{Ca}_{\text{shell}} < \delta^{44/42}\text{Ca}_{\text{marl}}$ (Figure 5.9). The systematic ~0.3‰ enrichment of $\delta^{44/42}\text{Ca}$ in calcite relative to aragonite precipitating from the same water, as noted by Gussone et al. (2005), appears to be confounded by additional processes at St. Agatha (Figure 5.9).

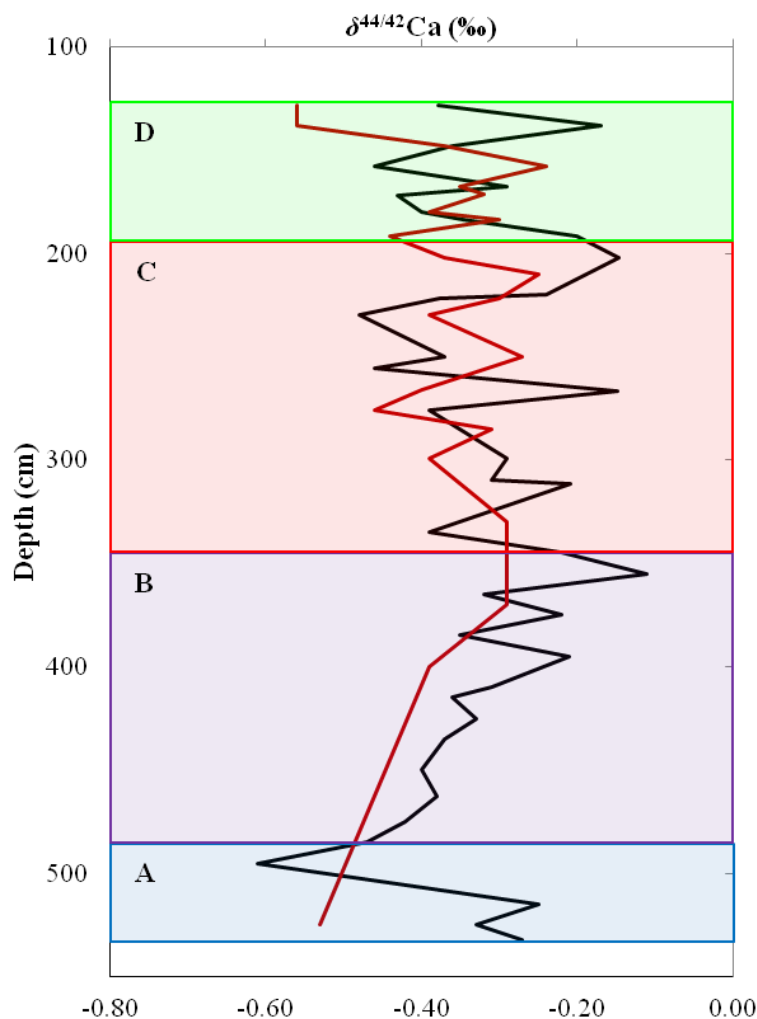


Figure 5.9: Depth versus $\delta^{44/42}\text{Ca}$ of marl calcite (red) and shell aragonite (black) of *G. parvus*. See section figu for discussion of Intervals A-D.

5.4 Environmental History of St. Agatha Marl Calcite

Here we combine the $\delta^{44/42}\text{Ca}$, $\delta^{18}\text{O}$, $\delta^{13}\text{C}$ and $^{87}\text{Sr}/^{86}\text{Sr}$ results for the St. Agatha system to infer the environmental history of marl precipitation (Figures 5.10 and 5.11). The marl section has been subdivided into four intervals (A to D) from the beginning of marl calcite crystallization at ~13,500 years BP until marl interface with the peat, which is dated at ~8,200 cal years BP (J. Walker and F. Longstaffe, personal communication, 2019).

For a large portion of the core, the marl (and shell) Ca-isotope data do not vary outside an error of 2SD ($\pm 0.1\%$; Table 4.6-4.7; Figures 4.7-4.8). In comparison with marl $\delta^{18}\text{O}$ data, which has

precision of $\pm 0.05\%$, however, similar variability is apparent for both isotopic systems. The variability observed in the Ca-isotope system may be real, despite not being outside of error.

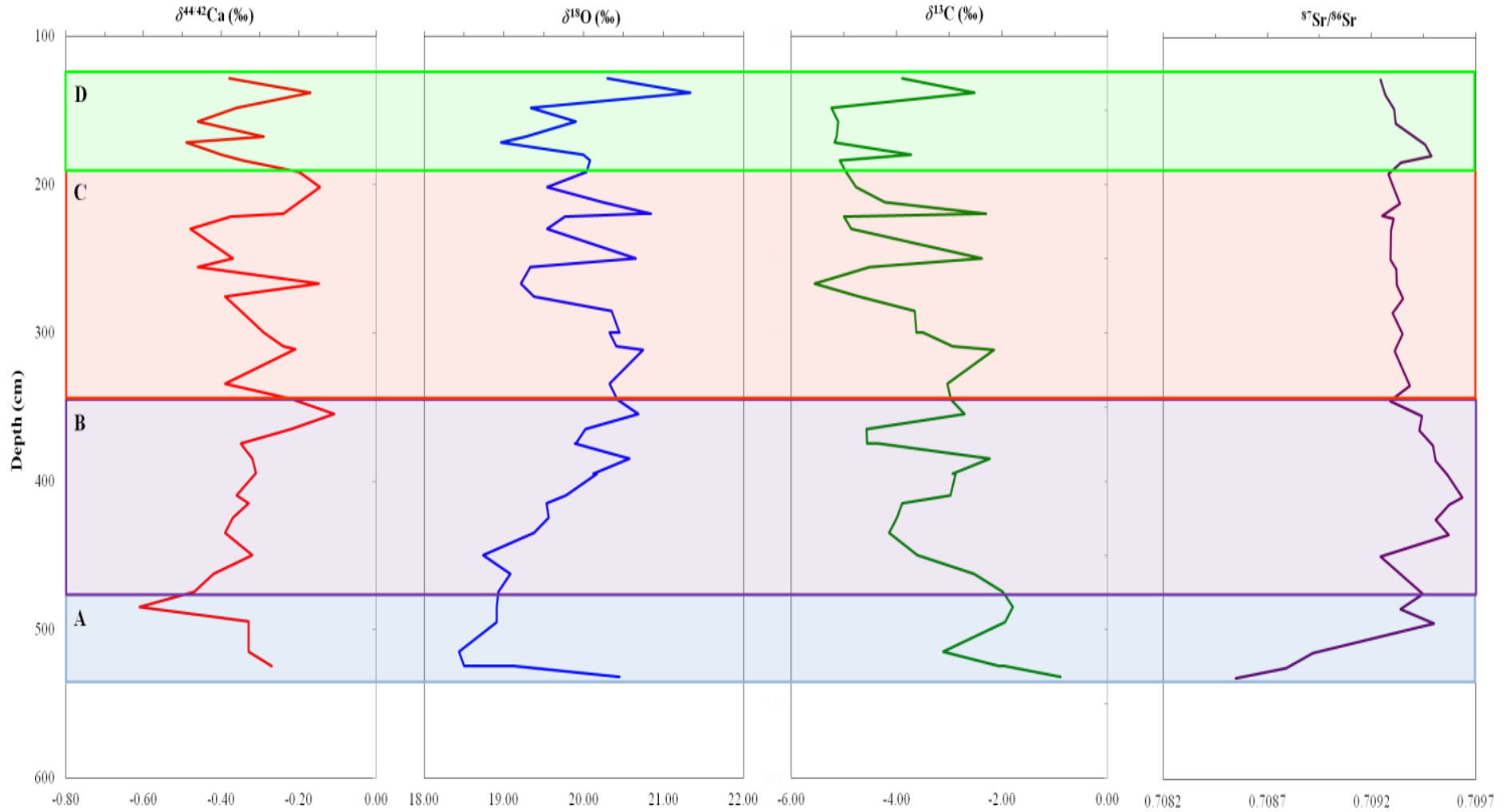


Figure 5.10: Depth versus $\delta^{44/42}\text{Ca}$ (red), $\delta^{18}\text{O}$ (dark blue), $\delta^{13}\text{C}$ (green) and $^{87}\text{Sr}/^{86}\text{Sr}$ (light blue) for marl calcite. Proposed Intervals A to D are outlined.

5.4.1 Interval A (532.0 to 475.0cm)

Interval A (532.0 to 475.0cm) contains the earliest stages of marl crystallization in the St. Agatha kettle lake system (Figure 5.10). Marl in this interval generally has the highest $\delta^{13}\text{C}$ and the lowest $\delta^{18}\text{O}$, $\delta^{44/42}\text{Ca}$ and $^{87}\text{Sr}/^{86}\text{Sr}$.

The initially low but rising $^{87}\text{Sr}/^{86}\text{Sr}$ ratios (0.708547 to 0.709446) are a defining feature of Interval A. As noted earlier, below 474.5cm the Sr-isotope ratios are most similar to brines from the Silurian Salina A-1 and A-2 units, fresh waters from the middle Devonian Lucas Formation aquifer, and most specifically, modern groundwater in the vicinity of St. Agatha. Above 475.0cm, $^{87}\text{Sr}/^{86}\text{Sr}$ increases, suggestive of a different and/or at least additional water source.

The low $\delta^{18}\text{O}_{\text{marl}}$ of Interval A (average $+19.0 \pm 0.7\text{‰}$ (1SD)) could arise from low $\delta^{18}\text{O}$ inputs and low evaporation, assuming a near constant temperature for marl precipitation. There is no O-isotope evidence for glacial meltwater in the St. Agatha system, even at the earliest stages of marl precipitation (F. Longstaffe, personal communication, 2016). This time period, however, is associated with cooler and moister conditions in southern Ontario (Edwards et al., 1996), which would have been accompanied by lower groundwater and precipitation $\delta^{18}\text{O}$. As discussed earlier, groundwater inflow was likely the major lake input during this interval, and groundwater is known to have lower $\delta^{18}\text{O}$ than coeval precipitation in cool climate regimes. Higher lake levels would also be typical of cooler and moister conditions. High lake levels and increased lake volume has been shown to produce lower $\delta^{18}\text{O}_{\text{marl}}$ (Li and Ku, 1997). The highest average $\delta^{13}\text{C}_{\text{marl}}$ occurs in Interval A ($-2.0 \pm 0.7\text{‰}$ (1SD)) and shows only limited covariation with $\delta^{18}\text{O}_{\text{marl}}$. As discussed earlier, weaker covariation is reflective of a more open lake system (Figure 5.4). The $\delta^{13}\text{C}_{\text{marl}}$ is likely reflective of groundwater DIC, derived mostly by dissolution of host carbonate rocks and overlying tills.

No samples of *G. parvus* were available from Interval A. The abundance of *G. parvus* decreased significantly below ~320cm in the core, consistent with cooler temperatures and deepening lake water (Yang et al., 2000), as suggested for the interval A time period.

Driven in particular by one sample with a particularly low $\delta^{44/42}\text{Ca}_{\text{marl}}$ (-0.61‰), Interval A also has the lowest average $\delta^{44/42}\text{Ca}_{\text{marl}}$ ($-0.41 \pm 0.12\text{‰}$) of the marl succession. Holmden (2009)

noted that enrichment of lighter Ca-isotopes in carbonates precipitated from solution is the product of rate-dependent, kinetic isotope fractionation. Marl calcite precipitates very rapidly once the trigger temperature and pH is reached in a lake, with whiting events lasting only hours to days.

Assuming a constant input (source) water $\delta^{44/42}\text{Ca}$, the low $\delta^{44/42}\text{Ca}_{\text{marl}}$ of Interval A may have arisen from overall cooler climatic conditions over the summer months, which led to lower primary productivity, particularly the bloom of blue-green algae that trigger marl precipitation. Hence the amount of marl precipitated during a whiting event would likely be less than under warmer conditions. If so, the available reservoir of the lighter Ca-isotopes (^{42}Ca , ^{40}Ca) relative to ^{44}Ca may have been unlimited, facilitating marl production with lower $\delta^{44/42}\text{Ca}_{\text{marl}}$, particularly if the rapid rate of marl crystallization caused it to proceed out of Ca-isotope equilibrium with water .

5.4.2 Interval B (475.0 to 345.0cm)

Interval B spans 475.0 to 345.0cm. Overall, it is characterized by upwards increasing $\delta^{44/42}\text{Ca}_{\text{marl}}$ and $\delta^{18}\text{O}_{\text{marl}}$, fluctuating $\delta^{13}\text{C}_{\text{marl}}$ and high and slightly variable marl $^{87}\text{Sr}/^{86}\text{Sr}$ (Figure 5.10 and 5.11). As shown in Figure 5.4, a transition from a more open lake system during Interval A to a more closed lake system begins near the base of Interval B. The shared, increasing upward trend of $\delta^{44/42}\text{Ca}_{\text{marl}}$ and $\delta^{18}\text{O}_{\text{marl}}$ ($r^2 = 0.48$), suggests a common process that drives this pattern. In comparison to the trend observed in $\delta^{44/42}\text{Ca}_{\text{marl}}$ and $\delta^{18}\text{O}_{\text{marl}}$ ($r^2 = 0.48$), the $\delta^{44/42}\text{Ca}_{\text{marl}}$ and $\delta^{13}\text{C}_{\text{marl}}$, exhibit only a weak overall increasing upward trend ($r^2=0.06$), which suggests that these isotopic systems have separate controls or are influenced by different mechanisms at different times.

More specifically, the $\delta^{18}\text{O}_{\text{marl}}$ generally increases from +18.7 to +20.7‰ upwards in Interval B, while $\delta^{13}\text{C}_{\text{marl}}$ cycles twice from as low as ~ -4.6 to as high as -2.0 ‰. The decoupling between $\delta^{18}\text{O}_{\text{marl}}$ and $\delta^{13}\text{C}_{\text{marl}}$ towards the base of Interval B likely records conditions just before transition from a more open to a more closed lake. Assuming a close-to-constant marl precipitation temperature, the overall increase in $\delta^{18}\text{O}_{\text{marl}}$ throughout Interval B is most simply attributed to higher source $\delta^{18}\text{O}_{\text{water}}$ and/or increased evaporation. Warmer conditions would result in higher $\delta^{18}\text{O}_{\text{water}}$ for both precipitation and groundwater fed by that precipitation (Abell and Williams,

1989). The correlation between $\delta^{13}\text{C}_{\text{marl}}$ and $\delta^{18}\text{O}_{\text{marl}}$ in Interval B from 474.5 to 344.5cm ($r^2 = 0.0$) is nonexistent, and since $r^2 < 0.49$, this indicates the interval was more open (Li and Ku, 1997). A more open lake system would not experience the evaporative effects necessary to increase the $\delta^{18}\text{O}_{\text{marl}}$ as was measured.

Upper portions of Interval B have the highest $\delta^{44/42}\text{Ca}_{\text{marl}}$ (-0.11‰) of the entire marl sequence, increasing from -0.42‰ near its bottom to -0.22‰ near its top. This increase could reflect a change in water input, but the $^{87}\text{Sr}/^{86}\text{Sr}$ does not suggest a major shift in water source throughout this interval (Figure 5.4). A rise in temperature of $\sim 12^\circ\text{C}$ could explain this increase, following the equation of Gussone et al. (2005) and assuming equilibrium. This explanation, however, is unlikely given the tendency of marl precipitation to be triggered at more or less a constant temperature, and the probability of Ca-isotope equilibrium during marl precipitation. We speculate instead that Ca-limitation during whiting events could explain the increasing $\delta^{44/42}\text{Ca}_{\text{marl}}$. An overall warming climate would encourage greater algal activity, thus driving an increase in the amount of marl produced. Ca-limitation would lead to progressively higher marl $\delta^{44/42}\text{Ca}$ as the relative abundances of the lighter Ca-isotopes (^{40}Ca and ^{42}Ca) in lakewater, which are preferred during kinetically driven marl precipitation, were depleted relative to ^{44}Ca . This process is akin to that of Rayleigh distillation in a cloud – considered as a closed system–, where overtime the $\delta^{18}\text{O}$ of precipitation gradually becomes lower as the availability of ^{18}O is reduced; in other words, ^{18}O preferentially leaves the cloud as precipitation, and ^{16}O remains as vapour. As the abundance of ^{18}O in the vapour decreases with progressive rainout, subsequent precipitation acquires lower and lower $\delta^{18}\text{O}$. Unlike Rayleigh distillation of water in a cloud arising from condensation at equilibrium, marl calcite crystallization in a lake is kinetically driven and equilibrium conditions cannot be presumed.

At depths less than $\sim 320.0\text{cm}$, the abundance of *G. parvus* increases, consistent with warmer and shallower waters in which macrophyte vegetation is prevalent. The $\delta^{18}\text{O}_{\text{marl}}$, $\delta^{13}\text{C}_{\text{marl}}$, and $\delta^{44/42}\text{Ca}$ of two shells were compared with coeval marl calcite. The average $\delta^{18}\text{O}_{\text{shell}}$ is $+21.1 \pm 0.4\text{‰}$ (1SD), $\sim 1.3\text{‰}$ higher than the average $\delta^{18}\text{O}_{\text{marl}}$ (Figure 5.5). Cooler temperatures would produce a larger carbonate-water O-isotope fractionation. This suggests that the average temperature of shell aragonite crystallization was lower than marl calcite, consistent with shell formation during spring and continuing through to fall, rather than at the peak of summer as is likely for marl. The

average $\delta^{13}\text{C}_{\text{shell}}$ is $-8.4 \pm 1.4\text{‰}$ (1SD), $\sim 5\text{‰}$ lower than the average $\delta^{13}\text{C}_{\text{marl}}$. This suggests that the DIC pool utilized by the shells had lower $\delta^{13}\text{C}$ than that utilized by marl calcite. This observation is consistent with increasing $\delta^{13}\text{C}_{\text{DIC}}$ related to summer algal productivity. Shell formation before and after this time would encounter a much less ^{13}C -enriched DIC pool. Significant differences were not observed between marl and shell $\delta^{44/42}\text{Ca}$ (Figure 5.9).

Overall, the isotopic data for Interval B signal a change from a more open lake characterized by cooler, deeper water and lower marl accumulation rates, to a more closed system characterized by greater summer warmth and increased lacustrine productivity. The variations in each of the proxy isotopic compositions are consistent with fluctuations in lake level driven largely by evaporation within an overall pattern of warmer and drier conditions relative to Interval A.

5.4.3 Interval C (345.0 to 192.0cm)

Interval C (345.0 to 192.0cm) exhibits variability across all isotopic systems except for $^{87}\text{Sr}/^{86}\text{Sr}$ (Figures 5.10 and 5.11). New Sr inputs to the lake with distinctly different Sr-isotope signatures did not occur. Values of $\delta^{44/42}\text{C}_{\text{marl}}$ cycle between -0.48 and -0.15‰ , with an average of $\sim 0.3\text{‰}$. Values of $\delta^{18}\text{O}_{\text{marl}}$ vary by $\sim 2\text{‰}$ ($+19.2$ to $+20.8\text{‰}$) in strong positive correlation ($r^2=0.82$) with a $\sim 3\text{‰}$ variation in $\delta^{13}\text{C}_{\text{marl}}$ (-5.6 to -2.2‰); this signifies an increasingly closed lake system (Li and Ku, 1997). Both $\delta^{44/42}\text{C}_{\text{marl}}$ and $\delta^{18}\text{O}_{\text{marl}}$ show a weak upwards trend towards lower values.

The progressive accumulation of marl calcite would have reduced the depth of the St. Agatha kettle lake, making it more susceptible to lake level fluctuations arising from changes in water inputs (I) and outputs (E), the latter mostly arising from evaporation. Increased abundances of *G. parvus* shells above $\sim 320\text{cm}$ are diagnostic of a generally warmer and shallower lake habitat (Yang et al., 2000), which had been established by the end of Interval B. That said, the cyclic oscillations in O-, C- and Ca-isotope compositions in Interval C, particularly for $\delta^{18}\text{O}_{\text{marl}}$, indicate alternating warmer and cooler conditions and associated variations in E/I under overall warmer conditions than existed during Interval A and most of Interval B.

Overall the data suggest warmer conditions than earlier in the St. Agatha kettle lake system. Nonetheless, both $\delta^{18}\text{O}_{\text{marl}}$ and $\delta^{13}\text{C}_{\text{marl}}$ show an overall trend of decrease from the beginning to the end of Interval C. Assuming that marl crystallization at about the same temperature each

year, lower values of $\delta^{18}\text{O}_{\text{marl}}$ most likely indicates a decrease in evaporation and/or water $\delta^{18}\text{O}_{\text{water}}$ inputs, consistent with higher lake levels and wetter conditions. The lower $\delta^{13}\text{C}_{\text{marl}}$ that accompanies decreases in $\delta^{18}\text{O}_{\text{marl}}$ is consistent with reduced algal productivity under cooler and wetter conditions. Higher values of both $\delta^{13}\text{C}_{\text{marl}}$ and $\delta^{18}\text{O}_{\text{water}}$ likewise signal a return to warmer conditions and greater lacustrine productivity.

Values of $\delta^{44/42}\text{Ca}_{\text{marl}}$ in Interval C fluctuate substantially. For most samples, higher $\delta^{44/42}\text{Ca}_{\text{marl}}$ correlates with higher $\delta^{18}\text{O}_{\text{marl}}$ and $\delta^{13}\text{C}_{\text{marl}}$ which is consistent with warming, increased primary productivity and Ca-limitation of marl production. In two exceptions (266.5cm, 201.5cm), however, spikes to higher $\delta^{44/42}\text{Ca}_{\text{marl}}$ (-0.15‰) are associated with lower $\delta^{18}\text{O}_{\text{marl}}$ ($+19.2\text{‰}$, $+19.5\text{‰}$) (Figure 5.11). By comparison, coexisting *G. parvus* has $\delta^{44/42}\text{Ca}_{\text{shell}}$ (-0.40‰ , -0.37‰ ; Figure 5.9) and $\delta^{18}\text{O}_{\text{shell}}$ ($+20.1\text{‰}$, $+21.4\text{‰}$; Figure 5.5) within its typical range of variation in Interval C. The cause of this variation in $\delta^{44/42}\text{Ca}_{\text{shell}}$ is unclear. Slower marl crystallization during a cooler period of lower productivity could perhaps have driven $\delta^{44/42}\text{Ca}_{\text{marl}}$ closer to equilibrium values, but this seems unlikely. Alternatively, an additional water source, with similar $^{87}\text{Sr}/^{86}\text{Sr}$ (and/or very low Sr content) but differing $\delta^{44/42}\text{Ca}_{\text{water}}$ may have been involved. Increased direct input of rain and snow, however, can probably be ruled out as such contributions would likely have had lower $\delta^{44/42}\text{Ca}_{\text{water}}$ and higher $\delta^{18}\text{O}_{\text{water}}$ than groundwater inputs. Also, any change in the sources of water inputs would need to have been specific to the period of marl formation.

The average $\delta^{18}\text{O}$ of shell aragonite in Interval C is $+21.1 \pm 0.7\text{‰}$ (1SD), $\sim 1\text{‰}$ higher than the average coeval marl calcite (Figure 5.5). The difference between the average $\delta^{18}\text{O}_{\text{shell}}$ and average $\delta^{18}\text{O}_{\text{marl}}$, however is slightly smaller in Interval C ($\sim 1\text{‰}$) than in Interval B ($\sim 1.3\text{‰}$). This suggests that the temperature difference between summer (marl) and spring to fall (shells) was probably less during Interval C than Interval B. At least three times during Interval C, shell aragonite and marl calcite $\delta^{18}\text{O}$ are more or less identical (Figure 5.4), which suggests an average temperature during the spring to fall period that was not much different from summer. The average $\delta^{13}\text{C}_{\text{shell}}$ ($-8.6 \pm 1.4\text{‰}$ (1SD)) in Interval C, however, remained at $\sim 5\text{‰}$ lower than coeval marl calcite, which is typical of the entire St. Agatha marl sequence.

5.4.4 Interval D (192.0 to 128.0cm)

Interval D spans depths from 192.0 to 128.0cm at which point the peat-marl interface is encountered. There is a small rise in $^{87}\text{Sr}/^{86}\text{Sr}$ at the base of Interval D followed by a steady but small decrease to lower ratios. No large changes in water inputs are indicated by the Sr-isotope compositions (Figure 5.10).

Values of $\delta^{44/42}\text{Ca}_{\text{marl}}$ (-0.49 to -0.17‰), $\delta^{18}\text{O}_{\text{marl}}$ ($+19.0$ to $+21.3\text{‰}$) and $\delta^{13}\text{C}_{\text{marl}}$ (-5.2 to -2.5‰) oscillate but generally increase upwards, reversing the gradual upward decrease noted for Interval C (Figure 5.10 and 5.11). Results for these isotopic systems tend to be positively correlated; the strongest correlation is between $\delta^{18}\text{O}_{\text{marl}}$ and $\delta^{13}\text{C}_{\text{marl}}$ ($r^2 = 0.71$), and the weakest correlation is between $\delta^{44/42}\text{Ca}_{\text{marl}}$ and $\delta^{13}\text{C}_{\text{marl}}$ ($r^2 = 0.19$). There is moderate correlation between $\delta^{18}\text{O}_{\text{marl}}$ and $\delta^{44/42}\text{Ca}_{\text{marl}}$ ($r^2 = 0.36$). There is a strong spike to higher values at 138.0cm, near the top of the section. There, the highest $\delta^{18}\text{O}_{\text{marl}}$ ($+21.3\text{‰}$) of the entire marl section is encountered, along with the second highest $\delta^{44/42}\text{Ca}_{\text{marl}}$ (-0.17‰). This overall trend to higher values in each of $\delta^{44/42}\text{Ca}_{\text{marl}}$, $\delta^{18}\text{O}_{\text{marl}}$ and $\delta^{13}\text{C}_{\text{marl}}$ is again interpreted – for the same reasons as discussed earlier – to reflect warming conditions in an ever-shallowing, closed-system lake that was being infilled by marl.

Marl precipitation ceased when conditions shifted to those of a bog that produced the peat deposits that overlie the marl. The uppermost part of the marl section is likely missing. Age-dating suggests a ~ 2800 yr gap between the top of the marl and the base of the peat (J. Walker and F. Longstaffe, personal communication, 2019).

The *G. parvus* average $\delta^{18}\text{O}$ is $+20.8 \pm 1.1\text{‰}$ (1SD), $\sim 1.1\text{‰}$ higher than coeval marl ($+19.9 \pm 0.7\text{‰}$ (1SD)), again reflective of a cooler average temperature for shell formation. As for Interval C, the difference between the average $\delta^{18}\text{O}_{\text{shell}}$ and $\delta^{18}\text{O}_{\text{marl}}$ ($\sim 0.8\text{‰}$) is smaller than in Interval B ($\sim 1.3\text{‰}$) (Figure 5.5), again indicating a smaller difference between average summer and spring to fall temperatures. The average *G. parvus* $\delta^{13}\text{C}_{\text{shell}}$ ($-10.4 \pm 1.2\text{‰}$ (1SD)) is the lowest of all intervals and $\sim 6\text{‰}$ lower than coeval $\delta^{13}\text{C}_{\text{marl}}$ ($-4.5 \pm 0.9\text{‰}$ (1SD)) (Figure 5.6). This suggests greater availability of low $\delta^{13}\text{C}_{\text{DIC}}$ during the shell formation period compared to that during marl crystallization when algal blooms would have caused residual DIC to be

enriched in ^{13}C . There was no systematic difference in shell and coeval marl $\delta^{44/42}\text{Ca}$, however, beyond those which can be attributed to analytical error.

5.4.5 Summary

Figure 5.12 summarizes the dominant environmental controls on $\delta^{44/42}\text{Ca}_{\text{marl}}$ (-0.61 to -0.11‰), $\delta^{18}\text{O}_{\text{marl}}$ ($+18.4$ to $+21.3\text{‰}$), and $\delta^{13}\text{C}_{\text{marl}}$ (-5.6 to -0.9‰) in Intervals A-D.

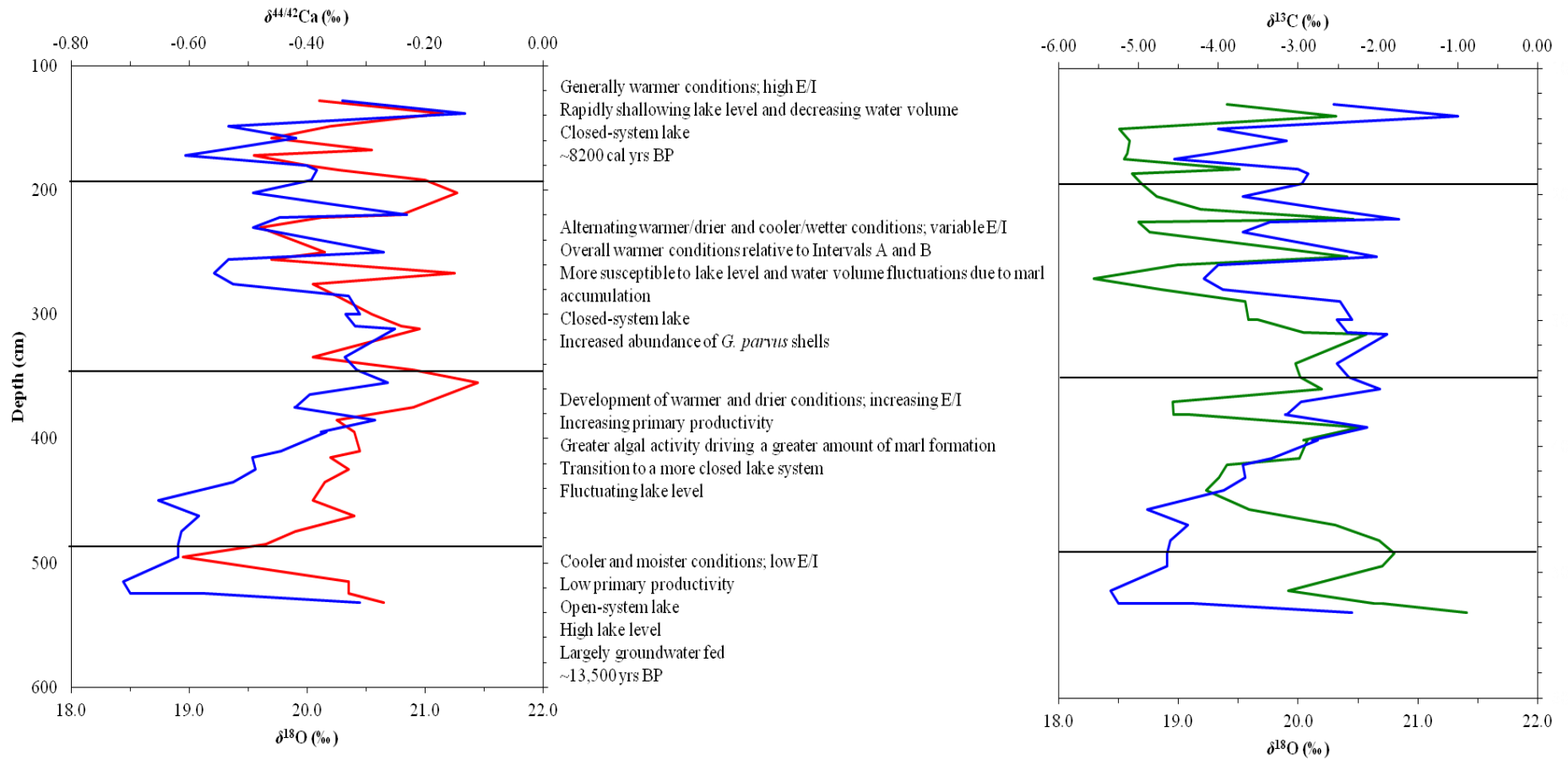


Figure 5.11: Controls on marl deposition in the St. Agatha kettle lake system. Depth (cm) versus $\delta^{44/42}\text{Ca}_{\text{marl}}$ (red) and $\delta^{18}\text{O}_{\text{marl}}$ (blue) (left), and $\delta^{13}\text{C}$ (green) and $\delta^{18}\text{O}$ (blue) (right).

Chapter 6

6 CONCLUSION

The St. Agatha kettle lake deposits of southern Ontario contain a ~400cm section of endogenic marl calcite, interspersed with biogenic aragonite (shells) deposited between ~13,500 and ~8,200 cal yrs BP (J. Walker and F. Longstaffe, personal communication, 2019). The availability of coeval calcite and aragonite in this stratigraphic sequence has been used to evaluate the dominant processes that have determined the measured Ca-isotope compositions of these freshwater carbonates. The carbonate $\delta^{18}\text{O}$, $\delta^{13}\text{C}$ and $^{87}\text{Sr}/^{86}\text{Sr}$ ratios have been used to help establish the climatic and environmental conditions and water sources during marl calcite crystallization, and hence inform interpretation of the carbonate $\delta^{44/42}\text{Ca}$.

This study developed an accurate and precise protocol to purify and extract Ca-isotopes from endogenic and biogenic carbonates, groundwater and bedrock, and a methodology for Ca-isotope measurements using high precision Multi-Collector ICPMS (MC-ICPMS). A multi-step Ca-purification protocol designed to remove interference products and OM from marl calcite and shell aragonite samples was adapted from Harouaka et al. (2016). The treatment used for bedrock samples was adapted from Moore et al. (2013), and included a multi-step procedure to remove OM and to isolate the sulphate fraction and any other mineral components. The Ca-separation column chromatographic protocol was adapted from Valdes et al. (2014), and was demonstrated to provide high yields and low Ca blanks. Full column yields were better than 97%, and blanks were on average $33 \pm 18\text{ng}$ (1SD), representing 0.04 – 0.15% of the total Ca loaded into a chromatographic column. Given the high Ca column yields from this protocol and the measured Ca isotopic composition of processed SRM 915b, corrections of sample Ca-isotope compositions were unnecessary.

High precision analyses were conducted at the Trent University Water Quality Center using a Thermo Neptune MC-ICPMS for Ca-isotope measurements and a Nu Instrument Plasma II MC-ICPMS for Sr-isotope ratio measurements. A total of 100 Ca-isotope measurements and 59 Sr-isotope ratio measurements of standards SRM 915b and OSIL Seawater, and samples of marl calcite, shell aragonite and groundwater, a reproducibility of 0.1‰ or better was achieved. These

results indicate that the collection of Ca-isotope measurements using a high precision MC-ICPMS, while challenging, is not only possible but provides comparable results with those reported for other methods, such as Thermal Ionization Mass Spectrometry (TIMS).

The successful collection of such a large number of marl calcite and shell aragonite Ca-isotope compositions using MC-ICPMS represents an important addition to the currently very limited data for freshwater lakes globally. In particular, these data help to shed new light onto the controls of Ca-isotope fractionation in carbonate-freshwater systems.

The sources of water to the St. Agatha kettle lake were thought to be strong contributors to the $\delta^{44/42}\text{Ca}$ of the marl calcite and shell aragonite, with groundwater and surface water/precipitation expected to be dominant sources. Higher Mg, Mn and Fe concentrations and lower Ba concentrations and $^{87}\text{Sr}/^{86}\text{Sr}$ ratios in the lowermost ~50cm of the marl compared to upper portions of the core indicate a shift in lakewater composition. These lower $^{87}\text{Sr}/^{86}\text{Sr}$ ratios trend towards modern groundwater $^{87}\text{Sr}/^{86}\text{Sr}$ ratios, which are typical of the region's Middle Devonian Lucas Formation. The higher $^{87}\text{Sr}/^{86}\text{Sr}$ ratios of marl calcite higher in the core better match mixing of shallow groundwater hosted by the region's Middle Devonian Amherstberg Formation, lower salinity regions portions of the Silurian Guelph Formation, and Sr-rich brines of the Guelph Formation and Cambrian units. Direct contributions of surface water (precipitation) are also possible.

While water source supplied the St. Agatha kettle lake with the necessary dissolved components for marl calcite crystallization, it is the evolution of the water in the lake that likely provided the strongest controls on the measured $\delta^{44/42}\text{Ca}$. Based on marl $\delta^{18}\text{O}$ and $\delta^{13}\text{C}$, the St. Agatha kettle lake appears to have initially been an open lake system, but transitioned to a closed lake system, beginning at ~50cm from the base of the core. Open lake systems have multiple inputs, outflows and are most strongly influenced by the isotope composition of source waters, whereas water in a closed lake system has a longer residence time and evaporative effects on its composition, and on lake level, are more prominent. This evolution from an open to a closed lake was likely a key factor controlling carbonate $\delta^{44/42}\text{Ca}$ in this system. With this control in mind, the isotopic variability observed in the St. Agatha marl deposits were subdivided into four intervals (A to D),

with their boundaries defined using changes in elemental concentration ratios and marl $\delta^{18}\text{O}$, $\delta^{13}\text{C}$ and $\delta^{44/42}\text{Ca}$.

Interval A (532.0 to 475.0cm) contains the earliest stages of marl crystallization, and is defined by rising $^{87}\text{Sr}/^{86}\text{Sr}$ ratios (0.708547 to 0.709446), low $\delta^{18}\text{O}_{\text{marl}}$, the highest average $\delta^{13}\text{C}_{\text{marl}}$ and low $\delta^{44/42}\text{Ca}_{\text{marl}}$. The rising $^{87}\text{Sr}/^{86}\text{Sr}$ ratios, as noted above, suggest a change in source water or additional source water contributions. Higher lake levels and increased lake volume, as well as greater groundwater inflows contribute to a lower $\delta^{18}\text{O}_{\text{marl}}$. This interval is associated with cooler, moister conditions and lower primary productivity, especially of the blue-green algae that commonly triggers marl precipitation. As a result, the amount of marl crystallized likely was less than during warmer periods, and the available reservoir of light Ca-isotopes was unlimited, facilitating lower $\delta^{44/42}\text{Ca}_{\text{marl}}$. Rate-dependent, kinetic isotope fractionation is likely a strong driver of marl calcite Ca-isotope compositions in the St. Agatha deposits, which leads to the low non-equilibrium values obtained for $\delta^{44/42}\text{Ca}_{\text{marl}}$.

Interval B (475.0 to 345.0cm) is defined by a general trend of increasing $\delta^{44/42}\text{Ca}_{\text{marl}}$ and $\delta^{18}\text{O}_{\text{marl}}$, fluctuating $\delta^{13}\text{C}_{\text{marl}}$ and overall high $^{87}\text{Sr}/^{86}\text{Sr}$ ratios. Most notably, this interval marks the transition from an open to a closed lake system. This interval is characterized by rising temperatures, which results in higher source $\delta^{18}\text{O}_{\text{water}}$ for precipitation and groundwater, and increased evaporation. Warmer temperatures encourage algal activity, which increases marl crystallization. Kinetically driven marl precipitation prefers lighter Ca-isotopes (^{40}Ca and ^{42}Ca). At times of increased marl crystallization, therefore, Ca-limitation could lead to higher $\delta^{44/42}\text{Ca}_{\text{marl}}$. Ca-limitation would necessitate the incorporation of heavier Ca-isotopes into marl calcite during times of increased carbonate production. The appearance of *G. parvus* shells further supports warmer temperatures during this interval.

Interval C (345.0 to 192.0cm) exhibits the greatest isotopic variability, except $^{87}\text{Sr}/^{86}\text{Sr}$ – the latter's constant ratios indicate little change in water sources during this time period. The accumulation of marl calcite in the St. Agatha kettle lake reduced the lake level, making it more susceptible to lake level fluctuations. Cyclic oscillations in O-, C-, and Ca-isotope compositions reflect alternating cooler and warmer conditions, with an overall trend to warmer conditions. Lower $\delta^{18}\text{O}_{\text{marl}}$ reflects a decrease in evaporation and/or $\delta^{18}\text{O}_{\text{water}}$ sources, and is accompanied by

lower $\delta^{13}\text{C}_{\text{marl}}$ consistent with reduced algal activity during cooler, wetter conditions, and vice versa. Higher $\delta^{44/42}\text{Ca}_{\text{marl}}$ mostly correlates with higher $\delta^{18}\text{O}_{\text{marl}}$ and $\delta^{13}\text{C}_{\text{marl}}$ during warming conditions, where algal activity increases and Ca-limitation occurs during kinetically-driven marl precipitation. The abundance of *G. parvus* shells is high in this interval, which is also indicative of overall warmer conditions and a shallower lake. Shell precipitation typically occurred at lower temperatures than marl calcite, consistent with shell growth from spring through fall.

Interval D (192.0cm to 128.0cm) contains the last stages of marl calcite crystallization, which ends at the marl-peat interface. The values for $\delta^{44/42}\text{Ca}_{\text{marl}}$, $\delta^{18}\text{O}_{\text{marl}}$ and $\delta^{13}\text{C}_{\text{marl}}$ oscillate widely, but increase overall upwards in the section. The lake level continued to shallow, a product of continued marl accumulation and warm conditions. Higher $\delta^{44/42}\text{Ca}_{\text{marl}}$ likely reflected greater Ca-limitation arising from a reduced lake volume and rising temperatures, both of which supported algal blooms until the death of the lake.

Overall, it appears that the dominant controls of $\delta^{44/42}\text{Ca}_{\text{marl}}$ in the St. Agatha kettle lake system were linked to rising temperatures, which led to increasing primary productivity, and consequently Ca-limitation in the lake water driven by extensive marl precipitation. Rate-dependent, kinetic isotope effects strongly affect the Ca-isotope fractionation in the carbonate-lake water system, leading to nonequilibrium values of $\delta^{44/42}\text{Ca}_{\text{marl}}$. Values of $\delta^{18}\text{O}_{\text{marl}}$ are driven by evaporation, and the composition of source water. Values of $\delta^{13}\text{C}_{\text{marl}}$ vary as a function of the DIC pool during marl precipitation, with higher $\delta^{13}\text{C}_{\text{DIC}}$ during times of increased algal activity and vice versa.

The St. Agatha kettle lake deposits are exceptionally unique and the $\delta^{18}\text{O}$, $\delta^{13}\text{C}$, $\delta^{44/42}\text{Ca}$ and $^{87}\text{Sr}/^{86}\text{Sr}$ ratios of the marl calcite and shelly aragonite can be used to obtain a focused environmental history of one freshwater lake in southern Ontario from the late Pleistocene to the middle Holocene. This study highlights in particular the complexity of Ca-isotope variation in freshwater carbonates and the need for additional detailed investigations and experiments to test the ideas presented in this thesis.

6.1 Future Work

Many questions remain unanswered. First, in future work the relationship between marl calcite and shell aragonite $\delta^{44/42}\text{Ca}$ could be explored in more detail, particularly through analysis of a

larger number of coeval samples. The systematic offset between the $\delta^{44/42}\text{Ca}$ of coeval calcite and aragonite typically reported in the literature was not always observed in this study, and the possible reasons for that difference (*e.g.*, temperature, rate of crystallization, Ca-limitation, metabolic processes) need to be understood.

Second, a greater number of species of shelly fauna should be analyzed. Exploration of inter-species variability in $\delta^{44/42}\text{Ca}_{\text{shell}}$ from the St. Agatha deposits could reveal more about the Ca-isotope structure of the lake and whether there was Ca-isotope partitioning between benthic and pelagic species. The initial work reported here hinted at the possible variability in $\delta^{44/42}\text{Ca}$ between clam species and mollusc species, but the results were not conclusive.

Third, an in-depth study is needed on the $\delta^{44/42}\text{Ca}$ of possible source waters. This could be achieved by analyzing the Ca-isotope composition of all Ca-rich minerals in the glacial tills and bedrock formations associated with the St. Agatha kettle lake deposits, and by collecting and analyzing the region's rainwater, surface water and all groundwater aquifers. These data would offer deeper insight into the role of source water variability on $\delta^{44/42}\text{Ca}_{\text{shell}}$.

Fourth, a Ca-isotope study of a modern lake actively precipitating marl calcite, preferably near St. Agatha, could explore in more detail the relative importance of variables such as algal productivity, marl crystallization rate, temperature and Ca-availability on $\delta^{44/42}\text{Ca}_{\text{marl}}$ and whether the initial Ca-isotope compositions undergo further isotopic exchange with porewaters after initial marl formation.

References

- Abell, P.I. (1985). Oxygen Isotope Ratios in Modern African Gastropod Shells: A Database for Paleoclimatology. *Chemical Geology*, **58**, 183-193.
- Abell, P.I., & Williams, M. A. J. (1989). Oxygen and Carbon Isotope Ratios in Gastropod Shells as Indicators of Paleoenvironments in the Afar Region of Ethiopia. *Palaeogeography, Palaeoclimatology, Palaeoecology*, **74**, 265-278.
- Andrén, H., Rodushkin, I., Stenberg, A., Malinosky, D., & Baxter, D.C. (2004). Sources of Mass Bias and Isotope Ratio Variation in Multi-collector ICP-MS: Optimization of Instrument Parameters based on Experimental Observations. *Journal of Analytical Atomic Spectrometry*, **19**, 1217-1224.
- Apolinarska, K., & Hammerlund, D. (2009). Multi-component Stable Isotope Records Form Late Weichselian and Early Holocene Lake Sediments at Imiołki, Poland: Palaeoclimatic and Methodological Implications. *Journal of Quaternary Science*, **24**, 948-959.
- Armstrong, D.K., & Dodge, J.E.P. (2007). Paleozoic Geology of Southern Ontario. *Ontario Geological Survey, Project Summary and Technical Document*.
- Banner, J.L. (2003). Radiogenic Isotopes: Systematics and Applications to Earth Surface Processes and Chemical Stratigraphy. *Earth Science Reviews*, **65**, 141-194.
- Baskaran, M. (2011). Handbook of Environmental Isotope Geochemistry. Springer. 7th Ed.
- Benson, L.V., Meyers, P.A., & Spencer, R.J. (1991). Change in the Size of Walker Lake During the Past 5000 Years. *Palaeogeography, Palaeoclimatology, Palaeoecology*, **81**, 189-214.
- Böhm, F., Joachimski, M.M., Dullo, W-C., Eisenhauer, A., Lehnert, H., Reitner, J., & Wörheide, G. (2000). Oxygen Isotope Fractionation in Marine Aragonite of Coralline Sponges. *Geochimica et Cosmochimica Acta*, **64**, 1695-1703.
- Boutton, T.W. (1991). Stable Carbon Isotope Ratios of Natural Materials: I. Sample Preparation and Mass Spectrometric Analysis. In: Carbon Isotope Techniques. Academic Press, New York.

- Brunskill, G.J. (1969). Fayetteville Green Lake, New York, II. Precipitation and Sedimentation of Calcite in a Meromictic Lake with Laminated Sediments. *Limnology and Oceanography*, **14**, 830-847.
- Burch, J.B. (1982). Freshwater Snails (Mollusca: Gastropoda) of North America. *United States Environmental Protection Agency*.
- Burke, W.H., Denison, R.E., Hetherington, E.A., Koepnick, R.B., Nelson, H.F., & Otto, J.B. (1982). Variation of Seawater $^{87}\text{Sr}/^{86}\text{Sr}$ Throughout Phanerozoic Time. *Geology*, **10**, 516-519.
- Capo, R.C., & Chadwick, O.A. (1999). Sources of Strontium and Calcium in Desert Soil and Calcrete. *Earth and Planetary Science Letters*, **170**, 61-72.
- Carré, M., Bentaleb, I., Bruguier, O., Ordinola, E., Barrett, N.T., Fontugne, M. (2006). Calcification Rate Influence on Trace Element Concentrations in Aragonitic Bivalve Shells: Evidences and Mechanisms. *Geochimica et Cosmochimica Acta*, **70**, 4906-4920.
- Carter, T.R., & Armstrong, D.K. (2010). The Subsurface Paleozoic Stratigraphy of Southern Ontario. Special Volume 7. Ontario Geological Survey.
- Carter, T.R., & Fortner, L. (2011). Regional Bedrock Aquifers and a Conceptual Groundwater Flow Model for Southern Ontario. *Petroleum Operations, Ministry of Natural Resources*.
- Carter, T.R., & Fortner, L. (2012). Regional Bedrock Aquifers and a Conceptual Groundwater Flow Model for Southern Ontario. *Petroleum Operations, Ministry of Natural Resources*.
- Cassidy, K.O. (2011). Evaluating Algal Growth at Different Temperatures. University of Kentucky. MSc Thesis.
- Cespuglio, G., Piccinetti, C., & Longinelli, A. (1999). Oxygen and Carbon Isotope Profiles from *Nassa Mutabilis* Shells (Gastropoda): Accretion Rates and Biological Behaviour. *Marine Biology*, **135**, 627-634.
- Clarke, A.H. (1981). The Freshwater Molluscs of Canada. National Museum of Natural Sciences, National Museums of Canada, Ottawa.
- Colla, C.A., Wimpenny, J., Y, Q-Z, Rustad, J.R., & Casey, W.H. (2013). Calcium-isotope Fractionation Between Solution and Solids with Six, Seven or Eight Oxygens Bound to Ca(II). *Geochimica et Cosmochimica Acta*, **121**, 363-373.

- Coplen, T.B. (2011). Guidelines and Recommended Terms for Expression of Stable-Isotope-Ratio and Gas-Ratio Measurement Results. *Rapid Communications in Mass Spectrometry*, **25**, 2538-2560.
- Dansgaard, W. (1964). Stable Isotopes in Precipitation. *Tellus*, **16**, 436-468.
- Dettman, D.L., Reische, A.K., & Lohmann, K.C. (1999). Controls on the Stable Isotope Composition of Seasonal Growth Bands in Aragonitic Fresh-water Bivalves (Unionidae). *Geochimica et Cosmochimica Acta*, **63**, 1049-1057.
- Dillon, R.T. (2000). *The Ecology of Freshwater Molluscs*. Cambridge University Press.
- Dollar, P.S., Frappe, S.K., & McNutt, R.H. *Geochemistry Formation Waters, Southwestern Ontario, Canada and Southern Michigan, USA: Implication for Origin and Evolution*. Published by *Ministry of Northern Development and Mines*. Ontario Geological Survey.
- Edwards, T. W. D., Wolfe, B.B., & MacDonald, G. M. (1996). Influence of Changing Atmospheric Circulation on Precipitation $\delta^{18}\text{O}$ – Temperature Relations in Canada During the Holocene. *Quaternary Research*, **46**, 211-218.
- Effler, S. (1984). Carbonate Equilibria and the Distribution of Inorganic Carbon in Saginaw Bay. *Journal of Great Lakes Research*, **10**, 3-14.
- Emrich, K., Ehalt, D.H., & Vogel, J.C. (1970). Carbon Isotope Fractionation During the Precipitation of Calcium Carbonate. *Earth and Planetary Science Letters*, **8**, 363-371.
- Fantle, M.S., & Tipper, T. (2014). Calcium isotopes in the Global Biogeochemical Ca Cycle: Implications for Development of a Ca Isotope Proxy. *Earth-Science Reviews*, **129**, 148-177.
- Fietzke, J., & Eisenhauer, A. (2006). Determination of Temperature-Dependent Stable Strontium Isotope ($^{88}\text{Sr}/^{86}\text{Sr}$) Fractionation via Bracketing Standard MC-ICP-MS. *Geochemistry Geophysics Geosystems*, **7**.
- Frappé, S.K., Fritz, P., & McNutt, R.H. (1984). Water-rock Interaction and Chemistry of Groundwaters from the Canadian Shield. *Geochimica et Cosmochimica Acta*, **48**, 1617-1627.
- Fritz, P., & Poplawski, S. (1974). ^{18}O and ^{13}C in the Shells of Freshwater Mollusc and Their Environments. *Earth and Planetary Science Letters*, **24**, 91-98.
- Gastmans, D., Hutcheon, I., Menegário, A.A., & Chang, H.K. (2016). Geochemical Evolution of Groundwater in a Basaltic Aquifer Based on Chemical and Stable Isotopic Data: Cases

- Study from the Northeastern Portion of Serra Geral Aquifer, São Paulo State (Brazil). *Journal of Hydrology*, **535**, 598-611.
- Gills, T.E. (1995). *Standard Reference Material 915a*. Gaithersburg: National Institute of Standards and Technology.
- Google Earth (2016, 2018, 2019). Saint Agatha, Ontario, Canada. <http://www.google.com/earth/>.
- Gothmann, A.M., Bender, M.L., Blättler, C.L., Swart, P.K., Giri, S.J., Adkins, J.F., Stolarski, J., & Higgins, J.A. (2016). Calcium Isotopes in Scleractinian Fossil Corals Since the Mesozoic: Implications for Vital Effects and Biomineralization Through Time. *Earth and Planetary Science Letters*, **444**, 205-214.
- Grace Andrews, M., Jacobson, A.D., Lehn, G.O., Horton, T.W., & Craw, D. (2016) Radiogenic and Stable Sr Isotope Ratios ($^{87}\text{Sr}/^{86}\text{Sr}$, $\delta^{88/86}\text{Sr}$) as Tracers of Riverine Cation Sources and Biogeochemical Cycling in the Milford Sound Region of Fiordland, New Zealand. *Geochimica et Cosmochimica Acta*, **173**, 284-303.
- Grabau, A.W. (1920). A Textbook of Geology Part I General Geology. C. Heath & Co. Publishers, Boston, New York, Chicago.
- Grossman, E.L., & Ku, T-H. (1986). Oxygen and Carbon Isotope Fractionation in Biogenic Aragonite: Temperature Effects. *Chemical Geology: Isotope Geoscience Section*, **59**, 59-74.
- Guillet, G.R. (1969). Marl in Ontario. *Ontario Department of Mines, Industrial Mine Report*.
- Gussone, N., Böhm, F., Eisenhauer, A., Dietzel, M., Heuser, A., Teichert, B.M.A., Reitner, J., Wörheide, G., & Dullo, W-C. (2005). Calcium Isotope Fractionation in Calcite and Aragonite. *Geochimica et Cosmochimica Acta*, **69**, 4485-4494.
- Gussone, N., Filipsson, H.L., & Kuhnert, H. (2015). Mg/Ca, Sr/Ca and Ca Isotope Ratios in Nethonic Foraminifers Related to Test Structure, Mineralogy and Environmental Controls. *Geochimica et Cosmochimica Acta*, **173**, 142-159.
- Gussone, N., Schmitt, A-D., Heuser, A., Wombacher, F., Dietzel, M., Tipper, E., & Schiller, M. (2016). Calcium Stable Isotope Geochemistry. Springer. 1st Ed.
- Halicz, L., Gaky, A., Belshaw, N.S., & Keith O’Nions, R. (1999). High-precision Measurement of Calcium Isotopes in Carbonates and Related Materials by Multiple Collector Inductively Coupled Plasma Mass Spectrometry (MC-ICP-MS). *Journal of Analytical Atomic Spectrometry*, **14**, 1835-1838.

- Harman, W. N. (1972). Benthic Substrates: Their Effect on Fresh-water Mollusca. *Ecology*, **53**, 271-277.
- Harouaka, K., Mansor, M., Macalady, J.L., & Fantle, M.S. (2016). Calcium Isotopic Fractionation in Microbially Mediated Gypsum Precipitates. *Geochimica et Cosmochimica Acta*, **184**, 114-131.
- Heumann, K.G., & Luecke, W. (1973). Calcium Isotope Ratios in Natural Carbonate Rocks. *Earth and Planetary Science Letters*, **20**, 341-346.
- Heuser, A., & Eisenhauer, A. (2008). The Calcium Isotope Composition ($\delta^{44/40}\text{Ca}$) of NIST SRM 915b and NIST SRM 1486. *Geostandards and Geoanalytical Research*, **32**, 311-315.
- Hippler, D., Schmitt, A-D., Gusone, N., Heuser, A., Stille, P., Eisenhauer, A., & Nagler, T. (2003). Calcium Isotopic Composition of Various Reference Materials and Seawater. *Geostandards Newsletter*, **27**, 13-19.
- Hoefs, J. (2015). *Stable Isotope Geochemistry*. Springer. 7th Ed.
- Holcomb, M., DeCarlo, T.M., Schoepf, V., Dissard, D., Tanaka, K., & McCulloch, M. (2015). Cleaning and Pre-treatment Procedures for Biogenic and Synthetic Calcium Carbonate Powders for Determination of Elemental and Boron Isotopic Compositions. *Chemical Geology*, **398**, 11-21.
- Holland, H.D., & Turekian, K.K. (2010). *Isotope Geochemistry: From the Treatise on Geochemistry*. Academic Press. 2nd Ed.
- Holmden, C. (2005). Measurement of $\delta^{44}\text{Ca}$ Using a ^{43}Ca - ^{42}Ca Double-spike TIMS Technique. *Saskatchewan Geological Survey, Summary of Investigations*, **1**.
- Holmden, C. (2009). Ca Isotope Study of Ordovician Dolomite, Limestone, and Anhydrite in the Williston Basin: Implications for subsurface Dolomitization and Local Ca Cycling. *Chemical Geology*, **268**, 180-188.
- Horwitz, E.P., McAlister, D.R., Bond, A.H., & Barrans Jr., R.E. (2005). Novel Extraction of Chromatographic Resins Based on Tetraalkyldiglycolamides; Characterization and Potential Application. *Solvent Extraction and Ion Exchange*, **23**, 319-344.
- Inoue, M., Gussone, N., Koga, Y., Iwase, A., Suzuki, A., Sakai, K., & Kawahata, H. (2015). Controlling Factors of Ca Isotope Fractionation in Scleractinian Corals Evaluated by Temperature, pH and Light Controlled Culture Experiments. *Geochimica et Cosmochimica Acta*, **167**, 80-92.

- Isotope Geochemistry (2003). Geolog 655, Lecture 5. Cornell University.
- Jacobson, A.D., & Holmden, C. (2008). $\delta^{44}\text{Ca}$ Evolution in a Carbonate Aquifer and its Bearing on the Equilibrium Factor for Calcite. *Earth and Planetary Science Letters*, **270**, 349-353.
- Jakopič, R., & Benedik, L. (2005). Tracer Studies on Sr Resin and Determination of ^{90}Sr in Environmental Samples. *Acta Chimica Slovenica*, **52**, 297-302.
- Karrow, P.F. (1974). Till Stratigraphy in Parts of Southwestern Ontario. *Geological Society of American Bulletin*, **85**, 761-768.
- Karrow, P.F. (1993). Quaternary Geology Stratford-Conestogo Area. *Ontario Geological Survey*, Report 283.
- Kasemann, S.A., Schmidt, D.N., Pearson, P.N., & Hawkesworth, C.J. (2008). Biological and Ecological Insights into Ca Isotopes in Planktic Foraminifers as a Paleotemperature Proxy. *Earth and Planetary Science Letters*, **271**, 292-302.
- Kayler, Z.E., Badrian, M., Frackowski, A., Rieckh, H., Nitzsche, K. N., Kalettka, T., Merz, C., & Gessler, A. (2018). Ephemeral Kettle Hole Water and Sediment Temporal and Spatial Dynamics Within an Agricultural Catchment. *Ecohydrology*, **11**.
- Kim, S-T., & O'Neil, J.R. (1997). Equilibrium Oxygen Isotope Effects in Synthetic Carbonates. *Geochimica et Cosmochimica Acta*, **61**, 3461-3475.
- Kulak, R.V. (2005). *Molluscan Paleoenvironments in Marl Deposits at St. Agatha, Ontario and Nichols Brook, New York*. University of Waterloo. MSc Thesis.
- Land and Water Policy Branch, Ministry of the Environment. (2009). Review of the State of Knowledge for the Waterloo and Paris/Galt Moraines. Prepared by: Blackport Hydrogeology Inc, Blackport and Associates Ltd, & AquaResource Inc.
- Lavens, P., & Sorgeloos, P. (1996). Manual on the Production and Use of Live Food for Aquaculture (FAO Fisheries Technical Paper No. 361). *Food and Agriculture Organization (FAO)*.
- Lehn, G.O., Jacobson, A.D., & Holmden, C. (2013). Precise Analysis of Ca Isotope Ratios ($\delta^{44/40}\text{Ca}$) Using an Optimized ^{43}Ca - ^{42}Ca Double-spike MC-TIMS Method. *International Journal of Mass Spectrometry*, **351**, 69-75.
- Lemarchand, D., Wasserburg, G.J., & Papanastassiou, D.A. (2004). Rate-Controlled Calcium Isotope Fractionation in Synthetic Calcite. *Geochimica et Cosmochimica Acta*, **68**, 4665-4678.

- Leng, M.J., & Marshall, J.D. (2004). Palaeoclimate Interpretation of Stable Isotope Data from Lake Sediment Archives. *Quaternary Science Reviews*, **23**, 811-831.
- Li, H.C., & Ku, T.L. (1997). $\delta^{13}\text{C} - \delta^{18}\text{O}$ Covariance as a Paleohydrological Indicator for Closed-Basin Lakes. *Paleogeography, Paleoclimatology, Paleoecology*, **133**, 69-80.
- Liu, Z. (2016). Stable Isotope Paleolimnology of Barry Lake, Ontario, Canada since AD ~1268. The University of Western Ontario. MSc Thesis.
- Lohmann, K.C., & Walker, J.C.G. (1989). The $\delta^{18}\text{O}$ Record of Phanerozoic Abiotic Marine Calcite Cements. *Geophysical Research Letters*, **16**, 319-322.
- Lyons, W.B., Bullen, T.D., & Welch, K.A. (2017). Ca Isotopic Geochemistry of an Antarctic Aquatic System. *Geophysical Research Letters*, **44**, 882-891.
- Macdonald, D.E. (1982). Marl Resources of Alberta. *Alberta Research Council, Earth Sciences Report 82-1*.
- Macdonald, R. (2012). The Late Quaternary History of Lake Huron and Michigan: A Stable Isotope Investigation of Sediment Cores and Modern Biogenic Carbonates. The University of Western Ontario. PhD Thesis.
- Marshall, B.D., & DePaolo, D.J. (1989). Calcium Isotopes in Igneous Rocks and the Origin of Granite. *Geochimica et Cosmochimica Acta*, **53**, 917-922.
- Martin, J.E., Tacail, T., Adnet, S., Girard, C., & Balter, V. (2015). Calcium Isotopes Reveal the Trophic Position of Extant and Fossil Elasmobranchs. *Chemical Geology*, **415**, 118-125.
- Matthews, J.A. (2014). *Strontium Isotopes*. In: Encyclopedia of Environmental Change: Three Volume Set. Sage Publishing, UK.
- McConnaughey, T. (1989). ^{13}C and ^{18}O Isotopic Disequilibrium in Biological Carbonates: II. *In vitro* Simulation of Kinetic Isotope Effects. *Geochimica et Cosmochimica Acta*, **53**, 163-171.
- McConnaughey, T.A., Burdett, J., Whelan, J.F., & Paull, C. K. (1997). Carbon Isotopes in Biological Carbonates: Respiration and Photosynthesis. *Geochimica et Cosmochimica Acta*, **61**, 611-622.
- McKillop, W.B. (1985). Distribution of Aquatic Gastropods Across The Ordovician Dolomite – Precambrian Granite Contact in Southeastern Manitoba, Canada. *Canadian Journal of Zoology*, **63**, 278-288.

- McNutt, R.H., Frapé, S.K., & Dollar, P.S. (1987). A Strontium, Oxygen and Hydrogen Isotopic Composition of Brines, Michigan and Appalachian Basins, Ontario and Michigan. *Applied Geochemistry*, **2**, 495-505.
- Miller, B.B., Tevesz, M.J.S., & Carney, J.S. (1998). Holocen Environmental Changes in the Whitefish Dunes Area, Door Peninsula, Northern Lake Michigan Basin, USA. *Journal of Paleolimnology*, **19**, 473-479.
- Moore, J., Jacobson, A.D., Holmden, C., & Craw, D. (2013). Tracking the Relationship Between Mountain Uplift, Silicate Weathering and Long-term CO₂ Consumption with Ca Isotopes: Southern Alps, New Zealand. *Chemical Geology*, **341**, 110-127.
- Morgan, J.L.L., Gordon, G.W., Arrua, R.C., Skulan, J.L., Anbar, A.D., & Bullen, T.D. (2011). High-Precision Measurement of Variations in Calcium Isotope Ratios in Urine by Multiple Collector Inductively Coupled Plasma Mass Spectrometry. *Analytical Chemistry*, **83**, 6956-6962.
- Moynier, F., Agranier, A., Hezel, D.C., & Bouvier, A. (2010). Sr Stable Isotope Composition of Earth, the Moon, Mars, Vesta and Meteorites. *Earth and Planetary Science Letters*, **300**, 359-366.
- Nelson, D.R., & McCulloch, M.T. (1989). Petrogenetic Applications of the ⁴⁰K-⁴⁰Ca Radiogenic Decay Scheme – A Reconnaissance Study. *Chemical Geology (Isotope Geoscience Section)*, **79**, 275-293.
- Oelkers, E.H., Pogge von Strandmann, P.A.E., & Mavromatis, V. (2019). The Rapid Resetting of the Ca Isotope Signatures of Calcite at Ambient Temperature During its Congruent Dissolution, Precipitation, and at Equilibrium. *Chemical Geology*, **512**, 1-10.
- OGSEarth, Paleozoic Geology KML. (2016) Published by *Ministry of Northern Development and Mines*, Government of Ontario (<https://www.mndm.gov.on.ca>).
- Owens, R.A., Day, C.C., Liu, Y-H., Pointing, M.D., Blättler, C.L., & Henderson, G.M. (2016). Calcium Isotopes in Caves as a Proxy for Aridity: Modern Calibration and Application to the 8.2 kyr Event. *Earth and Planetary Science Letters*, **443**, 129-138.
- Pourmand, A., & Dauphas, N. (2010). Distribution Coefficients of 60 Elements on TODGA Resin: Application to Ca, Lu, Hf, U and Th Isotope Geochemistry. *Talanta*, **81**, 741-753.

- Provincial Groundwater Monitoring Network (PGMN), Published by *Environment, Conservation and Parks*, Government of Ontario (<https://www.ontario.ca/data/provincial-groundwater-monitoring-network>), 2016.
- QCS-26-R ICP 26 Element Quality Control Standard, High Purity Standards.
(<https://highpuritystandards.com/qcs-26-r-icp-26-element-quality-control-standard/>)
- Ravera, O., Cenci, R., Beone, G.M., Dantas, M., & Lodigiani, P. (2003). Trace Element Concentrations in Freshwater Mussels and Macrophytes as Related to Those in Their Environment. *Journal of Limnology*, **62**, 61-70.
- Reynolds, C. (1984). *The Ecology of Freshwater Plankton*. Cambridge University Press.
- Rollion-Bard, C., Vigier, N., & Spezzaferri, S. (2007). In Situ Measurements of Calcium Isotopes by Ion Microprobe in Carbonates and Application to Foraminifera. *Chemical Geology*, **244**, 679-690.
- Romanek, C.S., Grossman, E.L., & Morse, J.W. (1992). Carbon Isotopic Fractionation in Synthetic Aragonite and Calcite: Effects of Temperature and Precipitation Rate. *Geochimica et Cosmochimica Acta*, **56**, 419-430.
- Rosenthal, Y., & Katz, A. (1989). The Applicability of Trace Elements in Freshwater Shells for Paleogeochemical Studies. *Chemical Geology*, 65-76, **78**.
- Russell, W.A., Papanastassiou, D.A., & Tombrello, T.A. (1978). Ca Isotope Fractionation on the Earth and Other Solar System Materials. *Geochimica et Cosmochimica Acta*, **42**, 1075-1090.
- Schiller, M., Paton, C., & Bizzarro, M. (2012). Calcium Isotope Measurement By Combined HR-MC-ICPMS and TIMS. *Journal of Analytical Atomic Spectrometry*, **27**, 38-49.
- Schmitt, A-D., Bracke, G., Stille, P., and Kiefel, B. (2001). The Calcium Isotope Composition of Modern Seawater Determined by Thermal Ionisation Mass Spectrometry. *Geostandards Newsletter*, **25**, 267-275.
- Schmitt, A-D., & Stille, P. (2004). The Source of Calcium in Wet Atmospheric Deposits: Ca-Sr Isotope Evidence. *Geochimica et Cosmochimica Acta*, **69**, 3463-3468.
- Sharp, Z. (2007). *Principles of Stable Isotope Geochemistry*. Pearson Prentice Hall. 1st Ed.
- Sime, N.G., De La Rocha, C.L., Tipper, E.T., Tripathi, A., Galy, A., & Bickle, M.J. (2005). Interpreting the Ca Isotope Record of Marine Biogenic Carbonates. *Geochimica et Cosmochimica Acta*, **71**, 3979-3989.

- Simon, J.L., DePaolo, D.J., & Moynier, F. (2009). Calcium Isotope Composition of Meteorites, Earth and Mars. *The Astrophysical Journal*, **702**, 707-715.
- Skuce, M.E. (2014). Isotope Fingerprinting of Shallow and Deep Groundwaters in Southwestern Ontario and its Applications to Abandoned Well Remediation. The University of Western Ontario. MSc Thesis.
- Skuce, M., Longstaffe, F.J., Carter, T.R., & Potter, J. (2015). Isotopic Fingerprinting of Groundwaters in Southwestern Ontario: Application to Abandoned Well Remediation. *Applied Geochemistry*, **58**, 1-13.
- Skulan, J., DePaolo, D.J., & Owens, T.L. (1997). Biological Control of Calcium Isotopic Abundances in the Global Calcium Cycle. *Geochimica et Cosmochimica Acta*, **61**, 2505-2510.
- Sorokin, C., & Krauss, R.W. (1962). Effects of Temperature and Illuminance on Chlorella Growth Uncoupled From Cell Division. *Plant Physiology*, **37**, 37-42.
- Spero, H. J. (1991). Opening the Carbon Isotope “Vital Effect” Black Box, 2, Quantitative Model for Interpreting Foraminiferal Carbon Isotope Data. *Paleoceanography*, **6**, 639-655.
- Stahl, W. (1968). Search for Natural Variations in Calcium Isotope Abundances. *Earth and Planetary Science Letters*, **5**, 171-174.
- Stahl, W., & Wendt, L. (1968). Fractionation of Calcium Isotopes in Carbonate Precipitation. *Earth and Planetary Science Letters*, **5**, 184-186.
- Steeffel, C.I., Druhan, J.L., & Maher, K. (2014). Modeling Coupled Chemical and Isotopic Equilibration Rates. *Procedia Earth and Planetary Science*, **10**, 208-217.
- Stötler, R.L., Frappe, S.K., El Mugammar, H.T., Johnston, C., Judd-Henrey, I., Harvey, F.E., Drimmie, R., & Jones, J.P. (2010). Geochemical Heterogeneity in a Small, Stratigraphically Complex Moraine Aquifer System (Ontario, Canada): Interpretation of Flow and Recharge Using Multiple Geochemical Parameters. *Hydrogeology Journal*, **19**, 101-115.
- Strong, A.E. (1978). Chemical Whitings and Chlorophyll Distributions in the Great Lakes as Viewed by Landsat. *Remote Sensing of Environment*, **7**, 61-78.
- Stuiver, M. (1970). Oxygen and Carbon Isotope Ratios of Fresh-Water Carbonates as Climatic Indicators. *Journal of Geophysical Research*, **75**, 5247-5257.

- Tacail, T., Albalat, E., Télouk, P.T., & Balter, V. (2014). A Simplified Protocol for Measurement of Ca Isotopes in Biological Samples. *Journal of Analytical Atomic Spectrometry*, **29**, 529-535.
- Talbot, M.R. (1990). A Review of the Paleohydrological Interpretation of Carbon and Oxygen Isotopic Ratios in Primary Lacustrine Carbonates. *Chemical Geology*, **80**, 261-279.
- Terlecky Jr., P.M. (1974). The Origin of a Late Pleistocene and Holocene Marl Deposit. *Journal of Sedimentary Petrology*, **44**, 456-463.
- Thompson, J.B., Schultze-Lam, S., Beveridge, T.J., & Des Marais, D.J. (1997). Whiting Events: Biogenic Origin Due to the Photosynthetic Activity of Cyanobacterial Picoplankton. *The American Society of Limnology and Oceanography*, **42**, 133-141.
- Tipper, E.T., Galy, A., & Bickle, M.J. (2006). Riverine Evidence for a Fractionated Reservoir of Ca and Mg on the Continents: Implications for the Oceanic Ca Cycle. *Earth and Planetary Science Letters*, **247**, 267-279.
- Tipper, E.T., Gaillardet, J., Galy, A., Leuvat, P., Bickle, M.J., & Capmas, F. (2010). Calcium Isotope Ratios in the World's Largest Rivers: A Constraint on the Maximum Imbalance of Oceanic Calcium Fluxes. *Global Biogeochemical Cycles*, **24**.
- Torres, J.M., Llauradó, M., Rauret, G., Bickel, M.m Altizitzoglou, T., & Pilviõ, R. (2000). Determination of ⁹⁰Sr in Aquatic Organisms by Extraction Chromatography: Method Validation. *Analytica Chimica Acta*, **414**, 101-111.
- Turner, J.V., Fritz, P., Karrow, P.F., & Warner, B.G. (1983). Isotopic and Geochemical Composition of Marl Lake Waters and Implications for Radiocarbon Dating of Marl Lake Sediments. *Canadian Journal of Earth Sciences*, **20**, 599-615.
- Valdes, M.C., Moreira, M., Foriel, J., & Moynier, F. (2014). The Nature of Earth's Building Blocks as Revealed by Calcium Isotopes. *Earth and Planetary Science Letters*, **394**, 135-145.
- Vander Putten, E., Dehairs, F., Keppens, E., & Baeyens, W. (2000). High Resolution Distribution of Trace Elements in the Calcite Shell layer of Modern *Mytilus Edulis*: Environmental and Biological Controls. *Geochimica et Cosmochimica Acta*, **64**, 997-1011.
- Veizer, J. (1989). Strontium Isotopes in Seawater Through Time. *Annual Review of Earth and Planetary Sciences*, **17**, 141-167.

- Veizer, J., & Compton, W. (1974). $^{87}\text{Sr}/^{86}\text{Sr}$ Composition of Seawater During the Phanerozoic. *Geochimica et Cosmochimica Acta*, **38**, 1461-1484.
- von Grafenstein, U., Erlernkeuser, H., & Trimborn, P. (1999). Oxygen and Carbon Isotopes in Modern Fresh-water Ostracod Valves: Assessing Vital Offsets and Autological Effects of Interest for Palaeoclimate Studies. *Palaeogeography, Palaeoclimatology, Palaeoecology*, **148**, 133-152.
- Vreeken, W.J. (1981). Distribution and Chronology of Freshwater Marls Between Kingston and Belleville, Ontario. *Canadian Journal of Earth Sciences*, **18**, 1228-1239.
- Warner, B.G., Kubiw, H.J., & Karrow, P.F. (1991). Origin of a Postglacial Kettle-fill Sequence Near Georgetown, Ontario. *Canadian Journal of Earth Science*, **28**, 1965-1974.
- Weis, D., Kieffer, B., Maerschalk, C., Barling, J., de Jong, J., Williams, G.A., Hanano, D., Pretorius, W., Mattielli, N., Scoates, J.S., Goolaerts, A., Friedman, R.M., & Mahoney, J.B. (2006). High Precision Isotopic Characterization of USGS Reference Materials by TIMS and MC-ICP-MS. *Geochemistry, Geophysics, Geosystems*, **7**.
- White, W.M. (2015). *Isotope Geochemistry*. Wiley.
- Wieser, M.E., Buhl, D., Bouman, C., & Schwieters, J. (2004). High Precision Calcium Isotope Ratio Measurements Using a Magnetic Sector Multiple Collector Inductively Coupled Plasma Mass Spectrometer. *Journal of Analytical Atomic Spectrometry*, **19**, 844-851.
- Wilson, J. (2016). Depositional and Environmental Controls on Oxygen and Carbon Isotope Compositions of Late Pleistocene to Mid-Holocene Shelly Fauna from the Huron Basin, Ontario, Canada. The University of Western Ontario. MSc Thesis.
- Yang, J., Karrow, P.F., & Mackie, G.L. (2000). Paleocological Analysis of Molluscan Assemblages in Two Marl Deposits in the Waterloo Region, Southwestern Ontario, Canada. *Journal of Paleolimnology*, **25**, 313-328.
- Yang, L. (2009). Accurate and Precise Determination of Isotopic Ratios by MC-ICP-MS: Review. *Mass Spectrometry Reviews*, **28**, 990-1011.
- Zhu, P., & Macdougall, J.D. (1998). Calcium Isotopes in the Marine Environment and the Oceanic Calcium Cycle. *Geochimica et Cosmochimica Acta*, **62**, 1691-1698.

Appendices

Appendix A

Additional Methodology

Strontium Isotopes

There are 4 long-lived stable or radiogenic isotopes of strontium (Sr), ^{84}Sr , ^{86}Sr , ^{87}Sr and ^{88}Sr . ^{87}Sr is a radiogenic isotope that forms from the emission of a negative beta (β)-particle during the decay of ^{87}Rb to ^{87}Sr (Veizer, 1989). This decay process has a half-life of 4.88×10^{10} years or 48.8 Ga (Veizer, 1989; Matthews, 2014). In geologic terms and relative to ^{87}Sr , isotopes ^{84}Sr , ^{86}Sr and ^{88}Sr are considered stable but can vary in abundances because of geological processes or nucleosynthetic anomalies in meteorites (Moynier et al., 2012). Radiogenic ^{87}Sr is reported relative to stable ^{86}Sr , and is expressed as an isotope ratio ($^{87}\text{Sr}/^{86}\text{Sr}$) in the literature and in this thesis.

Rubidium (Rb) is generally found in minerals such as clays, micas and feldspars, with the decay of ^{87}Rb found in these materials resulting in an increase in ^{87}Sr (McNutt et al., 1987). An enrichment in ^{87}Sr is characteristic of old continental rocks, such as cratons composed of granite, while low $^{87}\text{Sr}/^{86}\text{Sr}$ ratios are common in mantle rocks (Burke et al., 1982). As a result, the weathering of products of mantle and volcanic rocks will have low $^{87}\text{Sr}/^{86}\text{Sr}$ ratios, and the subsequent materials they are incorporated into will have a $^{87}\text{Sr}/^{86}\text{Sr}$ ratio that reflects this (Burke et al., 1982).

Table A1: The isotopes of Sr listed alongside their percent abundances.

Isotope	Abundance (%)
^{84}Sr	0.56
^{86}Sr	9.87
^{87}Sr	7.04
^{88}Sr	82.53

(Veizer, 1989; Matthews, 2014)

Sr isotopes remain relatively unchanged as they are incorporated into carbonates and can a useful tool in deciphering possible localities of water sources supplying the Saint Agatha kettle lake

deposits (Matthews, 2014). It is important to note that there may be large variability in Sr-isotope ratios measured in a given area, as they are strongly dependent on the geochemical composition of the catchment being considered, the hydrogeology of a specific area and the age of the materials being drained (Veizer and Compton, 1974). Sr-isotope ratios have other applications in global weathering cycles, source identification of sediments, timing of dolomitization events and tracing groundwater flow patterns, to name a few (Veizer, 1989; Dollar et al., 1991; Matthews, 2014; White, 2015).

Sr has a long residence time in oceans (≥ 4 million years) which can be attributed to its high solubility (White, 2015; Veizer, 1989). As a result, oceans are very well mixed and the isotopic composition is said to be homogenous (White, 2015). While the Sr-isotope composition of the ocean today is said to be homogenous, its composition has varied throughout geologic time (Figure A1). The variability in Sr seawater isotope compositions has been extensively studied and recorded, providing a Sr-isotope seawater record which is then used to infer the age of material analyzed (Figure A1) (Burke et al., 1982). The application of the Sr-isotope seawater curve in dating materials is referred to as Sr-isotope chronostratigraphy (White, 2015), and is a well established, globally recognized method. This technique, however, is dependent on the availability of reliable data for a given locality in a given time period and on the understanding of the materials being analyzed (White, 2015).

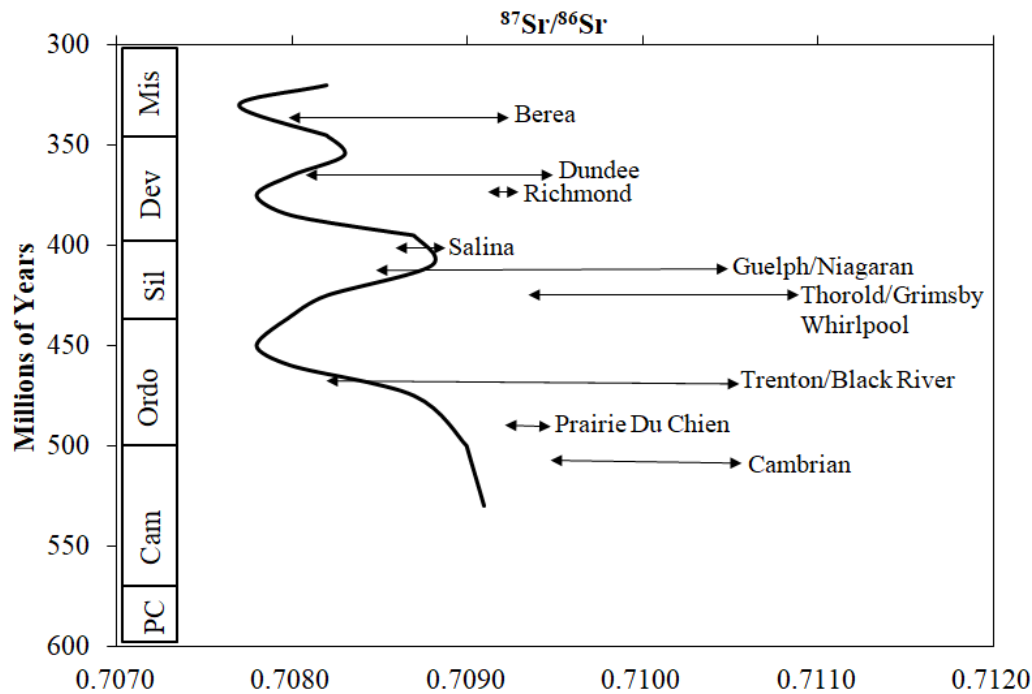


Figure A1: $^{87}\text{Sr}/^{86}\text{Sr}$ ratios of brines from the Michigan and northern Appalachian Basins from each of the formations identified (adapted from Burke et al. (1982) and Dollar et al. (1991)).

Dollar et al. (1991) determined that the Sr-isotope ratios determined for groundwater sampled from within a bedrock formation were higher than those determined for seawater of the same age, which was attributed to interactions with Rb-bearing minerals. This results in a Sr-isotope signature characteristic of each bedrock formation in southern Ontario. Bedrock formations containing Rb-bearing mineral phases and have undergone radiogenic decay will have a more enriched Sr-isotope signature, compared with those that lack Rb-bearing phases. For example, the Sr-isotope ratio of Cambrian bedrock ranges between 0.70930 and 0.71033, while Salina formation rocks range between 0.70839 and 0.70946. The Salina formation is composed primarily of dolomite, limestone, shale, and evaporates which preserve the Sr-isotope signature of seawater at the time of their formation. Figure A1 illustrates the deviation from the Sr-isotope seawater curve as measured for each formation in southern Ontario.

Local geology has been known play a large role in the $^{87}\text{Sr}/^{86}\text{Sr}$ isotope ratio measured as spatial differences in the Rb/Sr ratio of a formation will results in difference in the radiogenic ^{87}Sr content. The Salina formation has a large degree of interbedding, and spatial variability.

Variability across a formation will influence the composition of water that has come into contact with it, and can offer an isotope signature for determining source water (White, 2015).

Analytical Methods

Strontium Column Design

As noted above, a second column protocol was developed to remove Sr from samples (see 3.2.2 *Strontium*). This necessitated the creation of a set of micro-columns, formed from 5/16" heat shrinkable Teflon that was moulded around a pre-fitted former using a high temperature heat gun. This Teflon shrinks to ¼ of its original size.

Frits are also an important component of the Sr column design, as this medium porosity material fitted at the base of the resin bed prevents the flow of resin through the column and into the Teflon beaker below. This material was punched from a larger sheet using a 1/8" punch. The frits were cleaned for over a week in 20% HNO₃, and heated on a hot plate to ~80°C. Once cleaned, they were carefully placed at the base of the resin bed, allowing resin to be packed into the columns successfully.

Sr-resin

Eichrom Sr-resin (4,4'(5')-di-t-butylcyclohexano 18-crown-6 (crown ether)) is an organic solution, that when loaded into a chromatographic column, is designed to effectively and efficiently remove Sr from samples. Once loaded into a chromatographic column, Sr-resin has a bed density of 0.35g/ml. The micro-columns, once fully packed, contain ~0.07g of resin in each resin bed. This is important to note as this value can be used to determine the capacity of the resin bed, and the reusability of each column.

Resin Capacity

There have been multiple studies conducted that sought to determine the amount of Sr that can be loaded into a chromatographic column all the while still obtaining sufficient yields. Most notably, it was found that the resin capacity varies from 8.1 to 8.8mg/Sr per gram of Sr-resin used (Torres et al., 2000; Jakopič et al., 2005).

Using the bed density of each Sr-resin bed provided by Eichrom, as well as the experimentally determined resin bed capacity from Jakopič et al. (2005), the resin beds used in this study have a capacity of 0.567mg of Sr per column. The samples used in this study have very small concentrations of Sr which may indicate the ability to re-use each resin bed multiple times, assuming a sufficient washing protocol. It is important to note however, that the studies investigating the Sr-resin capacity used a protocol with acids at a higher concentration and found that overtime Sr yields dropped off, which was attributed to decomposition of the resin bed by strong acids (Jakopič et al. 2005). Another possible explanation for the decrease in Sr yields was attributed to the destruction of the crown ether in the fabric of the Sr-resin (Jakopič et al. 2005). As a result, it was determined that due to the non-linear degradation of the Sr-resin bed found by Jakopič et al. (2005), and the decreased Sr yields over time, each column was to be used a maximum of 3 times in this study before being discarded. Samples that have complex matrices may decrease the number of times the Sr-resin packed column may be re-used and can be assessed on a sample-to-sample basis based on the concentration of Sr found using the ICPMS at the University of Western Ontario. Due to the small amount of material available, aragonite rich shells typically contained ~150-500 $\mu\text{g/g}$ of Sr compared to the marl which contained ~250-2800 $\mu\text{g/g}$ depending on the sample.

To eliminate any sample carry over, extra washing steps were added prior to starting the Sr-column protocol and care was taken to ensure the columns were stored wet in a 20% HNO_3 acid bath with no air bubbles remaining within the column.

Sr Isotope Analysis

Analyses of the Sr fraction obtained from the Sr-resin columns were completed at the Trent University Water Quality Center in Peterborough, Ontario. These analyses were conducted using the Nu Instrument Plasma II MC-ICPMS at a concentration of 40 to 50ppb in 1ml or 1.5ml of 2% HNO_3 respectively. The concentration of these solutions was determined first by ICPMS at the University of Western Ontario. The samples were introduced in dry plasma mode using an Aridus II desolvating nebulizer and were bracketed by NBS 987 Sr standard to control precision, reproducibility and mass bias corrections. Additionally, BCR-2 USGS basalt was processed through the same procedure. The BCR-2 USGS basalt was used as an external standard to ensure that the Sr measured isotope compositions were accurate after chemistry. Published Sr isotope

ratios are available the for BCR-2 USGS basalt unlike the SRM 915b which is currently used as a Ca-isotope standard only. Due to the nature of the Ca column protocol, 15 purified SRM 915b Sr fractions were available for analysis to determine the $^{87}\text{Sr}/^{86}\text{Sr}$ ratios.

Table A2: $^{87}\text{Sr}/^{86}\text{Sr}$ ratios for SRM 915b with 2SD and 2SE for batches prepared for Ca-isotope measurements.

Batch #	$^{87}\text{Sr}/^{86}\text{Sr}$	2SD	2SE*
1	0.708004	0.000052	0.000007
2	0.708002	0.000055	0.000008
3	0.707994	0.000054	0.000008
4	0.707987	0.000051	0.000007
5	0.707994	0.000063	0.000009
6	0.708001	0.000051	0.000007
7	0.707985	0.000042	0.000006
8	0.707991	0.000050	0.000007
9	0.707991	0.000056	0.000008
10	0.708006	0.000041	0.000006
11	0.707991	0.000044	0.000006
12	0.707997	0.000059	0.000008
14	0.707988	0.000049	0.000007
15	0.707991	0.000047	0.000007
Average	0.707994	0.000051	0.000007

Appendix B

Additional Data Tables and Figures

Table B1: The amount of marl calcite (g) obtained and the weight (g) of material purified for further analyses.

Core (Name of core, Year)	Depth (cm)	Sample Obtained (g)	Material Processed (g)
1B, 2004	128.0 – 128.5	0.50277	0.10108
1B, 2004	138.0 – 138.5	0.51990	0.10079
1B, 2004	148.0 – 148.5	0.53965	0.10240
1C, 2004	157.5 – 158.0	0.51833	0.10438
1C, 2004	167.5 – 168.0	0.52394	0.10119
1C, 2004	171.5 – 172.0	0.79010	0.10126
1C, 2004	179.5 – 180.0	0.62192	0.10098
1C, 2004	183.5 – 184.0	0.53860	0.10076
1C, 2004	191.5 – 192.0	0.54130	0.10309
1C, 2004	201.5 – 202.0	0.58429	0.10074
1C, 2004	219.5 – 220.0	0.51476	0.10408
1C, 2004	221.5 – 222.0	0.62236	0.10057
1C, 2004	229.5 – 230.0	0.51530	0.10292
1D, 2004	249.5 – 250.0	0.51964	0.10362
1D, 2004	255.5 – 256.0	0.52132	0.10705
1D, 2004	266.5 – 267.0	0.60147	0.10078
1D, 2004	275.5 – 276.0	0.50945	0.10090
1D, 2004	285.5 – 286.0	0.51535	0.10395
1D, 2004	299.0 – 299.5	0.51430	0.10153
1E, 2004	309.0 – 309.5	0.60337	0.10121
1E, 2004	311.0 – 311.5	0.55000	0.10073
B7, 2015	334.5 – 335.0	0.51495	0.10383
B7, 2015	344.5 – 345.0	0.51261	0.10402
B7, 2015	354.5 – 355.0	0.51608	0.11080
B7, 2015	364.5 – 365.0	0.50749	0.10110
B7, 2015	374.5 – 375.0	0.51784	0.10266
B8, 2015	384.5 – 385.0	0.50560	0.10742
B8, 2015	394.5 – 395.0	0.51396	0.10252
B8, 2015	404.5 – 405.0	0.51496	0.10236
B8, 2015	409.5 – 410.0	0.52013	0.10274
B8, 2015	414.5 – 415.0	0.53405	0.10162
B8, 2015	424.5 – 425.0	0.52110	0.10327
B9, 2015	434.5 – 435.0	0.52345	0.10264
B9, 2015	449.5 – 445.0	0.52772	0.10388
B9, 2015	462.0 – 462.5	0.50549	0.10558
B9, 2015	474.5 – 475.0	0.52178	0.10256
B10, 2015	484.5 – 485.0	0.50883	0.10412
B10, 2015	494.5 – 495.0	0.52865	0.10312

B10, 2015	514.5 – 515.0	0.52370	0.10135
B10, 2015	524.5 – 525.0	0.52793	0.10410
B10, 2015	531.5 – 532.0	0.52939	0.10715

Table B2: *G. parvus* shell weight (g) consumed during processing and purification for further analyses.

Core (Name of core, Year)	Shell Species	Depth (cm)	Shell Weight (g)
1B, 2004	<i>G. parvus</i>	128.0 – 128.5	0.00128
1B, 2004	<i>G. parvus</i>	138.0 – 138.5	0.00022
1B, 2004	<i>G. parvus</i>	148.0 – 148.5	0.00117
1C, 2004	<i>G. parvus</i>	157.5 – 158.0	0.00080
1C, 2004	<i>G. parvus</i>	167.5 – 168.0	0.00210
1C, 2004	<i>G. parvus</i>	171.5 – 172.0	0.00205
1C, 2004	<i>G. parvus</i>	179.5 – 180.0	0.00165
1C, 2004	<i>G. parvus</i>	183.5 – 184.0	0.00212
1C, 2004	<i>G. parvus</i>	191.5 – 192.0	0.00057
1C, 2004	<i>G. parvus</i>	201.5 – 202.0	0.00081
1C, 2004	<i>G. parvus</i>	209.5 – 210.0	0.00017
1C, 2004	<i>G. parvus</i>	221.5 – 222.0	0.00092
1D, 2004	<i>G. parvus</i>	229.5 – 230.0	0.00083
1D, 2004	<i>G. parvus</i>	249.5 – 250.0	0.00034
1D, 2004	<i>G. parvus</i>	265.5 – 266.0	0.00051
1D, 2004	<i>G. parvus</i>	275.5 – 276.0	0.00218
1D, 2004	<i>G. parvus</i>	285.0 – 285.5	0.00094
1D, 2004	<i>G. parvus</i>	299.0 – 299.5	0.00291
B7, 2015	<i>G. parvus</i>	329.5 – 330.0	0.00763
B7, 2015	<i>G. parvus</i>	369.5 – 370.0	0.00486
B8, 2015	<i>G. parvus</i>	399.5 – 400.0	0.00113
B10, 2015	<i>G. parvus</i>	524.5 – 525.0	0.00044

Table B3: The weight (g) of shells selected at depths 219.5 - 220.0cm and 309.0 - 309.5cm.

Core (Name of core, Year)	Shell Label	Shell Species	Depth (cm)	Shell Weight (g)
1C, 2004	J1	<i>V. tricarinata</i>	219.5 – 220.0	0.00301
	H9	<i>V. tricarinata</i>		0.00050
	H6	<i>G. parvus</i>		0.00241
	J8	<i>G. parvus</i>		0.00147
	H7	<i>Pisidium Sp.</i>		0.00050
1E, 2004	D4	<i>V. tricarinata</i>	309.0 – 309.5	0.00162

D5	<i>V. tricarinata</i>	0.00244
D7	<i>G. parvus</i>	0.00054
E1	<i>G. parvus</i>	0.00120
D10	<i>Pisidium sp.</i>	0.00023

Table B4: The Ca concentration (ppm) in each marl calcite with the percentage (%) of each sample that is Ca.

Core	Depth (cm)	Concentration (ppm)	% of sample that is Ca*
1B	128.0 – 128.5	389061	39%
1B	138.0 – 138.5	317977	32%
1B	148.0 – 148.5	322857	32%
1C	157.5 – 158.0	326463	33%
1C	167.5 – 168.0	402711	40%
1C	171.5 – 172.0	391160	39%
1C	179.5 – 180.0	400243	40%
1C	183.5 – 184.0	437561	44%
1C	191.5 – 192.0	379298	38%
1C	201.5 – 202.0	409183	41%
1D	211.5 – 212.0	325580	33%
1C	219.5 – 220.0	335641	34%
1C	221.5 – 222.0	423508	42%
1D	229.5 – 230.0	414532	41%
1D	249.5 – 250.0	286730	29%
1D	255.5 – 256.0	306175	31%
1E	266.5 – 267.0	343722	34%
1D	275.5 – 276.0	511125	51%
1D	285.5 – 286.0	373294	37%
1D	299.0 – 299.5	457065	46%
1E	309.0 – 309.5	324727	32%
1E	311.0 - 311.5	426604	43%
B7	334.5 – 335.0	306408	31%
B7	344.5 – 345.0	312245	31%
B7	354.5 – 355.0	307834	31%
B7	364.5 – 365.0	297009	30%
B7	374.5 – 375.0	323615	32%
B8	384.5 – 385.0	314234	31%
B8	394.5 – 395.0	278814	28%
B8	404.5 – 405.0	264335	26%
B8	409.5 – 410.0	309733	31%
B8	414.5 – 415.0	333244	33%
B8	424.5 – 425.0	333123	33%
B9	434.5 – 435.0	339086	34%
B9	449.5 – 450.0	314520	31%
B9	462.0 – 462.5	404680	40%

B9	474.5 – 475.0	303875	30%
B10	484.5 – 485.0	352118	35%
B10	494.5 – 495.0	284485	28%
B10	514.5 – 515.0	299137	30%
B10	524.5 – 525.0	290781	29%
B10	531.5 – 532.0	283654	28%
Average		407799	35%

*% of each sample that is Ca = $\frac{(\text{conc. of Ca (ppm) in each sample})}{\text{initial mass of sample}} * 100$

Table B5: The normalized concentration (ppm) of important elements in marl calcite.

Core	Depth (cm)	Normalization Factor	Normalized Concentrations (ppm)						
			Mg	Cr	Mn	Fe	Zn	Sr	Ba
1B	128.0 – 128.5	1.03	6665.9	0.5	238.6	1399.0	50.4	248.4	491
1B	138.0 – 138.5	1.26	8800.2	0.3	196.2	992.0	31.1	300.7	700.4
1B	148.0 – 148.5	1.24	6820.6	0.6	378.0	1664.0	64.7	258.7	638.0
1C	157.5 – 158.0	1.23	7295.8	0.6	306.2	2505.8	46.6	298.5	684.5
1C	167.5 – 168.0	0.99	7149.1	0.4	327.8	950.7	41.2	265.2	564.2
1C	171.5 – 172.0	1.02	7064.7	0.5	264.3	1030.4	37.5	244.8	545.6
1C	179.5 – 180.0	1	8120.8	0.2	233.8	778.5	40.6	275.0	578.3
1C	183.5 – 184.0	0.91	7233.2	0.6	263.1	1870.4	83.1	255.0	559.0
1C	191.5 – 192.0	1.06	6960.0	0.6	301.3	1947.8	27.5	258.0	487.7
1C	201.5 – 202.0	1.03	7392.5	0.3	356.9	1769.7	43.1	337.0	613.9
1D	211.5 – 212.0	1.03	6158.5	0.8	212.6	2700.5	18.4	219.0	436.5
1C	219.5 – 220.0	1.07	7452.0	0.4	354.4	1735.5	133.1	326.3	573.5
1C	221.5 – 222.0	1.03	8847.3	2.2	474.5	2570.7	643.8	362.2	414.0
1D	229.5 – 230.0	0.97	7025.2	0.5	339.5	2418.4	24.7	317.8	551.7
1D	249.5 – 250.0	1.4	8149.2	0.4	433.8	2491.5	30.5	356.3	545.0
1D	255.5 – 256.0	1.31	7075.8	0.7	425.7	2644.8	38.3	306.4	508.3
1E	266.5 – 267.0	1.16	6332.9	0.4	372.5	1655.0	79.0	299.0	590.0
1D	275.5 – 276.0	0.78	7044.3	0.4	207.1	767.7	33.0	293.6	567.5
1D	285.5 – 286.0	1.07	8411.2	0.3	274.7	1368.7	24.4	318.8	542.0
1D	299.0 – 299.5	0.88	8356.6	0.4	267.5	906.3	56.1	327.0	591.0
1E	309.0 – 309.5	1.23	8223.1	0.4	305.6	1238.8	51.2	364.4	672.3
1E	311.0 – 311.5	0.94	8064.9	0.5	414.0	1660.3	86.5	331.8	526.4
B7	334.5 – 335.0	1.31	8182.5	0.3	322.7	872.4	11.0	312.5	529.4
B7	344.5 – 345.0	1.28	8618.2	0.3	330.2	865.2	30.5	314.1	529.6
B7	354.5 – 355.0	1.3	8664.5	0.3	289.3	655.0	18.0	325.2	539.8
B7	364.5 – 365.0	1.35	7180.0	0.3	230.7	496.0	50.4	227.6	462.7
B7	374.5 – 375.0	1.24	6825.0	0.2	235.7	579.0	26.1	284.5	452.3
B8	384.5 – 385.0	1.27	7485.6	0.3	300	1201.1	23.8	326.8	459.4

B8	394.5 – 395.0	1.44	7214.4	0.3	432.7	2829.8	25.4	311.5	438.1
B8	404.5 – 405.0	1.51	7210.7	0.3	324.8	2176.6	33.1	336.3	459.0
B8	409.5 – 410.0	1.29	6874.2	0.5	381.3	2511.1	29.8	358.3	369.0
B8	414.5 – 415.0	1.2	6472.8	0.4	210.0	1249.3	15.6	318.6	393.2
B8	424.5 – 425.0	1.2	6074.3	0.6	380.2	2916.3	31.5	301.0	340.1
B9	434.5 – 435.0	1.18	6368.8	0.6	278.6	1772.8	29.0	289.8	362.0
B9	449.5 – 450.0	1.27	6627.5	1.1	359.5	4403.3	43.0	341.5	309.4
B9	462.0 – 462.5	0.99	5877.4	0.7	369.9	3412.5	37.6	334.0	302.3
B9	474.5 – 475.0	1.32	7181.4	1.2	512.6	4713.3	86.2	467.8	240.0
B10	484.5 – 485.0	1.14	6906.1	0.7	486.6	4171.0	33.8	524.2	313.0
B10	494.5 – 495.0	1.41	10233.0	2.5	953.4	13160.0	65.4	811.0	78.4
B10	514.5 – 515.0	1.34	10513.8	2.1	691.1	11539.7	45.6	1155.3	166.0
B10	524.5 – 525.0	1.38	12085.2	1.6	787.4	10686.3	37.8	1581.8	254.4
B10	531.5 – 532.0	1.41	11616.2	1.4	729.9	9912.7	25.5	3979.1	216.0

Table B6: Elemental ratios of marl calcite.

Core	Depth (cm)	Elemental Ratios				
		Mg/Fe	Fe/Ca	Mn/Ca	Ba/Ca	Sr/Ca
1B	128.0 – 128.5	0.017	0.0035	0.0006	0.0012	0.0006
1B	138.0 – 138.5	0.022	0.0025	0.0005	0.0018	0.0008
1B	148.0 – 148.5	0.017	0.0042	0.0009	0.0016	0.0006
1C	157.5 – 158.0	0.018	0.0063	0.0008	0.0017	0.0007
1C	167.5 – 168.0	0.018	0.0024	0.0008	0.0014	0.0007
1C	171.5 – 172.0	0.018	0.0026	0.0007	0.0014	0.0006
1C	179.5 – 180.0	0.020	0.0019	0.0006	0.0015	0.0007
1C	183.5 – 184.0	0.018	0.0047	0.0007	0.0014	0.0006
1C	191.5 – 192.0	0.017	0.0049	0.0008	0.0012	0.0006
1C	201.5 – 202.0	0.017	0.0042	0.0008	0.0015	0.0008
1D	211.5 – 212.0	0.018	0.0081	0.0006	0.0013	0.0007
1C	219.5 – 220.0	0.021	0.0049	0.0010	0.0016	0.0009
1C	221.5 – 222.0	0.020	0.0059	0.0011	0.0010	0.0008

1D	229.5 – 230.0	0.018	0.0060	0.0008	0.0014	0.0008
1D	249.5 – 250.0	0.020	0.0062	0.0011	0.0014	0.0009
1D	255.5 – 256.0	0.018	0.0066	0.0011	0.0013	0.0008
1E	266.5 – 267.0	0.016	0.0041	0.0009	0.0015	0.0007
1D	275.5 – 276.0	0.018	0.0019	0.0005	0.0014	0.0007
1D	285.5 – 286.0	0.021	0.0034	0.0007	0.0014	0.0008
1D	299.0 – 299.5	0.021	0.0023	0.0007	0.0015	0.0008
1E	309.0 – 309.5	0.021	0.0031	0.0008	0.0017	0.0009
1E	311.0 – 311.5	0.020	0.0042	0.0010	0.0013	0.0008
B7	334.5 – 335.0	0.021	0.0022	0.0008	0.0013	0.0008
B7	344.5 – 345.0	0.022	0.0022	0.0008	0.0013	0.0008
B7	354.5 – 355.0	0.022	0.0016	0.0007	0.0014	0.0008
B7	364.5 – 365.0	0.018	0.0012	0.0006	0.0012	0.0007
B7	374.5 – 375.0	0.017	0.0014	0.0006	0.0011	0.0007
B8	384.5 – 385.0	0.019	0.0030	0.0007	0.0012	0.0008
B8	394.5 – 395.0	0.018	0.0071	0.0011	0.0011	0.0008
B8	404.5 – 405.0	0.018	0.0054	0.0008	0.0012	0.0008
B8	409.5 – 410.0	0.017	0.0063	0.0010	0.0009	0.0009
B8	414.5 – 415.0	0.016	0.0031	0.0005	0.0010	0.0008
B8	424.5 – 425.0	0.015	0.0073	0.0010	0.0009	0.0008
B9	434.5 – 435.0	0.016	0.0044	0.0007	0.0009	0.0007
B9	449.5 – 450.0	0.017	0.0110	0.0009	0.0008	0.0009
B9	462.0 – 462.5	0.015	0.0085	0.0009	0.0008	0.0008
B9	474.5 – 475.0	0.018	0.0120	0.0013	0.0006	0.0012
B10	484.5 – 485.0	0.017	0.0100	0.0012	0.0008	0.0013
B10	494.5 – 495.0	0.026	0.0330	0.0024	0.0002	0.0020
B10	514.5 – 515.0	0.026	0.0290	0.0017	0.0004	0.0029
B10	524.5 – 525.0	0.030	0.0270	0.0020	0.0006	0.0040
B10	531.5 – 532.0	0.029	0.0250	0.0018	0.0005	0.0100

Table B7: The normalized concentration (ppm) of important elements in shell aragonite. Samples concentrations noted with a "/" indicates the concentration was below the detection limit of the ICPMS.

Core	Depth (cm)	Shell Label	Normalized Concentrations (ppm)						
			Mg	Cr	Mn	Fe	Zn	Sr	Ba
1B	128.0 – 128.5	M2	140.1	0.3	80.0	45.5	128.0	246.6	208.0
1B	138.0 – 138.5	M8	662.4	2.4	65.6	/	409.3	298.7	348.8
1B	148.0 – 148.5	N4	129.4	/	38.4	55.7	341.4	255.0	189.5
1C	157.5 – 158.0	P2	212.6	0.1	27.6	/	1020.9	274.3	147.7
1C	167.5 – 168.0	P7	75.1	/	53.9	/	42.8	241.2	130.6
1C	171.5 – 172.0	P8	69.9	0.5	39.6	23.8	98.4	242.5	175.0
1C	179.5 – 180.0	Q3	201.3	0.1	67.4	25.5	150.4	341.2	202.8
1C	183.5 – 184.0	Q5	82.1	0.1	53.8	8.3	101.6	246.1	170.3
1C	191.5 – 192.0	Q9	670.3	/	37.5	6.3	396.9	342.2	3683.1
1C	201.5 – 202.0	R5	189.4	3.1	295.6	/	524.2	470.8	738.7
1C	209.5 – 210.0	R9	1039.1	1.8	80.3		773.7	269.2	3962.3
1C	221.5 – 222.0	S7	261.3	0.4	46.3	116.2	1183.8	306.3	195.4
1D	229.5 – 230.0	T9	481.9	0.1	122.2	/	221.61	294.0	1279.7
1D	249.5 – 250.0	V1	1769.4	3.5	44.5	95.5	13749.8	212.1	217.8
1D	265.5 – 266.0	V9	466.4	0.8	43.1	/	104.8	382.6	1120.2
1D	275.5 – 276.0	W5	95.0	0.5	67.2	51.4	95.5	217.9	227.5
1D	285.0 – 285.5	X1	375.9	/	97.1	31.3	298.4	362.7	1088.4
1D	299.0 – 299.5	X8	108.2	0.2	31.0	9.15	174.2	252.2	165.3
B7	329.5 – 330.0	AA4	46.5	/	185.9	12.9	1.3	298.3	130.4
B7	369.5 – 370.0	AA3	42.0	/	66.8	5.7	/	299.5	125.9
B8	399.5 – 400.0	AA5	59.6	/	51.1	8.5	/	383.1	102.2
B10	524.5 – 525.0	Y3	124.3	/	145.1	20.7	/	1616.4	82.9

Table B8: The Ca concentration (ppm) in shell aragonite with the percentage (%) of each sample that is Ca.

Core	Depth (cm)	Concentration (ppm)	% of sample that is Ca*
1B	128.0 – 128.5	375102	38%
1B	138.0 – 138.5	466327	47%
1B	148.0 – 148.5	292521	29%
1C	157.5 – 158.0	410759	41%
1C	167.5 – 168.0	387249	39%
1C	171.5 – 172.0	381281	38%
1C	179.5 – 180.0	381681	38%
1C	183.5 – 184.0	256937	26%
1C	191.5 – 192.0	251409	25%
1C	201.5 – 202.0	329575	33%
1D	209.5 – 210.0	633324	63%
1C	221.5 – 222.0	437471	44%
1D	229.5 – 230.0	228195	23%
1D	249.5 – 250.0	1026703	103%
1E	265.5 – 266.0	567337	57%
1D	275.5 – 276.0	422322	42%
1D	285.0 – 285.5	348737	35%
1D	299.0 - 299.5	385391	39%
1E	329.5 – 330.0	406792	41%
1E	369.5 – 370.0	432245	43%
B7	399.5 – 400.0	416646	42%
B10	524.5 – 525.0	439545	44%
Average		421707	42%

*% of each sample that is Ca = $\frac{(\text{conc. of Ca (ppm) in each sample})}{\text{initial mass of sample}} * 100$

Table B9: Concentration of *V. tricarinata*, *G. parvus*, and *Pisidium sp.* analyzed at 219.5 – 220cm and 309.5 – 310cm.

Core	Depth (cm)	Shell Label	Shell Species	Concentration (ppm)							
				Mg	Ca	Cr	Mn	Fe	Zn	Sr	Ba
1B	219.5 -220.0	J1	<i>V. tricarinata</i>	126.5	285088.1	0.78	26.1	/	90.7	264.0	303.0
		H9	<i>V. tricarinata</i>	475.4	292831.9	/	23.7	1965.8	126.2	224.4	2247.4
		H6	<i>G. parvus</i>	61.4	295590.2	0.02	17.3	/	57.9	286.7	413.4
		J8	<i>G. parvus</i>	171.9	260949.9	/	21.0	/	104.7	289.6	621.4
		H7	<i>Pisidium sp.</i>	160.5	365372.2	2.0	5.7	121.4	/	259.3	32.9
1E	309.5 – 310.0	D4	<i>V. tricarinata</i>	107.3	274348.0	/	19.7	/	161.2	172.0	589.2
		D5	<i>V. tricarinata</i>	78.9	299281.3	0.51	12.6	/	67.0	267.1	621.9
		D7	<i>G. parvus</i>	185.3	378383.5	/	16.2	/	376.1	470.4	1731.9
		E1	<i>G. parvus</i>	428.8	533619.1	2.1	36.3	/	527.8	711.3	4819.0
		D10	<i>Pisidium sp.</i>	2438.3	399548.6	1.3	25.3	94.0	/	286.0	47.43

Table B10: A comparison of the elemental data obtained in this study and the published elemental data reported in the Provincial Groundwater Monitoring Network (PGMN) water chemistry database, provided by the Government of Ontario; (a) W427 is found to the southwest of the St. Agatha kettle lake deposits b) W36 is located to the northeast of the St. Agatha kettle lake deposits.

Groundwater Sampling Location W427:

a)

Year Reported	Na	Mg	K	Ca	Cr	Mn	Fe	Zn	Sr	Ba
2002	18.4	68.7	1.95	425.0	0.0005	0.0520	1.830	0.001	9.63	0.0097
2003	23.4	70.8	1.95	442.0	0.0010	0.0546	2.190	0.002	9.35	0.0091
2009	21.7	68.6	1.96	432.0	0.0006	0.0492	2.230	0.003	9.51	0.0079
2009	21.6	7-2	1.91	438.0	0.0000	0.0497	2.310	0.001	9.36	0.0082
2010	20.6	71.9	1.98	440.0	0.0000	0.0512	2.340	0.003	9.28	0.0081
2011	24.0	75.3	2.23	431.0	0.0000	0.0567	2.440	0.008	9.63	0.0084
2012	26.4	80.4	2.48	452.0	0.0000	0.0510	2.410	0.003	9.29	0.0075
2013	20.7	72.3	1.89	440.0	0.0004	0.0488	2.350	0.003	9.03	0.0082

2014	19.8	70.8	2.62	457.0	0.0005	0.0477	1.999	0.003	9.32	0.0075
2015	21.9	69.1	2.65	412.0	0.0002	0.0488	2.420	0.003	9.92	0.0077
This Study (2016)	4.7	72.9	1.04	471.1	0.0000	0.0531	2.304	0.055	9.16	0.0673

Groundwater Sampling Location W36:

b)

Year Reported	Na	Mg	K	Ca	Cr	Mn	Fe	Zn	Sr	Ba
2005	20.0	61.6	2.15	267.0	0.0011	0.0990	1.530	0.0027	9.18	0.016
2008	20.5	62.7	2.04	279.0	0.0002	0.0889	1.460	0.0022	8.65	0.013
2010	20.6	62.1	2.03	269.0	0.0003	0.0716	1.380	0.0021	8.72	0.012
2010	20.0	62.7	1.95	281.0	0.0002	0.0739	1.370	0.0034	8.79	0.011
2011	20.2	63.2	2.22	286.0	0.0003	0.0772	1.450	0.0032	8.66	0.012
2012	18.6	61.8	1.93	298.0	0.0002	0.0691	1.370	0.0031	8.60	0.011
2013	19.8	61.4	1.92	272.0	0.0006	0.0769	1.310	0.0034	8.44	0.012
2014	19.5	56.7	1.93	271.0	0.0002	0.0836	1.200	0.0053	8.38	0.021
2015	20.8	62.2	2.73	283.0	0.0001	0.0809	1.130	0.0053	8.90	0.017
This Study (2016)	4.88	69.0	1.24	342.9	0.0002	0.0916	1.518	0.0484	9.30	0.058

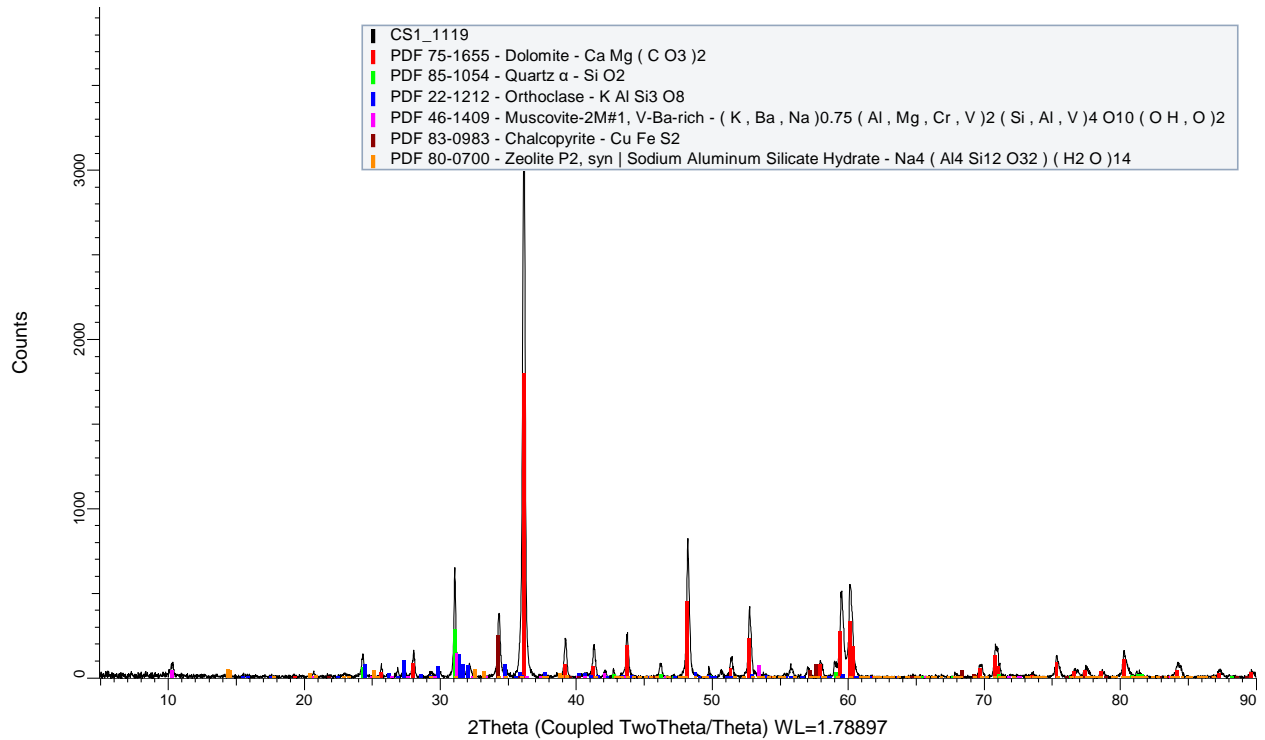


Figure B1: XRD diffraction pattern of Core 1119 sample 1, with peak matching completed using EVA software. The sample is taken from the Salina E member of the Upper Silurian Formation.

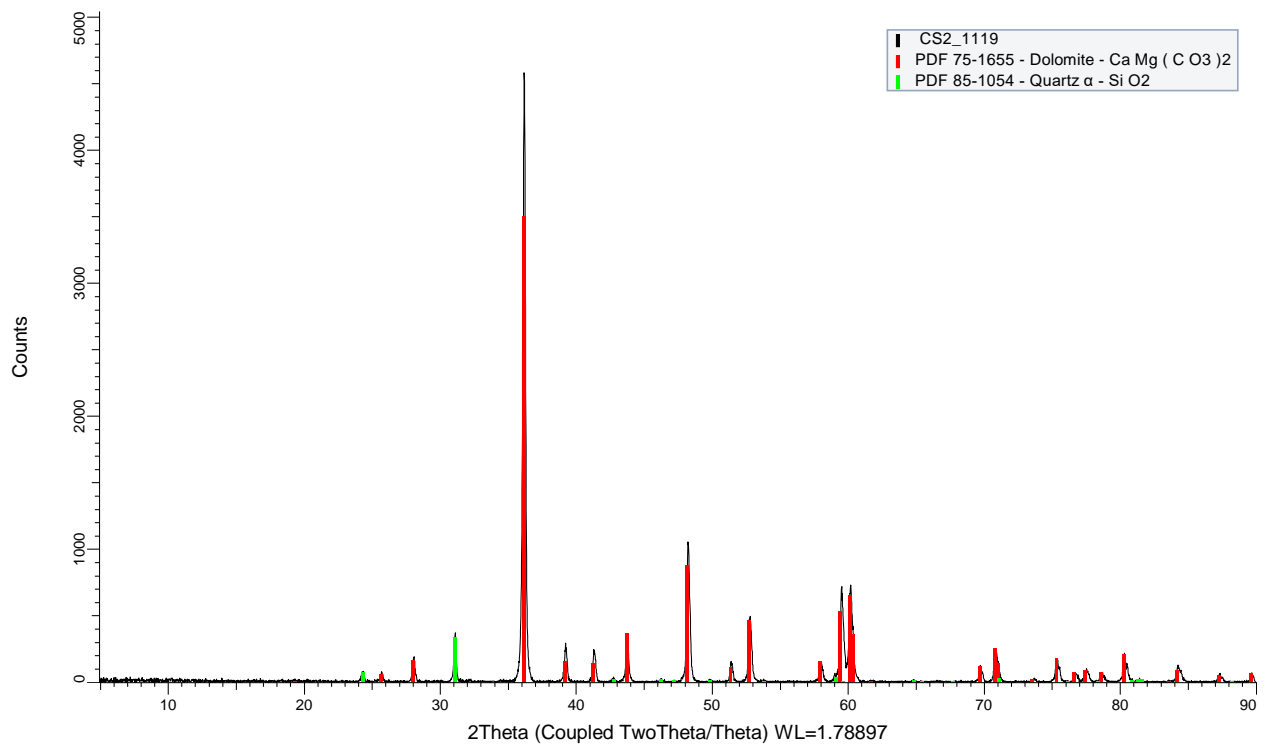


Figure B2: XRD diffraction pattern of Core 1119 sample 2, with peak matching completed using EVA software. The sample is taken from the Salina E member of the Upper Silurian Formation.

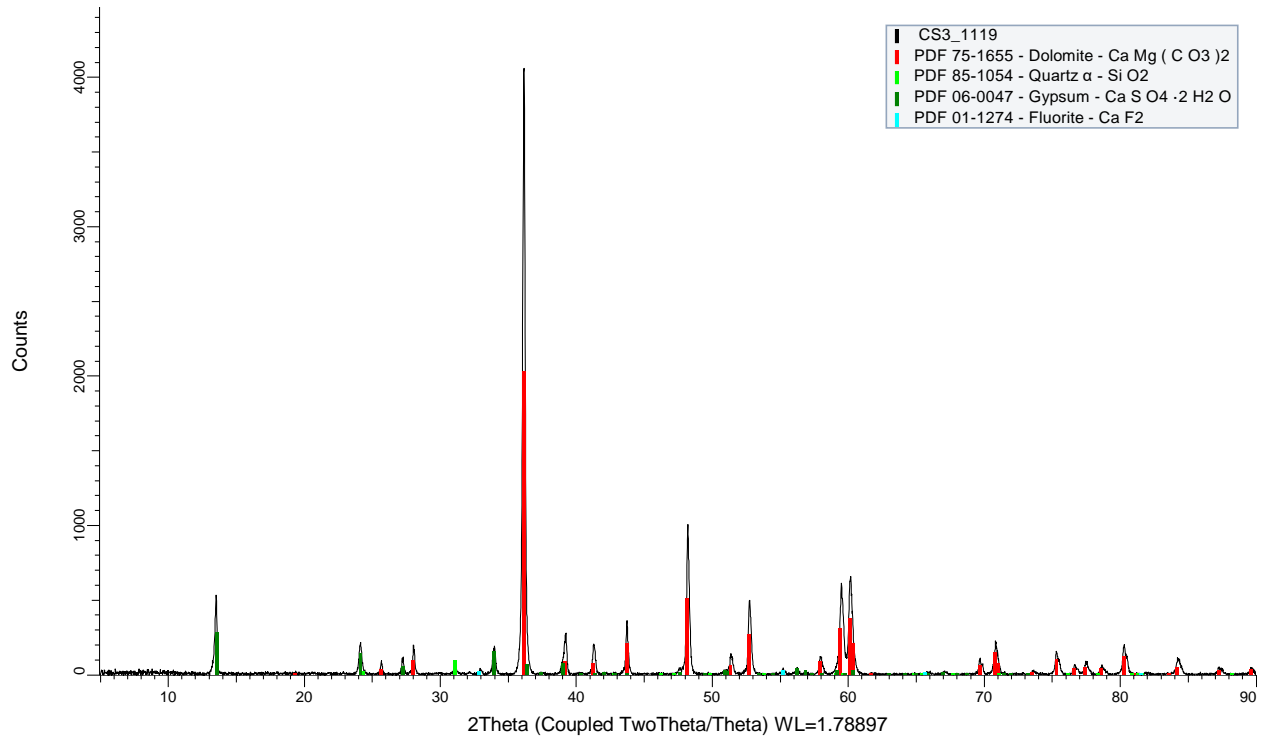


Figure B3: XRD diffraction pattern of Core 1119 sample 3, with peak matching completed using EVA software. The sample is taken from the Salina C member of the Upper Silurian Formation.

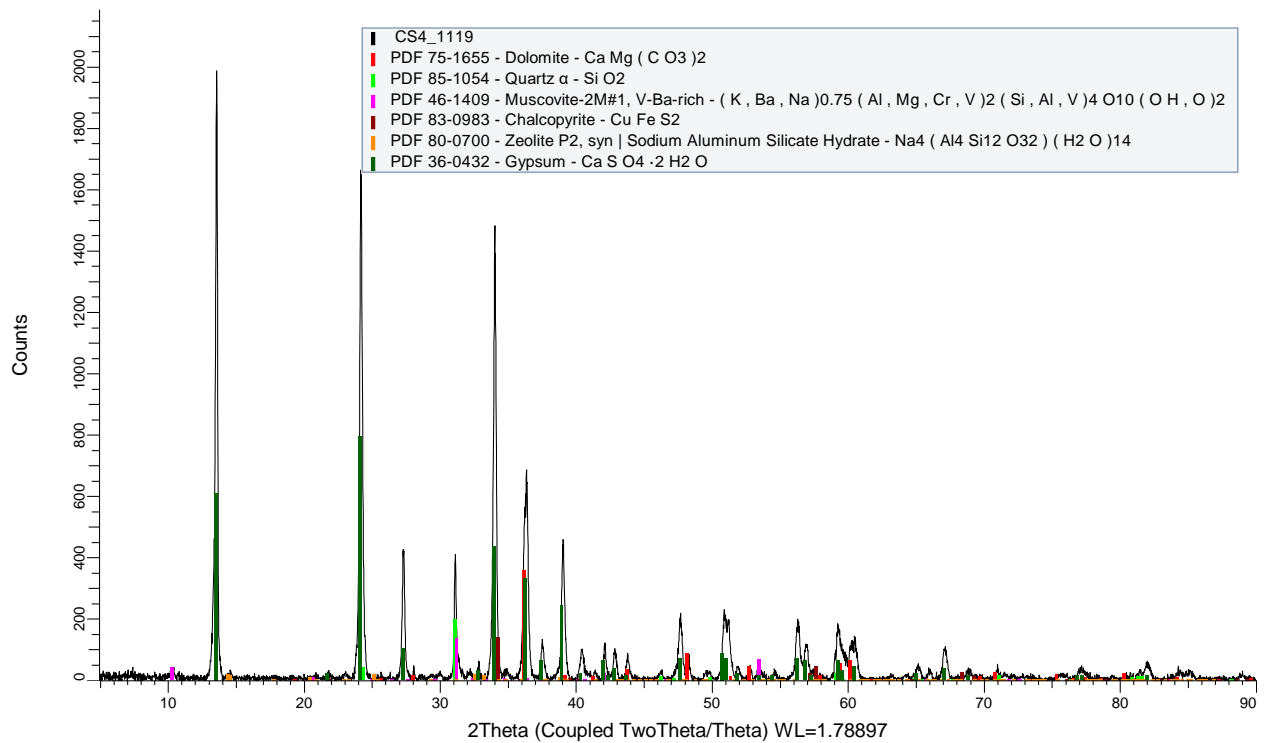


Figure B4: XRD diffraction pattern of Core 1119 sample 4, with peak matching completed using EVA software. The sample is taken from the Salina A2 member of the Upper Silurian Formation.

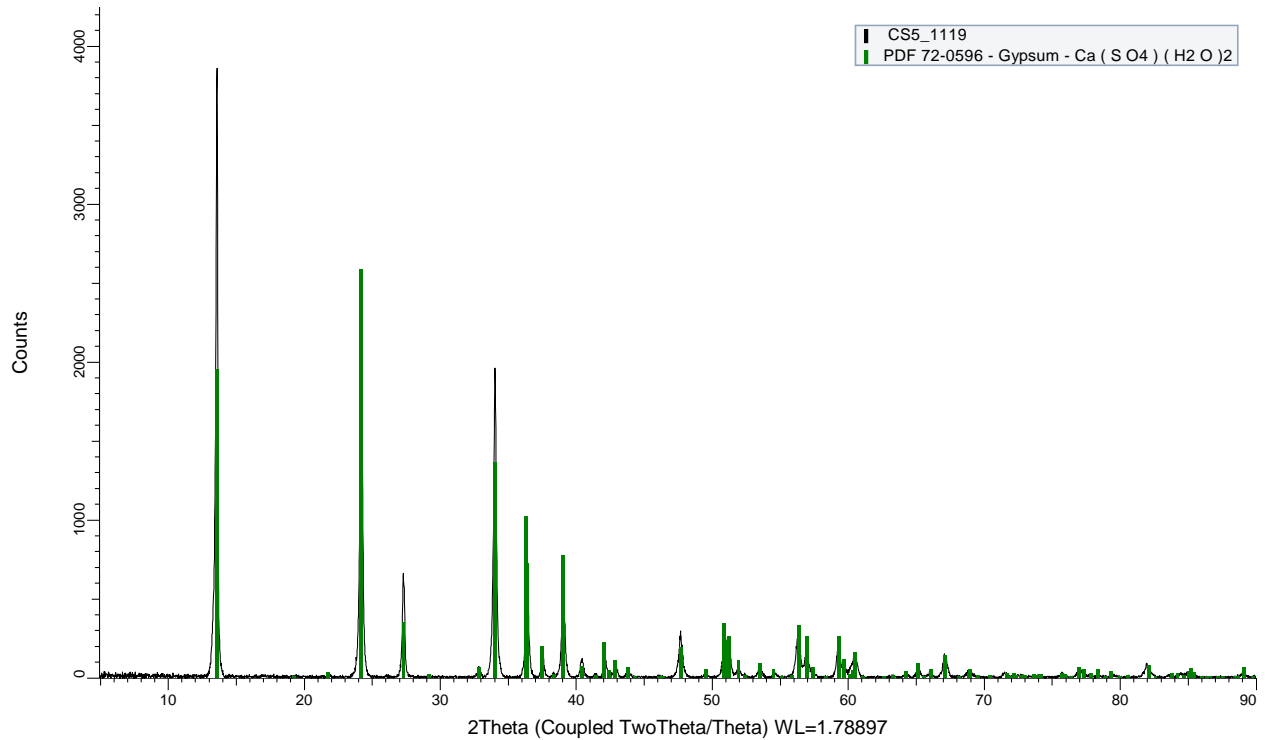


Figure B5: XRD diffraction pattern of Core 1119 sample 5, with peak matching completed using EVA software. The sample is taken from the Salina A2 member of the Upper Silurian Formation.

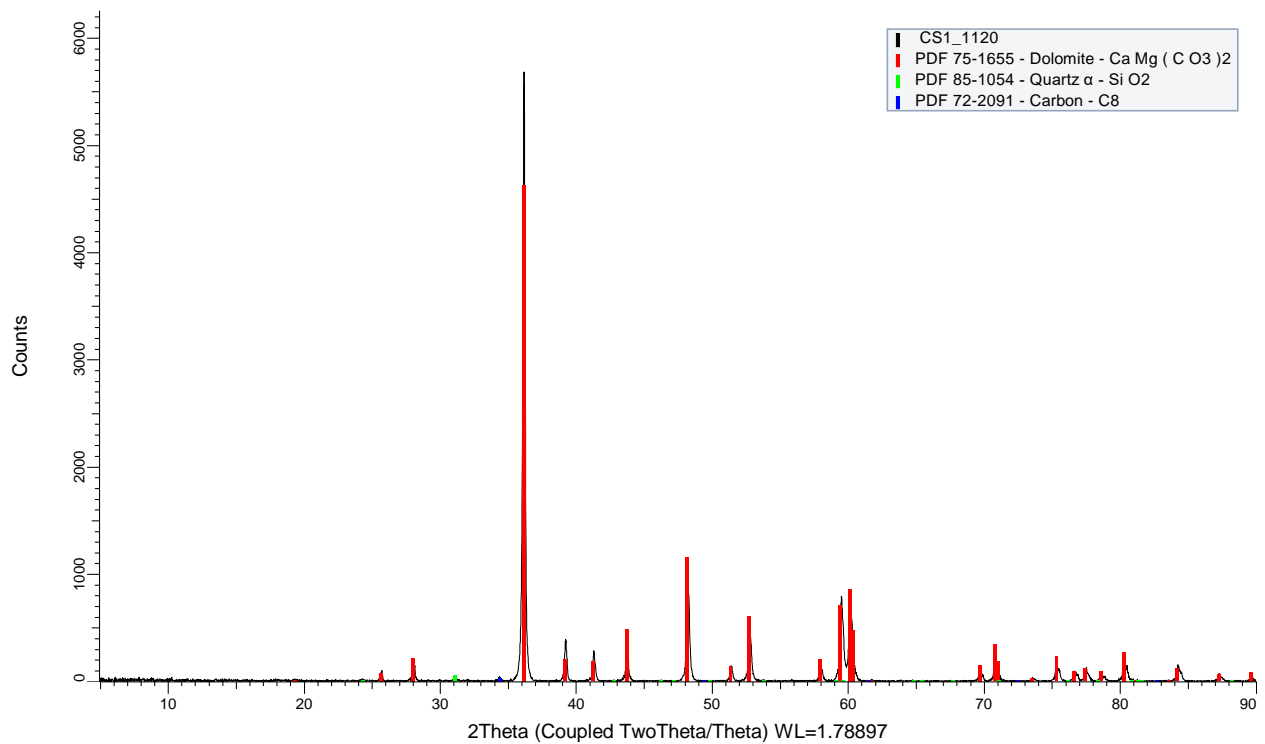


Figure B6: XRD diffraction pattern of Core 1120 sample 1, with peak matching completed using EVA software. The sample is taken from the Salina E member of the Upper Silurian Formation.

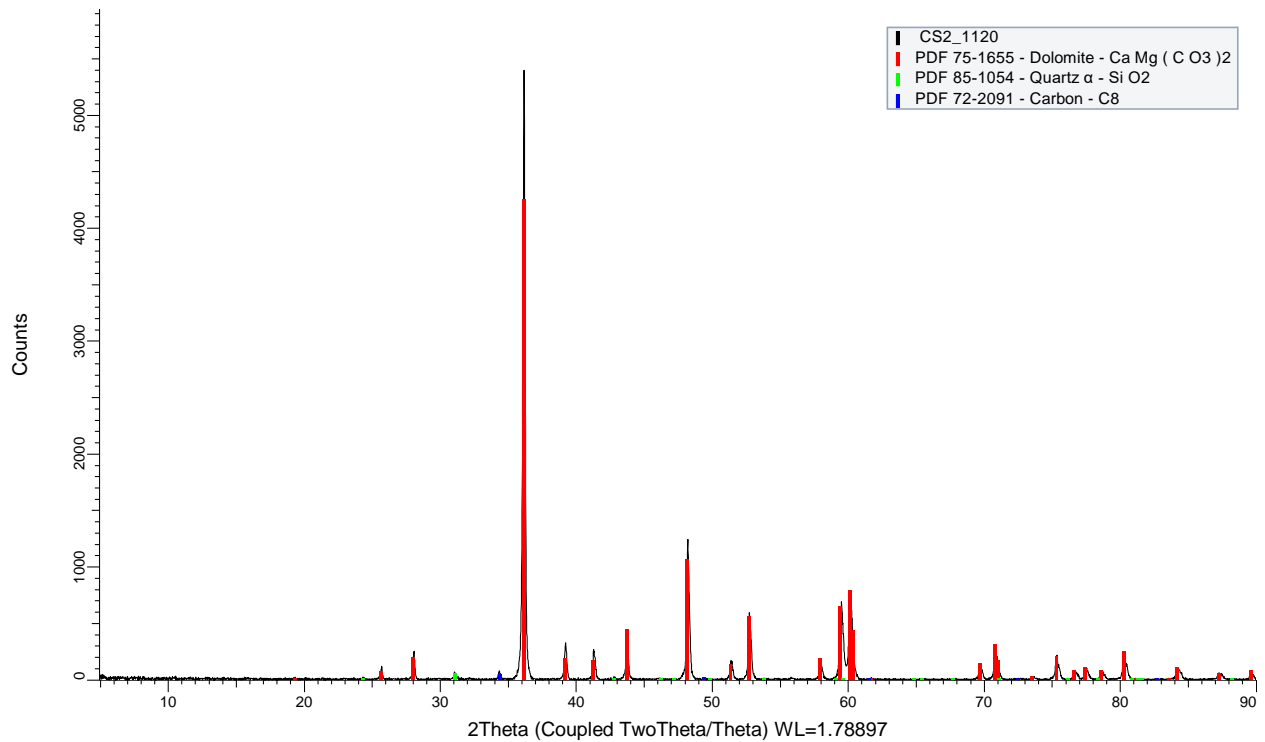


Figure B7: XRD diffraction pattern of Core 1120 sample 2, with peak matching completed using EVA software. The sample is taken from the Salina E member of the Upper Silurian Formation.

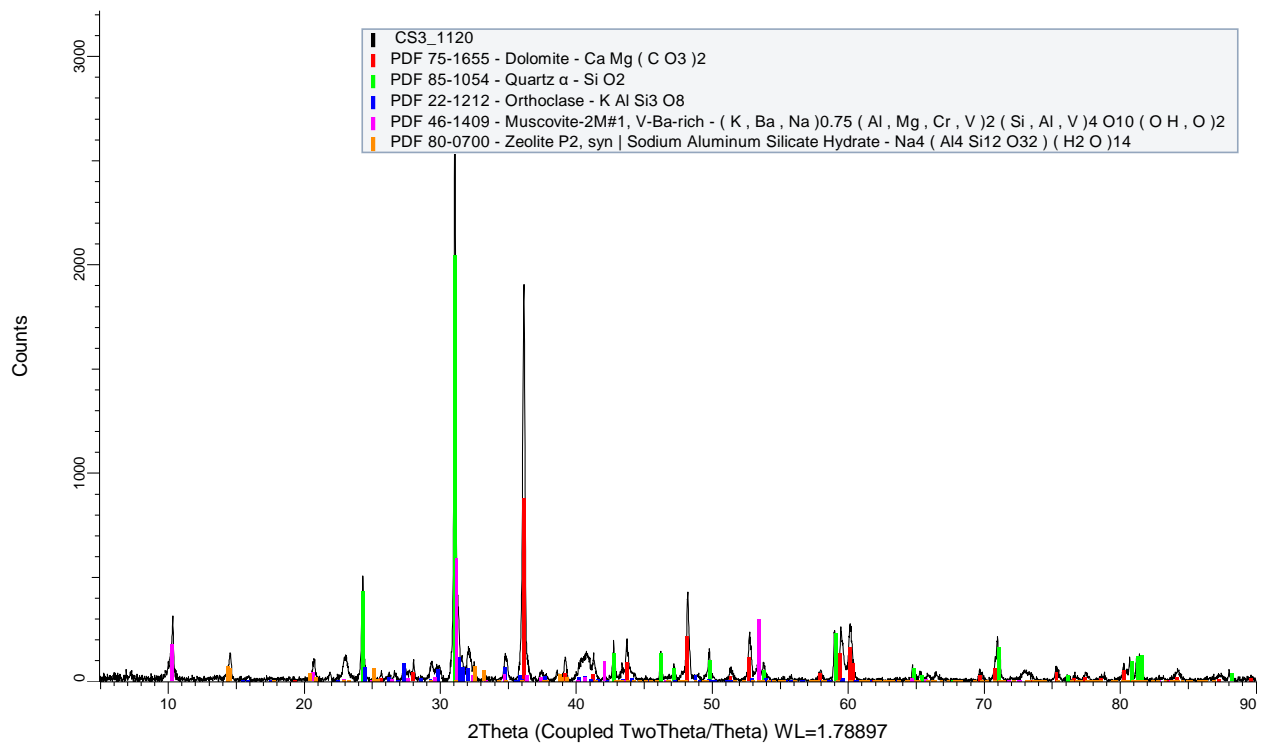


Figure B8: XRD diffraction pattern of Core 1120 sample 3, with peak matching completed using EVA software. The sample is taken from the Salina C member of the Upper Silurian Formation.

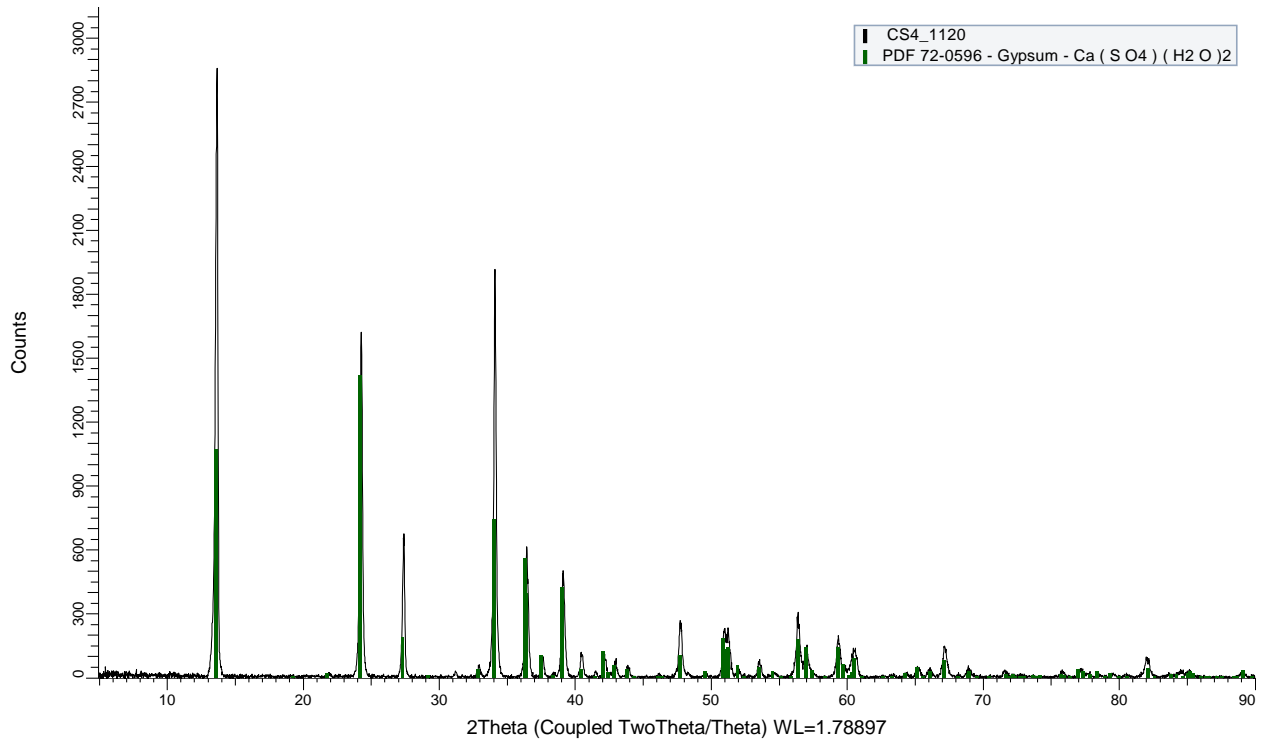


Figure B9: XRD diffraction pattern of Core 1120 sample 4, with peak matching completed using EVA software. The sample is taken from the Salina A2 member of the Upper Silurian Formation.

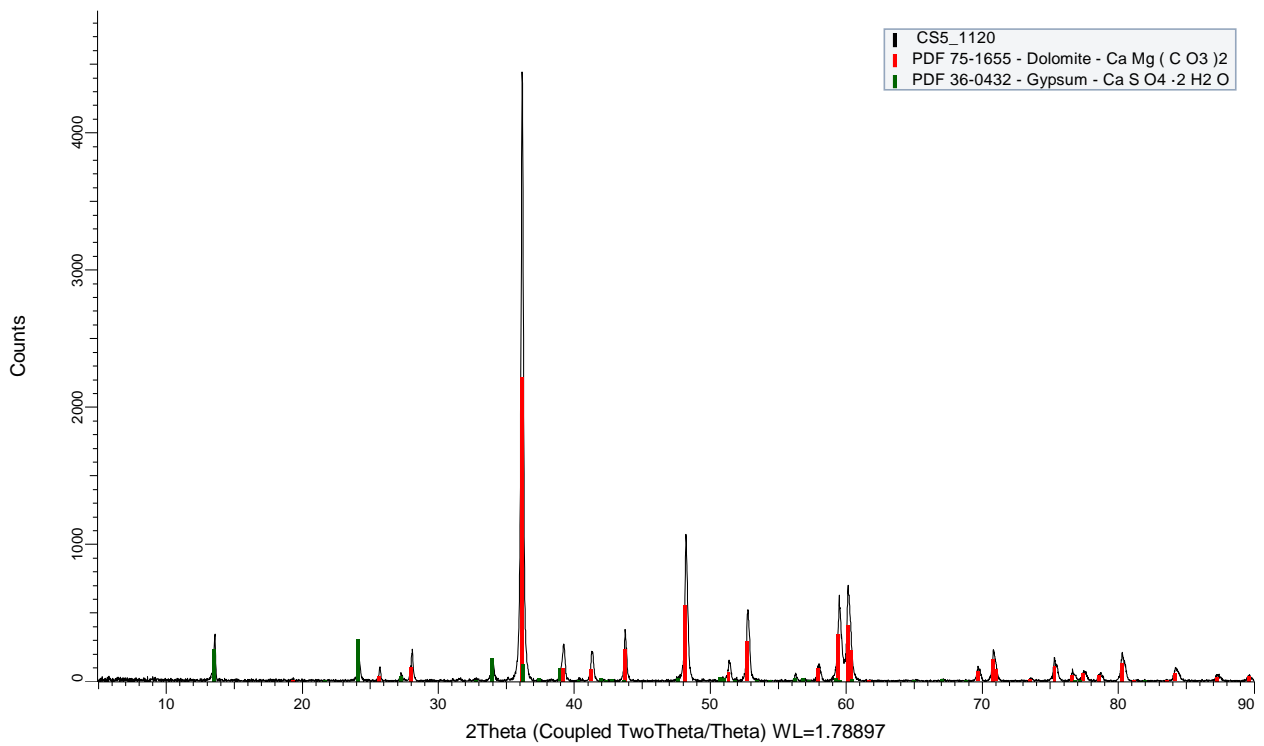


Figure B10: XRD diffraction pattern of Core 1120 sample 5, with peak matching completed using EVA software. The sample is taken from the Salina A2 member of the Upper Silurian Formation.

Curriculum Vitae

Name: Emma-Dawn Ferguson

Post-secondary Education and Degrees: The University of Western Ontario
London, Ontario, Canada
2010-2015 B.Sc.

The University of Western Ontario
London, Ontario, Canada
2015-2019 M.Sc.

Related Work Experience Teaching Assistant and Research Assistant
The University of Western Ontario
2015-2017

Research Assistant
The University of Western Ontario
2015